Phevamine A, a small molecule that suppresses plant immune responses

Erinn M. O'Neill[a,1], Tatiana S. Mucyn[b,c,1], Jon B. Patteson[a], Omri M. Finkel[b,c], Eui-Hwan Chung[b,c], Joshua A. Baccile[d,e,2], Elisabetta Massolo[a,3], Frank C. Schroeder[d,e], Jeffery L. Dangl[b,c], and Bo Li[a,4]

[a]Department of Chemistry, University of North Carolina at Chapel Hill, Chapel Hill, NC 27599; [b]Howard Hughes Medical Institute, University of North Carolina at Chapel Hill, Chapel Hill, NC 27599; [c]Department of Biology, University of North Carolina at Chapel Hill, Chapel Hill, NC 27599; [d]Boyce Thompson Institute, Cornell University, Ithaca, NY 14853; and [e]Department of Chemistry and Chemical Biology, Cornell University, Ithaca, NY 14853

Edited by Sheng Yang He, Michigan State University, East Lansing, MI, and approved August 10, 2018 (received for review March 3, 2018)

Bacterial plant pathogens cause significant crop damage worldwide. They invade plant cells by producing a variety of virulence factors, including small-molecule toxins and phytohormone mimics. Virulence of the model pathogen *Pseudomonas syringae* pv. *tomato* DC3000 (*Pto*) is regulated in part by the sigma factor HrpL. Our study of the HrpL regulon identified an uncharacterized, three-gene operon in *Pto* that is controlled by HrpL and related to the *Erwinia hrp*-associated systemic virulence (*hsv*) operon. Here, we demonstrate that the *hsv* operon contributes to the virulence of *Pto* on *Arabidopsis thaliana* and suppresses bacteria-induced immune responses. We show that the *hsv*-encoded enzymes in *Pto* synthesize a small molecule, phevamine A. This molecule consists of L-phenylalanine, L-valine, and a modified spermidine, and is different from known small molecules produced by phytopathogens. We show that phevamine A suppresses a potentiation effect of spermidine and L-arginine on the reactive oxygen species burst generated upon recognition of bacterial flagellin. The *hsv* operon is found in the genomes of divergent bacterial genera, including ∼37% of *P. syringae* genomes, suggesting that phevamine A is a widely distributed virulence factor in phytopathogens. Our work identifies a small-molecule virulence factor and reveals a mechanism by which bacterial pathogens overcome plant defense. This work highlights the power of omics approaches in identifying important small molecules in bacteria–host interactions.

natural products | genome mining | phytopathogen | virulence factor | plant immunity

Bacterial small molecules play key roles in pathogen–plant interactions. *Pseudomonas syringae*, a phylogenetically diverse species of bacteria responsible for many crop diseases, employs a myriad of virulence factors, including secreted protein effectors delivered to host cells by the type III secretion system (T3SS) and small molecules (1, 2). Coronatine, syringomycin, syringopeptin, tabtoxin, and phaseolotoxin are among the small-molecule virulence factors produced by various strains of *P. syringae*, acting as phytohormone mimics or phytotoxins (1). For example, coronatine disrupts plant immune signaling by mimicking the structure of the plant hormone jasmonic acid-isoleucine (1, 3), and phaseolotoxin contributes to virulence by interfering with the synthesis of L-arginine and polyamines in plants (4, 5). While many protein effectors have been extensively studied in *P. syringae*, only a limited number of small molecules have been identified. The genomes of *P. syringae* and other phytopathogens encode potential biosynthetic enzymes (6, 7). Identifying the cryptic small molecules synthesized by these enzymes may reveal new virulence mechanisms that could be targeted to control plant infection.

Many phytopathogenic virulence factors function to suppress plant immune responses (8, 9). The first layer of the plant immune system relies on the recognition of conserved microbe-associated molecular patterns (MAMPs) by host pattern recognition receptors to generate MAMP-triggered immunity (MTI) (10). The MTI signaling cascade includes receptor kinase activation, reactive oxygen species (ROS) production, calcium influx, mitogen-activated protein kinase activation, defense gene activation, and callose deposition at the plant cell wall (*SI Appendix*, Fig. S1); each of these steps can be targeted by virulence factors (10). The sigma factor HrpL controls the expression of *P. syringae* virulence factors including the T3SS and its associated effector genes (11). HrpL also regulates genes responsible for the biosynthesis of coronatine in some, but not all, *P. syringae* strains (12, 13). Our recent study identified a number of uncharacterized HrpL-regulated genes that encode putative biosynthetic enzymes for small molecules (12). We therefore proposed that these HrpL-regulated genes are responsible for synthesizing small molecules that play a role in virulence (12).

In this study, we focus on an HrpL-regulated three-gene biosynthetic operon *PSPTO_0873–0875* from *P. syringae* pv. *tomato* DC3000 (*Pto*) (12, 14). This operon shares 66–85% homology with *hrp* (hypersensitive response and pathogenicity)-associated systemic virulence (*hsv*) genes from *Erwinia amylovora* (15). The *hsv* operon was implicated in the virulence of *E. amylovora* on apple shoots (16), but the small molecule(s) produced by *hsv*-encoded enzymes are unknown. Here, we confirm that the *Pto hsv* operon acts as a *P. syringae* virulence factor on *Arabidopsis thaliana* and demonstrate that the *hsv* operon dampens host immune responses in both *A. thaliana* and *Nicotiana benthamiana*. We demonstrate that the enzymes encoded by the *hsv*

Significance

Bacterial pathogens cause plant diseases that threaten the global food supply. To control diseases, it is important to understand how pathogenic bacteria evade plant defense and promote infection. We identify from the phytopathogen *Pseudomonas syringae* a small-molecule virulence factor—phevamine A. Both the chemical structure and mode of action of phevamine A are different from known bacterial phytotoxins. Phevamine A promotes bacterial growth by suppressing plant immune responses, including both early (the generation of reactive oxygen species) and late (the deposition of cell wall reinforcing callose in leaves and leaf cell death) markers. This work uncovers a widely distributed, small-molecule virulence factor and shows the power of a multidisciplinary approach to identify small molecules important for plant infection.

Author contributions: E.M.O., T.S.M., J.L.D., and B.L. designed research; E.M.O., T.S.M., J.B.P., O.M.F., and E.-H.C. performed research; J.B.P., O.M.F., J.A.B., E.M., and F.C.S. contributed new reagents/analytic tools; E.M.O., T.S.M., J.L.D., and B.L. analyzed data; and E.M.O., T.S.M., J.L.D., and B.L. wrote the paper.

The authors declare no conflict of interest.

This article is a PNAS Direct Submission.

[1]E.M.O. and T.S.M. contributed equally to this work.

[2]Present address: Division of Chemistry and Chemical Engineering, California Institute of Technology, Pasadena, CA 91125.

[3]Present address: Department of Chemistry, Università degli Studi di Milano, 20133 Milan, Italy.

[4]To whom correspondence should be addressed. Email: boli@email.unc.edu.

This article contains supporting information online at www.pnas.org/lookup/suppl/doi:10.1073/pnas.1803779115/-/DCSupplemental.

operon synthesize a small molecule that is important for virulence. By integrating heterologous expression, metabolomics, and in vitro biosynthesis, we identify a bioactive small molecule, phevamine A, a conjugate of L-phenylalanine, L-valine, and a modified spermidine. We further show that phevamine A suppresses the potentiation of MAMP-induced ROS bursts by spermidine and L-arginine. Thus, phevamine A is a small-molecule virulence factor that promotes bacterial growth and virulence, in part by suppressing plant immune responses.

Results and Discussion

The *P. syringae hsv* Operon Promotes Virulence and Suppresses Defense Responses. To investigate the function of the *hsv* operon, we first generated independent clean deletion mutants in *Pto*. The parental strain, *Pto*, and the two mutants, *Pto*_Δ*hsv*1, *Pto*_Δ*hsv*2 were used to infect *A. thaliana* Col-0 seedlings by dip inoculation (*SI Appendix*, *Materials and Methods*) and the growth of these bacteria was monitored. We observed that the mutants grew slightly less than the *Pto* strains (*SI Appendix*, Fig. S2) in two independent experiments, but this reduced growth trend was not statistically significant. This observation is not surprising, as *Pto* is an aggressive pathogen on *A. thaliana* and its large suite of virulence factors can act collectively (17). It is therefore rare to observe significant loss of virulence phenotypes when deleting a single candidate virulence factor from this strain. To circumvent this problem, we used a weakly pathogenic *Pto* derivative deficient in coronatine production (*Pto* DC3118, hereafter *Pto*-Cor$^-$) (17) to generate independent *hsv* mutants *Pto*-Cor$^-$Δ*hsv*1, and *Pto*-Cor$^-$Δ*hsv*2. Three days postinfection, significantly less bacteria for *Pto*-Cor$^-$Δ*hsv*1 and *Pto*-Cor$^-$Δ*hsv*2 were recovered from the seedlings than *Pto*-Cor$^-$ (Fig. 1*A*). This result indicates that *hsv* is required for full virulence *in planta*.

We next addressed whether the *hsv* operon had an effect on host callose deposition, a cell wall reinforcing response typically triggered during MTI (18, 19) (*SI Appendix*, Fig. S1). Several type III secretion effector proteins can inhibit callose deposition (20–24) and thus may obscure phenotypes resulting from *hsv* deletion. We therefore generated two independent *hsv* clean deletions in *Pto*D28E (*Pto*D28EΔ*hsv*1 and *Pto*D28EΔ*hsv*2), a strain lacking 28 different type III secretion effectors (25). *Pto*D28E, *Pto*D28EΔ*hsv*1, and *Pto*D28EΔ*hsv*2 were used to infiltrate 4-wk-old leaves of *A. thaliana*. Both *Pto*D28EΔ*hsv* alleles induced higher callose deposition than *Pto*D28E (Fig. 1*B*); complementation of *Pto*D28EΔ*hsv*2 with constitutively expressed *hsv* reduced the level of callose back to that induced by *Pto*D28E (Fig. 1*C*). These results demonstrate that *hsv* suppresses a late marker of plant defense at the cell wall.

Conversely, we also examined whether *hsv* expression is sufficient to suppress plant callose deposition induced by a nonpathogenic bacterium. The *hsv* operon was constitutively expressed in *Pseudomonas fluorescens Pf*0-1 (*Pf*0-1), a strain that lacks both *hsv* and a T3SS, but still induces callose deposition (Fig. 1*D*) (26). Expression of *hsv* had no effect on the level of *Pf*0-1-induced callose deposition (Fig. 1*D*). A *Pf*0-1 derivative engineered to contain a complete *P. syringae* T3SS locus (*Pf*0-1+T3SS) (27) induced more callose than wild-type *Pf*0-1 (*SI Appendix*, Fig. S3), suggesting that *Pf*0-1 T3SS components are recognized by the plant (28). Expression of *hsv* in the *Pf*0-1+T3SS strain reduced the level of callose back to the level elicited by wild-type *Pf*0-1 (Fig. 1*D* and *SI Appendix*, Fig. S3). Thus, *hsv* suppresses the callose deposition induced by *Pf*0-1 T3SS components. To extend this observation, we evaluated the activities of these *P. fluorescens* strains on a second plant species, *N. benthamiana*. Infiltration of *N. benthamiana* leaves with *Pf*0-1 or *Pf*0-1-expressing *hsv* had no effect; the tissue infiltrated with bacteria was identical to the noninfiltrated tissue (Fig. 1*E*). In contrast, infiltration with *Pf*0-1+T3SS elicited a dose-dependent leaf cell death. This response was suppressed by *hsv* expression (Fig. 1*E*). Thus, *hsv* suppresses the cell death caused by a component of the T3SS or the linked harpin gene transferred from *P. syringae* pv. *syringae* to *Pf*0-1 (29, 30).

***hsv*-Encoded Enzymes Synthesize Three Related Small Molecules.** The *hsv* operon encodes three enzymes, including a putative amidinotransferase, HsvA, and two putative ATP-grasp–type enzymes, HsvB and HsvC (Fig. 2*A*). To test the hypothesis that these *hsv*-encoded enzymes synthesize small molecules, we conducted *hsv* heterologous expression and comparative metabolomics experiments. The *hsv* cluster was overexpressed in *Escherichia coli* as a heterologous host to enhance small molecule production. Organic extracts of culture supernatants were analyzed using liquid-chromatography-coupled high-resolution mass spectrometry (LC-HRMS) to generate metabolomic profiles for comparison. Three species with mass-to-charge ratios (*m*/*z*) of 287.255, 434.324, and 581.392 were present at high levels in the *hsv*-expressing *E. coli*, but were absent in the control *E. coli* carrying the empty vector (Fig. 2*B* and *SI Appendix*, Figs. S4–S6). The species with the *m*/*z* of 287.255 and 434.324 were also detected by LC-HRMS in the culture extract of the wild-type *Pto*, but not in *Pto*Δ*hsv* (Fig. 2*C* and *SI Appendix*, Fig. S5). The production of the metabolite with the *m*/*z* of 434.324 is also observed in *Pto* overexpressing *hrpL*, but is reduced by *hrpL* deletion (Fig. 2*C*), consistent with the regulation of *hsv* by *hrpL* (12). This metabolite was detected at the same level in the supernatants of both *Pf*0-1- and *Pf*0-1+T3SS-expressing *hsv* (*SI Appendix*, Fig. S7), indicating that secretion of the compound is independent of the T3SS.

We analyzed the structures of the identified metabolites from *E. coli* and *P. syringae* strains expressing the *hsv* operon by tandem MS, which revealed that these metabolites share similar MS fragments (*SI Appendix*, Figs. S8 and S9) and likely possess related structures. The mass differences between 287.255 and 434.324, and between 434.324 and 581.392 are both 147.068, corresponding to the mass of a phenylalanine in an amide linkage. Based on these data, we propose that the structures of the compounds with the *m*/*z* of 434.324 and 581.392 contain one and two phenylalanines, respectively. We name the identified metabolites phevamine A (*m*/*z* 434.324; PHVA), phevamine B (*m*/*z* 581.392; PHVB) and prephevamine (*m*/*z* 287.255; pPHV).

In Vitro Biosynthesis of Phevamines Reveals Structures. To characterize the structures of phevamines, we reconstituted the biosynthetic enzymes encoded by the *hsv* operon in vitro. HsvA shares homology with amidinotransferases that transfer an amidino group from arginine to an amine, suggesting the presence of an amidino group. HsvB and HsvC belong to the ATP-grasp enzyme superfamily consisting of ATP-dependent enzymes that condense carboxylic acids with amines, suggesting the presence of amide linkages in the phevamines and prephevamine (31). HsvA, HsvB, and HsvC were overexpressed in *E. coli* and purified as recombinant proteins. We reconstituted the activity of HsvA by incubating L-arginine, the donor of the amidino group for amidinotransferases, in the presence of a variety of physiologically relevant amines as acceptors, including L-lysine as well as spermidine and spermine, which are polyamines produced by *P. syringae* (32, 33). We found that HsvA preferentially modifies spermidine and generates amidinospermidine (Fig. 3*A* and *SI Appendix*, Figs. S10 and S11). Subtracting the mass of amidinospermidine from that of prephevamine results in a mass consistent with a valine in an amide linkage. We therefore proposed amidinospermidine is condensed with L-Val as the second biosynthetic step to generate prephevamine (Fig. 3*A*). Both ATP-grasp enzymes, HsvB and HsvC, were examined for this condensation activity in the presence of amidinospermidine, L-Val, ATP, and Mg^{2+}. Only HsvC catalyzes prephevamine formation (Fig. 3*A* and *SI Appendix*, Fig. S10). Data from analyzing product formation by LC-HRMS and measuring phosphate released in the assay suggest

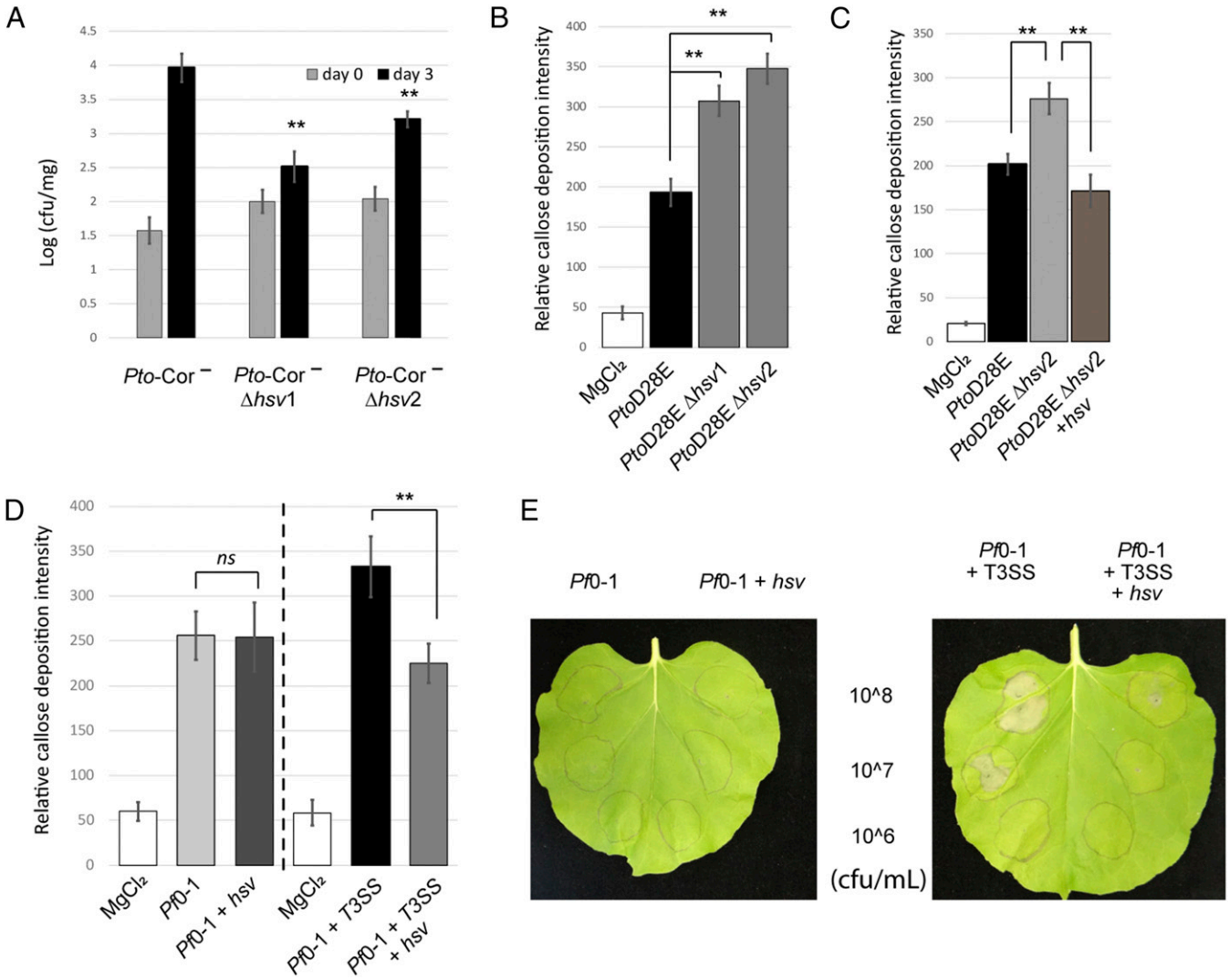

Fig. 1. The *hsv* operon is required for virulence and suppresses defense responses. (*A*) *Pto*-Cor⁻Δ*hsv* mutants display reduced growth on *A. thaliana* seedlings compared with *Pto*-Cor⁻. This experiment was repeated three times with similar results. (*B*) *Pto*D28EΔ*hsv* mutants induce higher callose deposition than *Pto*D28E on 4-wk-old *A. thaliana* leaves. The experiment is a representative of four independent replicates. (*C*) Complementation of *hsv* in *Pto*D28EΔ*hsv2* (*Pto*D28EΔ*hsv2* + *NptII::hsv*) reestablishes callose deposition to levels triggered by *Pto*D28E. This assay is a representative of two independent replicates. (*D*) The *hsv* operon suppresses callose deposition when coexpressed in *Pf*0-1 with T3SS, but not when expressed in *Pf*0-1. The callose deposition was monitored as in *B* after infiltration of *Pf*0-1 or *Pf*0-1 expressing *hsv*. This assay was performed twice with similar results. *Pf*0-1+T3SS and *Pf*0-1+T3SS-expressing *hsv* were tested separately with at least three replicate experiments for each strain. (*E*) The *hsv* operon in *Pf*0-1 suppresses T3SS-mediated cell death in *N. benthamiana*. *Pf*0-1-derived strains were inoculated at three different concentrations (colony-forming units per milliliter). Pictures were taken 20-h postinfiltration. This assay was repeated four times with similar results. ** indicates *t* test, *P* value < 0.01. Error bars represent ±SE. Relative callose intensity represents the number of callose deposits observed per field. cfu/mg, colony-forming units per milligram of plant tissue; ns, not significant.

that L-phenylalanine is a structural component of the phevamines (*SI Appendix*, Fig. S12). To validate this proposal, we incubated prephevamine with HsvB and L-Phe, and the formation of phevamine A and phevamine B was indeed observed (Fig. 3*A* and *SI Appendix*, Figs. S10 and S13). This result also indicates that HsvB can catalyze two rounds of condensation with L-Phe. Tandem MS analysis of phevamine A suggests that the amidino group is connected to the propylamine end of spermidine (Fig. 3*B* and *SI Appendix*, Fig. S9).

Having identified that phevamines consist of L-Phe, L-Val, and amidinospermidine, we next determined the connectivity of these components by NMR analysis. Due to high polarity, phevamines were difficult to isolate from bacterial culture extracts. To isolate sufficient materials for NMR, we developed in vitro biosynthetic methods for phevamine A and phevamine B (*Methods*). From 16 mL of in vitro enzymatic assays, 5.7 mg of phevamine A and 5.5 mg of phevamine B were purified. These compounds were analyzed by ^{1}H, (^{1}H,^{1}H)-COSY, (^{1}H,^{13}C)-HMBC, and (^{1}H,^{13}C)-HSQC NMR experiments (Fig. 3*C* and *SI Appendix*, Figs. S14–S21). The NMR data support that the amidino group is linked to the propylamine side of spermidine and that phevamine B contains an additional L-Phe at the *N*-terminus of phevamine A. Phevamine B was only detected under conditions of heterologous expression and in vitro synthesis, but not in the culture extract of *Pto* (*SI Appendix*, Fig. S6), suggesting that phevamine B is unlikely a physiologically relevant molecule. The production of phevamine B may be due to the overexpression of HsvB in *E. coli* and the high concentration of HsvB and L-Phe added in vitro. Thus, we focused on phevamine A for further structural characterization. To confirm the absolute stereochemistry, we developed a total synthesis method for phevamine A (*SI Appendix*, *Materials and Methods*). Synthetic

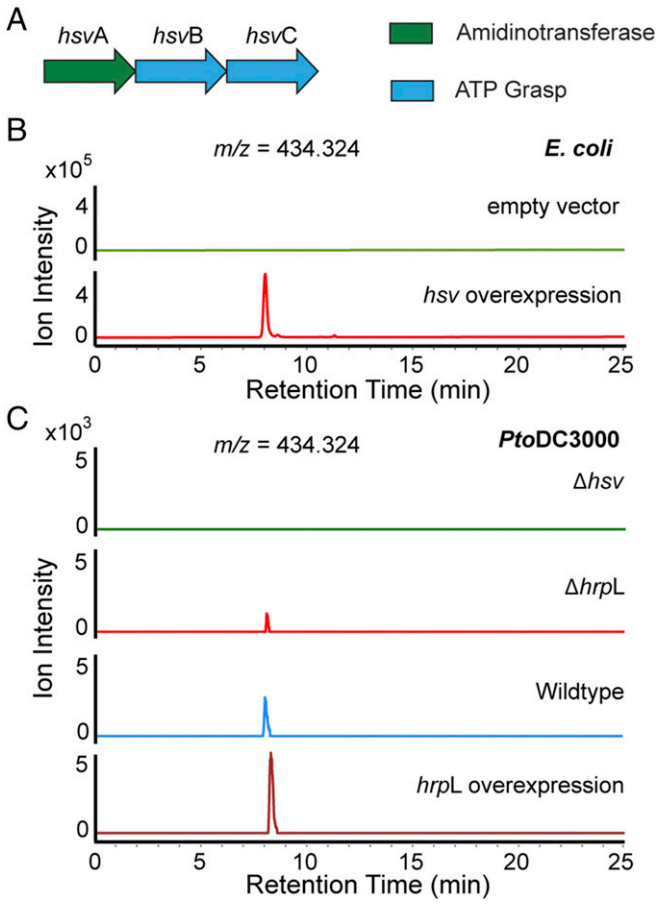

Fig. 2. Metabolomics reveals the small molecules synthesized by *hsv*-encoded enzymes. (*A*) Graphical representation of the *hsv* operon. (*B*) Comparative metabolomics analysis in *E. coli*. Overexpression of *hsv* produces a molecule with an *m/z* of 434.324 (green), which is absent in *E. coli* harboring the empty vector (red). (*C*) Comparative metabolomics analysis in *Pto*. The molecule with the *m/z* of 434.324 is absent in Δ*hsv* (green) and reduced in Δ*hrpL* (red), but present in both wild-type *Pto* (blue) and *Pto* overexpressing *hrpL* (maroon). Extracted ion chromatograms for 434.324 are shown in *B* and *C*. The slight change in retention time is due to the hydrophilicity of this molecule. Experiments presented in *B* and *C* were repeated at least three times.

and in vitro isolated phevamine A exhibit identical ^{1}H and ^{13}C NMR signals, and the same LC retention time and MS fragmentation pattern as the species detected in the bacterial culture extract (Fig. 3*D* and *SI Appendix*, Figs. S14–S22). These results confirmed the structure assignment for phevamine A and provided materials for biological activity testing of this molecule. In an initial activity test, we examined the ability of phevamine A to bind ferric iron using a chromeazurol S assay and observed no significant binding to ferric iron (*SI Appendix*, Fig. S23), suggesting phevamine A is unlikely acting as a siderophore.

Comparative Genomics Suggests a Potential Host Target for Phevamines. We investigated the phylogenetic distribution of *hsv* in bacterial genomes using MultiGeneBlast that identifies homologous gene clusters based on sequence similarity and gene synteny (34). We found that *hsv* is widely distributed across plant-pathogenic bacterial genera including *Pseudomonas*, *Erwinia*, and *Pantoea*. We compared the distribution of the *hsv* operon to those biosynthetic gene clusters encoding known *P. syringae* phytotoxins, focusing on coronatine, mangotoxin, syringolin, phaseolotoxin, and tabtoxin (Fig. 4*A* and Dataset S1) (1, 35). The *hsv* operon is present in ~37% of *P. syringae* (107 out of 292) and is the most widely distributed gene cluster of the six analyzed. The *hsv* operon rarely cooccurs with any of the aforementioned small-molecule biosynthetic clusters. This anticorrelation is especially prominent between *hsv* and phaseolotoxin biosynthetic genes in the genomes of otherwise extremely closely related strains of *P. syringae* pv. *actinidiae* (36). We previously showed that functionally redundant virulence factors rarely cooccur in the same strain (37). Specifically, the small molecule coronatine and three different type III secretion system protein effectors use four distinct mechanisms to target the same host defense signaling pathway, and only genes responsible for a single mechanism are typically found in any given *P. syringae* genome (37). Based on the clear anticorrelation of *hsv* with the phaseolotoxin biosynthetic genes, and the knowledge that phaseolotoxin targets host arginine and polyamine biosynthesis by inhibiting ornithine carbamoyltransferase and ornithine decarboxylase (Fig. 4*B*) (4, 5, 38), we hypothesized that the action of phevamine A involves polyamines and/or arginine. This hypothesis is consistent with previous implication of polyamine function in plant immune responses (39, 40). Furthermore, our genomic analysis revealed that many *P. syringae* strains do not contain the biosynthetic gene clusters for phevamine A or the five other phytotoxins described herein (Fig. 4*A*). These strains could produce different small molecules that might play a role in bacteria–plant interaction.

Polyamines and Arginine Potentiate an Early MTI Response. We investigated the effect of arginine and polyamines on the MTI response induced by the well-studied MAMP flg22, a short peptide derived from the *Pseudomonas* flagellin (18). We monitored the ROS burst following recognition of flg22 by the pattern recognition receptor FLS2 (*SI Appendix*, Fig. S1) (41, 42). The polyamines putrescine, spermidine, and spermine potentiated the flg22-induced ROS burst in *N. benthamiana*, resulting in an earlier and larger amplitude response (Fig. 5 *A* and *B* and *SI Appendix*, Fig. S24*A*). The potentiation was dose-dependent (*SI Appendix*, Fig. S24*B*). Spermidine alone induced only a slight ROS burst (*SI Appendix*, Fig. S24*C*) (40), and the increase of the flg22-induced ROS burst in the presence of spermidine was higher than an additive effect (*SI Appendix*, Fig. S24*C*). The potentiation by spermidine was also observed in *A. thaliana*, but was not observed in the flg22 receptor mutant *fls2* (Fig. 5*C* and *SI Appendix*, Fig. S25 *A* and *B*). Spermidine potentiation was also observed using the elicitor elf18 (*SI Appendix*, Fig. S25*C*) (43). Surprisingly, the *Arabidopsis* Ca^{2+} burst induced by flg22 was reduced in the presence of spermidine (Fig. 5*D* and *SI Appendix*, Figs. S1 and S25*D*). Arginine had a similar effect on ROS burst in *A. thaliana* and *N. benthamiana*, while L-citrulline did not (*SI Appendix*, Figs. S26 and S27). Thus, spermidine and arginine potentiate MAMP-induced ROS bursts in both plant species, and spermidine modulates the flg22-induced Ca^{2+} burst, at least in *A. thaliana*. These results are consistent with previously proposed functions of polyamines in plant defense responses (39, 40), including up-regulation of polyamine biosynthesis in plants following challenge with bacterial pathogens (44–47), subsequent polyamine transport to the apoplast (44), and increased resistance toward *Pseudomonas viridiflava* observed after exogenous addition of spermine (47).

Phevamine A Suppresses Spermidine and Arginine Potentiation of the flg22-Induced ROS Burst. The anticorrelation of phevamine A- and phaseolotoxin-encoding genes suggested that phevamines might impair the effect of spermidine and arginine on the early MAMP-dependent ROS burst. We therefore tested whether phevamine A could impair the effect of exogenously supplied spermidine and arginine in the MTI-induced ROS burst potentiation assay. Leaf disks of *N. benthamiana* were challenged with flg22 in the presence of phevamine A, spermidine, or both (Fig. 5*A*). We observed

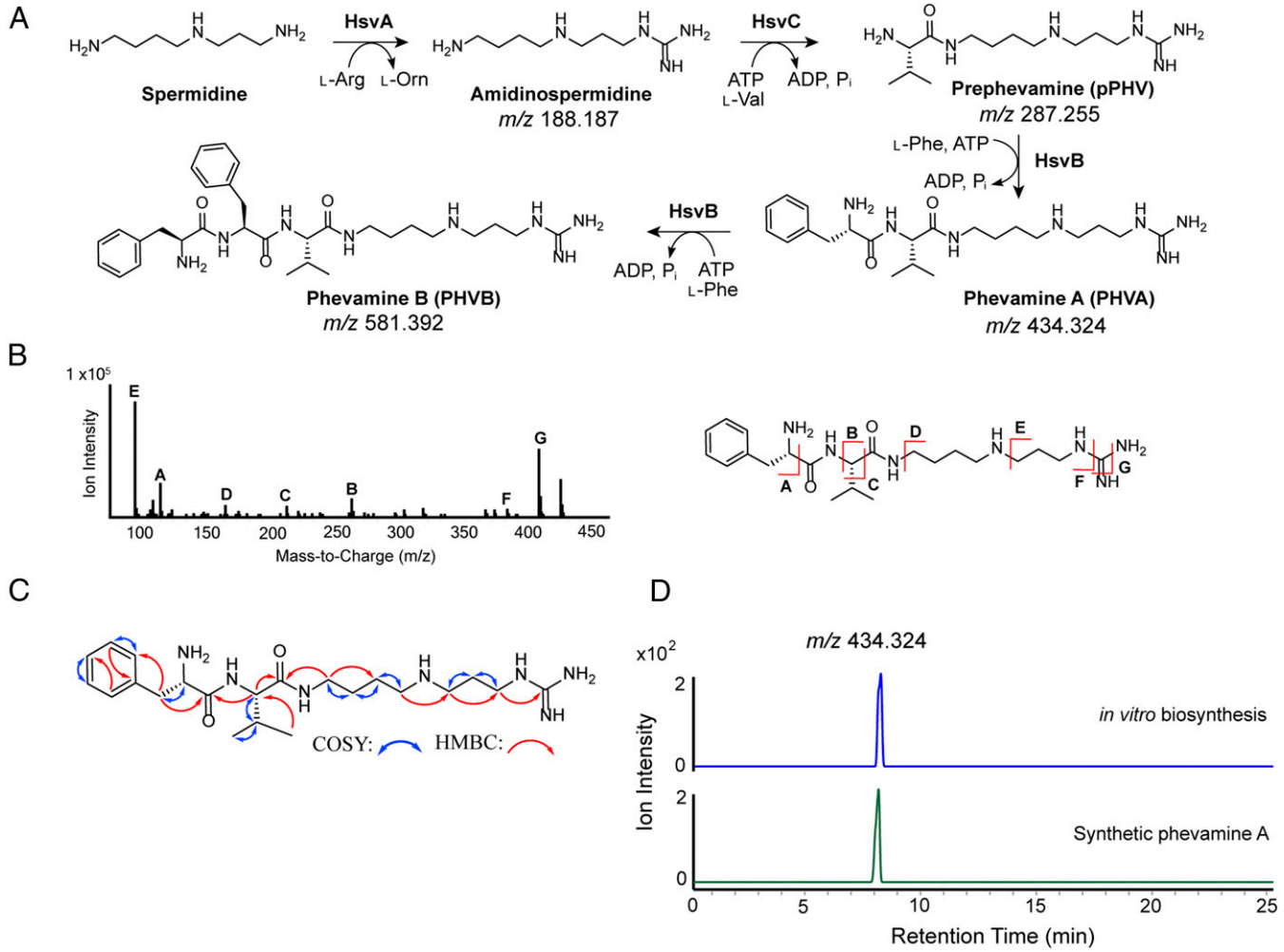

Fig. 3. Structural characterization and biosynthesis of prephevamine and the phevamines. (*A*) Biosynthetic pathway of prephevamine and the phevamines based on in vitro characterization. (*B*) Structural analysis of phevamine A produced by *E. coli* overexpressing *hsv* using tandem MS. (*C*) COSY and (^{1}H,^{13}C)-HMBC correlations of in vitro synthesized and purified phevamine A. (*D*) Extracted ion chromatograms of phevamine A (*m/z*, 434.324) produced via in vitro enzymatic synthesis (blue) or total chemical synthesis (green).

that phevamine A suppressed the spermidine potentiation of the flg22-induced ROS burst in *N. benthamiana*, but did not directly affect the flg22 response (Fig. 5*A*). We noted that prephevamine also suppressed the spermidine potentiation of the flg22-induced ROS burst, but phevamine B did not (Fig. 5*B*). This result is consistent with our observation that phevamine B is not naturally produced by *Pto* (*SI Appendix*, Fig. S6). In contrast, only phevamine A suppressed the spermidine-mediated flg22-induced ROS burst in *A. thaliana* leaf disks in a similar experimental setup (Fig. 5*C*). This indicates that the molecular mechanism(s) of the spermidine potentiation might differ slightly between *N. benthamiana* and *A. thaliana*.

Spermidine affects both the flg22-induced ROS and Ca^{2+} bursts (Fig. 5*D* and *SI Appendix*, Fig. S24*C*). We therefore tested the effect of phevamine A on the flg22-induced Ca^{2+} burst in the presence and absence of spermidine using a transgenic *A. thaliana* line that expresses the aequorin reporter (48). As noted above, spermidine suppressed the flg22-induced Ca^{2+} burst, but the addition of phevamine A did not affect this suppression. Phevamine A also had no direct effect on the Ca^{2+} burst induced by flg22 (Fig. 5*D*). These data suggest that phevamine A acts downstream of the Ca^{2+} burst.

Additionally, both phevamine A and prephevamine were tested for their effect on the ROS potentiation mediated by arginine in both *N. benthamiana* and *A. thaliana*. Phevamine A, but not prephevamine, could suppress the arginine-mediated potentiation of the flg22-induced ROS burst in *N. benthamiana* (*SI Appendix*, Fig. S27). This may imply that the potentiation mediated by spermidine and arginine in *N. benthamiana* involves slightly divergent molecular mechanism(s), supported by the different potentiation phenotypes for prephevamine. Similarly, only phevamine A and not prephevamine could inhibit the arginine potentiation of the flg22-induced ROS burst in *A. thaliana*.

Overall, we observed that phevamine A consistently suppressed both the spermidine- and arginine-mediated potentiation of the flg22-induced ROS burst across two divergent plant species. Thus, phevamine A is likely the most physiologically relevant small molecule produced by the *hsv* operon in *Pto*.

Conclusions

We identify a bacterial small-molecule virulence factor, phevamine A. The biosynthesis of phevamine A is controlled by the HrpL virulence regulator in *P. syringae*. Interestingly, phevamine A shares structural similarity with insect polyamine toxins: argiotoxin from the orb-weaver spider, and philanthotoxin from the Egyptian solitary wasp, both of which contain a polyamine and two amino acids, and are powerful neurotoxins that target

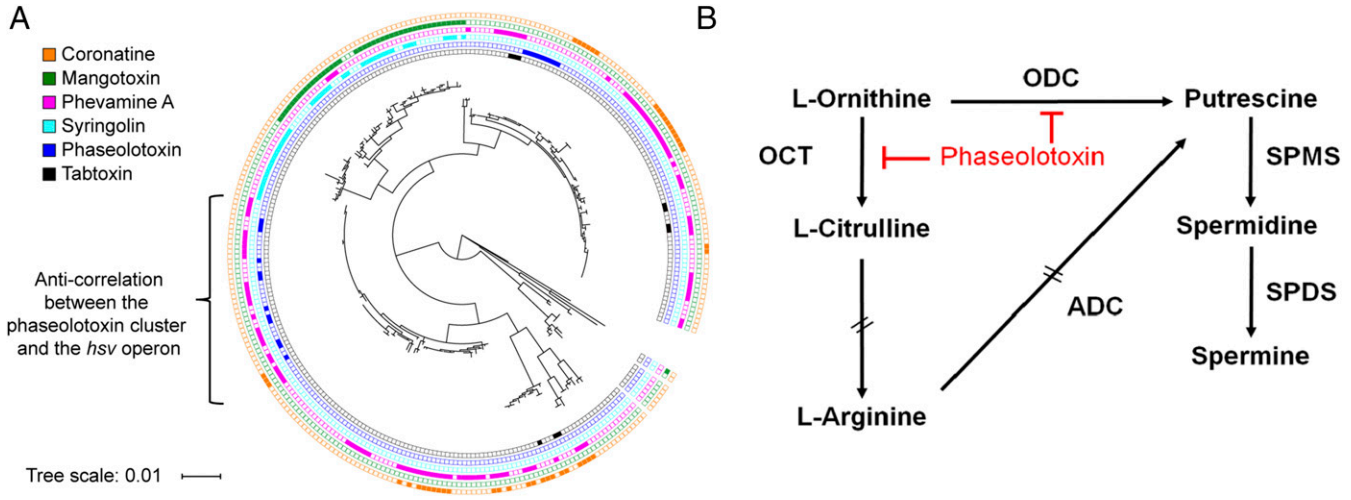

Fig. 4. Distribution of the *hsv* operon and other toxins among *P. syringae* and graphical representation of polyamine biosynthesis and action of phaseolotoxin. (*A*) Phylogenetic tree of 292 *P. syringae* strains and the distribution of coronatine, mangotoxin, phevamine A, syringolin, phaseolotoxin, and tabtoxin biosynthetic genes, from the outer ring to the inner ring. The tree scale represents the nucleotide substitution per site. (*B*) Phaseolotoxin inhibits the arginine and polyamine pathways by suppressing the activity of ornithine decarboxylase (ODC) and ornithine carbamoyltransferase (OCT). ADC, arginine decarboxylase; SPDS, spermidine synthase; SPMS, spermine synthase. Double dashed arrows represent pathways with intermediates not shown. Reproduced from ref. 60 with permission from American Society for Microbiology.

ion channels (49, 50). The structural similarity suggests related mechanisms, which will be the focus of future studies.

The importance of phevamine A in bacterial virulence has been demonstrated in two different pathogens, *E. amylovora* (16) and *P. syringae* in this study. We show that the *hsv* operon and purified phevamine A can suppress both early and late markers of plant immune responses. Specifically, the *hsv* operon suppresses T3SS/harpin-induced callose deposition and host cell death. The phylogenetic distribution of the *hsv* operon suggested that phevamine A is a conserved virulence factor among bacterial phytopathogens. The anticorrelation of *hsv* and the biosynthetic genes for phaseolotoxin within a closely related clade of *P. syrinage* pv. *actinidiae* genomes suggested functional redundancy between phevamine A and phaseolotoxin. We demonstrated that phevamine A impairs plant immune signal potentiation by polyamines and arginine, while it is known that phaseolotoxin targets the synthesis of polyamines and arginine.

Our discovery of phevamine A also provided the opportunity to describe functions for polyamines in the potentiation of the MAMP-induced ROS burst induced by flg22, expanding the role of polyamines as important defense mediators. Our results are consistent with a model (*SI Appendix*, Fig. S28) in which *P. syringae* uses either phaseolotoxin or phevamine A to dampen host immune output by altering polyamine biosynthesis or the signaling capacity of polyamines, respectively. We speculate that components of the T3SS and/or harpins may be recognized at the cell surface, acting as elicitors of MTI subject to polyamine potentiation and suppression by phevamine A.

We show that two ATP-grasp enzymes are responsible for assembling phevamine A. These enzymes belong to a large superfamily of enzymes that catalyze amide bond formation by activating carboxylic acids through phosphorylation (51). ATP-grasp–type enzymes are widely used by bacteria for the synthesis of diverse small molecules, including the virulence factors phaseolotoxin, dapdiamide, and mangotoxin (52–54). Studies of these enzymes in a marine proteobacterium and a soil actinomycete have led to the discovery of small molecules with distinct structures but unknown functions (55, 56). Still, most biosynthetic operons containing ATP-grasp–type enzymes have eluded genome-guided discovery. Our study suggests that targeted mining of uncharacterized ATP-grasp enzymes will likely lead to novel small molecules.

Our approach for identifying cryptic small molecules builds on the rich knowledge of pathogen gene expression and integrates comparative genomic analysis, biochemical enzyme reconstitution, and physiological assays. Bacterial genomes harbor many biosynthetic operons of unknown function; therefore, this approach holds potential for identifying many more small molecules essential for bacteria–host interactions.

Methods

Metabolite Extraction for Metabolomics. *E. coli*, *P. syringae*, and *P. fluorescens* cultures (100 mL) were spun down at 3,500 × *g* and 4 °C for 10 min. Solvent extractions were performed using an equal volume of supernatant to chloroform-methanol (2:1:1). The top aqueous layer was separated into a round-bottom flask and concentrated under vacuum. The dried-down material was resuspended and transferred to a small glass vial, concentrated under reduced pressure, and stored at −20 °C until MS analysis.

MS and MS/MS Analysis. Culture extracts, in vitro synthesized phevamines, and chemically synthesized phevamine A, were analyzed by Agilent 6520 accurate-mass quadrupole-time of flight (Q-TOF) LC/MS using a Phenomenex Kinetex 5-μm C18 column (100 Å, 150 mm × 4.60 mm). Mobile phases were water and acetonitrile, each containing 0.1% formic acid. The gradient was held at 2% acetonitrile for 2 min before ramping up to 45% acetonitrile over 17 min at a flow rate of 0.4 mL/min. For each sample, *m/z* 434.324 was selected at a retention time of 8 ± 5 min and analyzed by MS fragmentation. Targeted MS/MS was conducted using 30-V collision energy, 970.9-ms/s acquisition time, and a 4 *m/z* isolation width.

Preparative Scale in Vitro Enzymatic Synthesis of Phevamines. One milliliter, one-pot enzymatic assays for phevamine A were conducted at room temperature for 2 h. Assays contained 5 mM L-arginine, 5 mM spermidine, 1 mM L-valine, 0.5 mM L-phenylalanine, 100 mM Hepes (pH 7.5), 2 mM $MgCl_2$, 1 mM ATP, 20 μM HsvA, 10 μM HsvB, 10 μM HsvC, and water. The reaction was then quenched with 1 mL acetonitrile to precipitate protein overnight at −20 °C. The precipitated proteins were removed by centrifugation. Phevamines were purified from the supernatant using one round of preparative HPLC, and two rounds of analytical HPLC using conditions described in *SI Appendix, Materials and Methods*.

Plant Material and Bacterial Growth. *A. thaliana* was grown in walk-in growth rooms maintained at 21 °C/18 °C (day/night) with a 9-h/15-h (day/night) cycle. *N. benthamiana* was grown in a walk-in growth room maintained at

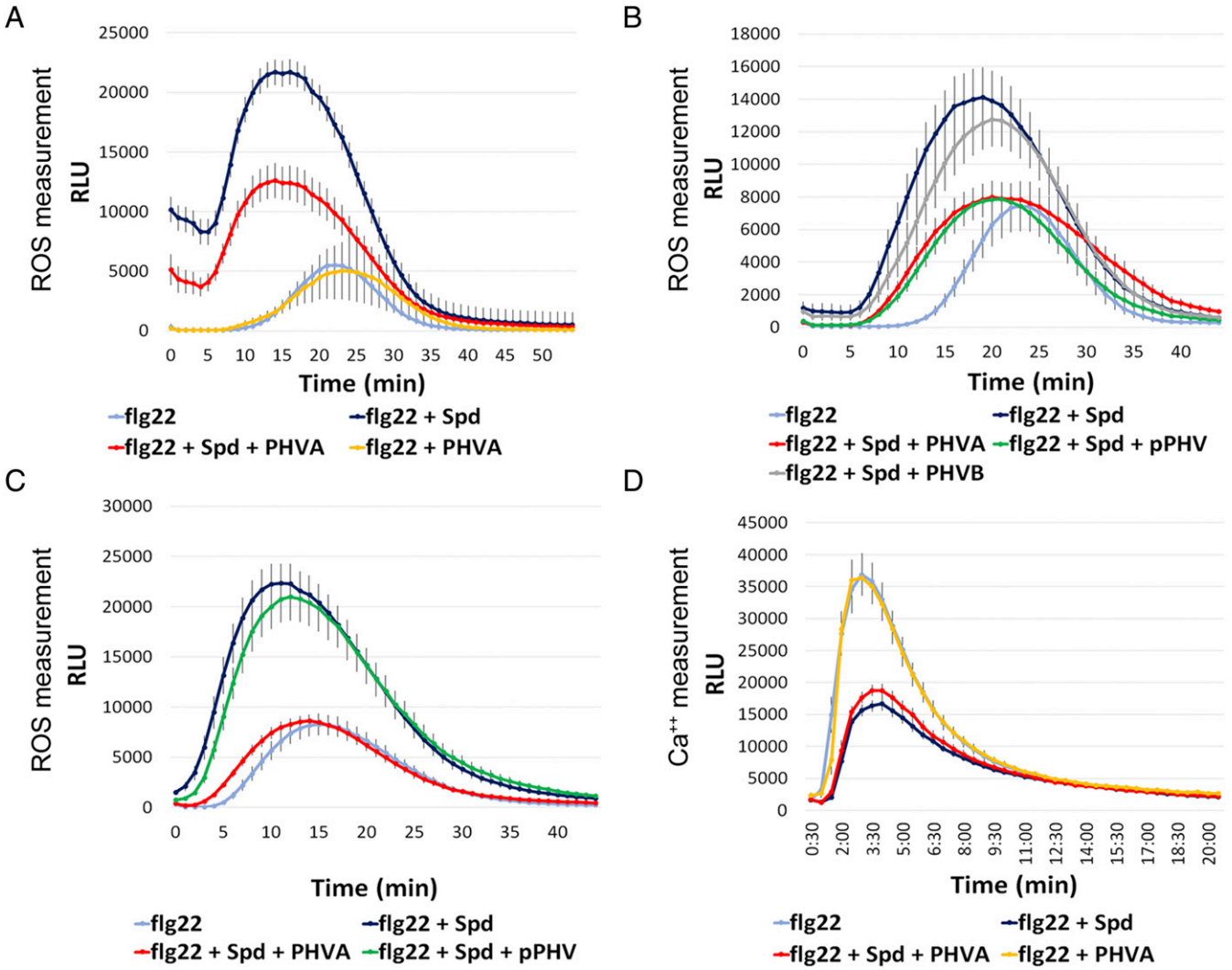

Fig. 5. Effect of the phevamines and prephevamine on the spermidine potentiation of the ROS burst and suppression of the calcium burst. (*A*) Phevamine A suppresses the spermidine potentiation of the flg22-induced ROS burst in *N. benthamiana*, but does not affect the flg22-induced ROS burst directly. Leaf disks were treated with 50 nM flg22, with or without spermidine at 400 μM, and with or without phevamine A at 400 μM. (*B*) Phevamine A and prephevamine suppress the spermidine potentiation in *N. benthamiana*, but phevamine B does not. Leaf disks were treated with flg22 at 10 nM, spermidine, phevamines, and prephevamine were used at 300 μM. (*C*) In *Arabidopsis*, phevamine A suppresses the spermidine potentiation, while prephevamine does not. Leaf disks were treated with flg22 at 10 nM, spermidine and phevamines were used at 300 μM. (*D*) Phevamine A does not affect the flg22-induced Ca^{2+} burst, or the reduction of this burst by spermidine. Leaf disks were treated with flg22 at 20 nM, spermidine and phevamine A were used at 300 μM. Error bars represent SEs. PHVA, phevamine A; PHVB, phevamine B; pPHV, prephevamine; RLU, relative luminescence units; Spd, spermidine. All experiments presented here were repeated at least three times.

26 °C/22 °C with a 12-h/12-h (day/night) cycle and a LGM550 professional LED grow light system (LED Grow Master Global). For maintenance and transformation, *Pseudomonas* strains were grown in King's B media at 28 °C. For infiltration or dipping *in planta*, *Pseudomonas* strains were grown in liquid culture overnight with the appropriate antibiotics, then plated on a Petri dish and incubated overnight before resuspension in 10 mM $MgCl_2$.

Bacterial Growth Assay. *Pto*, *Pto*Δ*hsv*, *Pto*-Cor$^-$, and *Pto*-Cor$^-$Δ*hsv* cells were resuspended in 10 mM $MgCl_2$ to a final concentration of 2×10^5 cfu/mL. Twenty-day-old *A. thaliana* Col-0 seedlings were dipped in bacterial solutions supplemented with Silwet L-77 (Momentive), and growth was assessed at day 0 and 3-d postinfection as described by Tornero and Dangl (57). Eight samples containing three seedlings were collected for each treatment.

Callose Deposition Measurement. Three- to 5-wk-old *Arabidopsis* plants were infiltrated with *Pseudomonas* strains at an OD_{600} of 0.2 in 10 mM $MgCl_2$ and collected after about 20 h. To visualize callose deposition, leaves were stained with aniline blue (58). The tissue was cleared and dehydrated with 96% ethanol overnight at 37 °C. Cleared leaves were washed with distilled water and then stained in 0.01% aniline blue in 150 mM K_2HPO_4 (pH 9.5) for 4 h at room temperature. Stained samples were washed and mounted in distilled water and examined by epifluorescence (LEICA M205 FA) with 100× magnification. Images were taken at the region below the infiltrated zone of each leaf. Counting of accumulated callose foci was carried out using ImageJ (NIH). For each treatment, 10–20 leaves were processed.

Phylogenetic Analysis. The phylogenetic history of *P. syringae* was inferred from Yang et al. (37). Protein sequences of toxin biosynthetic genes listed in Dataset S1 were used as basic local alignment search tool (BLAST) queries to search for homologous protein sequences in the 292 *P. syringae* genomes [available as of January 2017, Pathosystems Resource Integration Center (PATRIC)]. A hit with over 80% protein sequence identity was considered positive. The tree was visualized using interactive tree of life (iTOL) (59).

ROS Burst Measurement. Leaf disks from 4-wk-old *A. thaliana* Col-0, or *N. benthamiana* were placed into a 96-well plate with 100 μl of water in each well. Twelve leaf disks were used per treatment. After overnight incubation for *Arabidopsis* leaf disks, or 20 h for *N. benthamiana* leaf disks, each sample was treated with 100 μl of reaction mix, including 17 mg/mL of luminol (Sigma), 10 mg/mL of horseradish peroxidase (Sigma), distilled water, flg22 at

concentrations ranging from 5 to 100 nM, L-arginine, and polyamines at concentrations typically ranging from 200 to 800 μM. Phevamines and prephevamine were used at the same concentration as L-arginine (Sigma) or spermidine. Luminescence was measured immediately with 0.5-s integration and 1-min interval over 45 min using a SpectraMax L (Molecular Devices). For each experiment, 8–12 leaf-disks per condition were monitored. The flg22 peptide (QRLSTGSRINSAKDDAAGLQIA) was synthesized by Genscript (41).

ACKNOWLEDGMENTS. We thank Dr. Albert Bowers for helpful discussions of the manuscript, Dr. Gary Pielak for the naming of the phevamines, Dr. Jillian Tyrrell for cloning the *hsv* operon into the pLIC-His vector, Dr. Jake Malone for sharing the pBBR5 plasmid, Dr. Jim Jorgenson and Katherine Simpson for helpful discussion of isolation of phevamines, and Kevin Santa Maria for assistance with MultiGeneBlast. This work is supported by the Rita Allen Foundation and the David and Lucile Packard Foundation (B.L.), National Institutes of Health (R00 GM099904 to B.L., 5T32 GM008500 to J.A.B., and R01 GM112739-01 to F.C.S.), the National Science Foundation (IOS-1257373 to J.L.D.), and the Howard Hughes Medical Institute. J.L.D. is an Investigator of the Howard Hughes Medical Institute, and F.C.S. is a Faculty Scholar of the Howard Hughes Medical Institute.

1. Bender CL, Alarcón-Chaidez F, Gross DC (1999) *Pseudomonas syringae* phytotoxins: Mode of action, regulation, and biosynthesis by peptide and polyketide synthetases. *Microbiol Mol Biol Rev* 63:266–292.
2. Katagiri F, Thilmony R, He SY (2002) The *Arabidopsis thaliana-Pseudomonas syringae* interaction. *Arabidopsis Book* 1:e0039.
3. Geng X, Jin L, Shimada M, Kim MG, Mackey D (2014) The phytotoxin coronatine is a multifunctional component of the virulence armament of *Pseudomonas syringae*. *Planta* 240:1149–1165.
4. Ferguson A, Johnston J (1980) Phaseolotoxin: Chlorosis, ornithine accumulation and inhibition of ornithine carbamoyltransferase in different plants. *Physiol Plant Pathol* 16:269–275.
5. Bachmann A, Matile P, Slusarenko A (1998) Inhibition of ornithine decarboxylase activity by phaseolotoxin: Implications for symptom production in halo blight of French bean. *Physiol Mol Plant Pathol* 53:287–299.
6. Gulick AM (2017) Nonribosomal peptide synthetase biosynthetic clusters of ESKAPE pathogens. *Nat Prod Rep* 34:981–1009.
7. Gross H, Loper JE (2009) Genomics of secondary metabolite production by *Pseudomonas spp*. *Nat Prod Rep* 26:1408–1446.
8. Gimenez-Ibanez S, Chini A, Solano R (2016) How microbes twist jasmonate signaling around their little fingers. *Plants (Basel)* 5:9.
9. Toruño TY, Stergiopoulos I, Coaker G (2016) Plant-pathogen effectors: Cellular probes interfering with plant defenses in spatial and temporal manners. *Annu Rev Phytopathol* 54:419–441.
10. Yu X, Feng B, He P, Shan L (2017) From chaos to harmony: Responses and signaling upon microbial pattern recognition. *Annu Rev Phytopathol* 55:109–137.
11. Fouts DE, et al. (2002) Genomewide identification of *Pseudomonas syringae* pv. *tomato* DC3000 promoters controlled by the HrpL alternative sigma factor. *Proc Natl Acad Sci USA* 99:2275–2280.
12. Mucyn TS, et al. (2014) Variable suites of non-effector genes are co-regulated in the type III secretion virulence regulon across the *Pseudomonas syringae* phylogeny. *PLoS Pathog* 10:e1003807.
13. Weingart H, Stubner S, Schenk A, Ullrich MS (2004) Impact of temperature on in planta expression of genes involved in synthesis of the *Pseudomonas syringae* phytotoxin coronatine. *Mol Plant Microbe Interact* 17:1095–1102.
14. Lan L, Deng X, Zhou J, Tang X (2006) Genome-wide gene expression analysis of *Pseudomonas syringae* pv. *tomato* DC3000 reveals overlapping and distinct pathways regulated by *hrpL* and *hrpRS*. *Mol Plant Microbe Interact* 19:976–987.
15. Oh CS, Beer SV (2005) Molecular genetics of *Erwinia amylovora* involved in the development of fire blight. *FEMS Microbiol Lett* 253:185–192.
16. Oh CS, Kim JF, Beer SV (2005) The Hrp pathogenicity island of *Erwinia amylovora* and identification of three novel genes required for systemic infection. *Mol Plant Pathol* 6: 125–138.
17. Kvitko BH, et al. (2009) Deletions in the repertoire of *Pseudomonas syringae* pv. *tomato* DC3000 type III secretion effector genes reveal functional overlap among effectors. *PLoS Pathog* 5:e1000388.
18. Gómez-Gómez L, Felix G, Boller T (1999) A single locus determines sensitivity to bacterial flagellin in *Arabidopsis thaliana*. *Plant J* 18:277–284.
19. Bowles DJ (1990) Defense-related proteins in higher plants. *Annu Rev Biochem* 59: 873–907.
20. Hauck P, Thilmony R, He SY (2003) A *Pseudomonas syringae* type III effector suppresses cell wall-based extracellular defense in susceptible *Arabidopsis* plants. *Proc Natl Acad Sci USA* 100:8577–8582.
21. DebRoy S, Thilmony R, Kwack YB, Nomura K, He SY (2004) A family of conserved bacterial effectors inhibits salicylic acid-mediated basal immunity and promotes disease necrosis in plants. *Proc Natl Acad Sci USA* 101:9927–9932.
22. de Torres M, et al. (2006) *Pseudomonas syringae* effector AvrPtoB suppresses basal defence in *Arabidopsis*. *Plant J* 47:368–382.
23. Nomura K, et al. (2006) A bacterial virulence protein suppresses host innate immunity to cause plant disease. *Science* 313:220–223.
24. Underwood W, Zhang S, He SY (2007) The *Pseudomonas syringae* type III effector tyrosine phosphatase HopAO1 suppresses innate immunity in *Arabidopsis thaliana*. *Plant J* 52:658–672.
25. Cunnac S, et al. (2011) Genetic disassembly and combinatorial reassembly identify a minimal functional repertoire of type III effectors in *Pseudomonas syringae*. *Proc Natl Acad Sci USA* 108:2975–2980.
26. Silby MW, et al. (2009) Genomic and genetic analyses of diversity and plant interactions of *Pseudomonas fluorescens*. *Genome Biol* 10:R51.
27. Thomas WJ, Thireault CA, Kimbrel JA, Chang JH (2009) Recombineering and stable integration of the *Pseudomonas syringae* pv. *syringae* 61 *hrp/hrc* cluster into the genome of the soil bacterium *Pseudomonas fluorescens Pf*0-1. *Plant J* 60:919–928.
28. Oh H-S, Park DH, Collmer A (2010) Components of the *Pseudomonas syringae* type III secretion system can suppress and may elicit plant innate immunity. *Mol Plant Microbe Interact* 23:727–739.
29. He SY, Huang H-C, Collmer A (1993) *Pseudomonas syringae* pv. *syringae* harpin$_{Pss}$: A protein that is secreted via the Hrp pathway and elicits the hypersensitive response in plants. *Cell* 73:1255–1266.
30. Charkowski AO, et al. (1998) The *Pseudomonas syringae* pv. *tomato* HrpW protein has domains similar to harpins and pectate lyases and can elicit the plant hypersensitive response and bind to pectate. *J Bacteriol* 180:5211–5217.
31. Fawaz MV, Topper ME, Firestine SM (2011) The ATP-grasp enzymes. *Bioorg Chem* 39: 185–191.
32. Michael AJ, Furze JM, Rhodes MJ, Burtin D (1996) Molecular cloning and functional identification of a plant ornithine decarboxylase cDNA. *Biochem J* 314:241–248.
33. Hamana K, Sakamoto A, Tachiyanagi S, Terauchi E (2003) Polyamine profiles of some members of the gamma subclass of the class Proteobacteria: Polyamine analysis of twelve recently described genera. *Microbiol Cult Collect* 19:3–11.
34. Medema MH, Takano E, Breitling R (2013) Detecting sequence homology at the gene cluster level with MultiGeneBlast. *Mol Biol Evol* 30:1218–1223.
35. Baltrus DA, et al. (2011) Dynamic evolution of pathogenicity revealed by sequencing and comparative genomics of 19 *Pseudomonas syringae* isolates. *PLoS Pathog* 7: e1002132.
36. McCann HC, et al. (2013) Genomic analysis of the Kiwifruit pathogen *Pseudomonas syringae* pv. *actinidiae* provides insight into the origins of an emergent plant disease. *PLoS Pathog* 9:e1003503, and erratum (2013) 9:10.1371/annotation/af157ddc-200a-4105-b243-3f01251cc677.
37. Yang L, et al. (2017) *Pseudomonas syringae* type III effector HopBB1 promotes host transcriptional repressor degradation to regulate phytohormone responses and virulence. *Cell Host Microbe* 21:156–168.
38. Mitchell RE (1976) Isolation and structure of a chlorosis-inducing toxin of *Pseudomonas phaseolicola*. *Phytochemistry* 15:1941–1947.
39. Hussain SS, Ali M, Ahmad M, Siddique KH (2011) Polyamines: Natural and engineered abiotic and biotic stress tolerance in plants. *Biotechnol Adv* 29:300–311.
40. Jiménez-Bremont JF, et al. (2014) Physiological and molecular implications of plant polyamine metabolism during biotic interactions. *Front Plant Sci* 5:95.
41. Zipfel C, et al. (2004) Bacterial disease resistance in *Arabidopsis* through flagellin perception. *Nature* 428:764–767.
42. Chinchilla D, Bauer Z, Regenass M, Boller T, Felix G (2006) The *Arabidopsis* receptor kinase FLS2 binds flg22 and determines the specificity of flagellin perception. *Plant Cell* 18:465–476.
43. Kunze G, et al. (2004) The *N* terminus of bacterial elongation factor Tu elicits innate immunity in *Arabidopsis* plants. *Plant Cell* 16:3496–3507.
44. Yoda H, et al. (2009) Polyamines as a common source of hydrogen peroxide in host- and nonhost hypersensitive response during pathogen infection. *Plant Mol Biol* 70:103–112.
45. Ward JL, et al. (2010) The metabolic transition during disease following infection of *Arabidopsis thaliana* by *Pseudomonas syringae* pv. *tomato*. *Plant J* 63:443–457.
46. Lou Y-R, Bor M, Yan J, Preuss AS, Jander G (2016) *Arabidopsis* NATA1 acetylates putrescine and decreases defense-related hydrogen peroxide accumulation. *Plant Physiol* 171:1443–1455.
47. Gonzalez ME, et al. (2011) Perturbation of spermine synthase gene expression and transcript profiling provide new insights on the role of the tetraamine spermine in *Arabidopsis* defense against *Pseudomonas viridiflava*. *Plant Physiol* 156:2266–2277.
48. Knight H, Trewavas AJ, Knight MR (1996) Cold calcium signaling in *Arabidopsis* involves two cellular pools and a change in calcium signature after acclimation. *Plant Cell* 8:489–503.
49. Nelson JK, Frølund SU, Tikhonov DB, Kristensen AS, Strømgaard K (2009) Synthesis and biological activity of argiotoxin 636 and analogues: Selective antagonists for ionotropic glutamate receptors. *Angew Chem Int Ed Engl* 48:3087–3091.
50. Kromann H, et al. (2002) Solid-phase synthesis of polyamine toxin analogues: Potent and selective antagonists of Ca^{2+}-permeable AMPA receptors. *J Med Chem* 45: 5745–5754.
51. Ogasawara Y, Dairi T (2017) Biosynthesis of oligopeptides using ATP-grasp enzymes. *Chemistry* 23:10714–10724.
52. Hollenhorst MA, Clardy J, Walsh CT (2009) The ATP-dependent amide ligases DdaG and DdaF assemble the fumaramoyl-dipeptide scaffold of the dapdiamide antibiotics. *Biochemistry* 48:10467–10472.
53. Arai T, Kino K (2008) A novel L-amino acid ligase is encoded by a gene in the phaseolotoxin biosynthetic gene cluster from *Pseudomonas syringae* pv. *phaseolicola* 1448A. *Biosci Biotechnol Biochem* 72:3048–3050.
54. Carrión VJ, Arrebola E, Cazorla FM, Murillo J, de Vicente A (2012) The *mbo* operon is specific and essential for biosynthesis of mangotoxin in *Pseudomonas syringae*. *PLoS One* 7:e36709.

55. Blasiak LC, Clardy J (2010) Discovery of 3-formyl-tyrosine metabolites from *Pseudoalteromonas tunicata* through heterologous expression. *J Am Chem Soc* 132:926–927.
56. Ogasawara Y, et al. (2016) Exploring peptide ligase orthologs in *Actinobacteria*: Discovery of pseudopeptide natural products, ketomemicins. *ACS Chem Biol* 11: 1686–1692.
57. Tornero P, Dangl JL (2001) A high-throughput method for quantifying growth of phytopathogenic bacteria in *Arabidopsis thaliana*. *Plant J* 28:475–481.
58. Kim MG, et al. (2005) Two *Pseudomonas syringae* type III effectors inhibit RIN4-regulated basal defense in *Arabidopsis*. *Cell* 121:749–759.
59. Letunic I, Bork P (2016) Interactive tree of life (iTOL) v3: An online tool for the display and annotation of phylogenetic and other trees. *Nucleic Acids Res* 44:W242–W245.
60. Carrión VJ, et al. (2013) The *mangotoxin biosynthetic operon* (*mbo*) is specifically distributed within *Pseudomonas syringae* genomospecies 1 and was acquired only once during evolution. *Appl Environ Microbiol* 79:756–767.

Phevamine A, a bacterial small molecule that suppresses plant immune response

Supporting Information Appendix

Erinn M. O'Neill, Tatiana S. Mucyn, Jon B. Patteson, Omri M. Finkel, Eui-Hwan Chung, Joshua A. Baccile, Elisabetta Massolo, Frank C. Schroeder, Jeffery L. Dangl, and Bo Li

Materials and Methods

General

All chemicals were purchased from Sigma-Aldrich or Fisher. Primers were ordered from Integrated DNA Technology (Table S3). Polymerase, restriction enzymes, and ligase were purchased from New England Biolabs. DNA manipulation kits were purchased from Qiagen and Thermo Scientific. PCR reactions were carried out using an Eppendorf Nexus GSX1 thermocycler with Q5 DNA polymerase. General genetic manipulation of *E. coli* was carried out using standard protocols (1). LC-MS data was obtained using an Agilent 6520 accurate-mass Q-TOF LC/MS. Preparative HPLC was carried out using a Phenomenex Luna 10 µm C18 (2) column on a Varian Prostar instrument equipped with a PDA detector. Further purification was carried out using a Phenomenex Kinetex 5 µm C18 column (100 Å, 150 mm x 4.60 mm) on a Shimadzu HPLC equipped with an SPD-20A UV-vis detector. NMR spectra were obtained using a Bruker 600 MHz spectrometer or a Bruker Avance^{III} HD 800 MHz spectrometer unless otherwise noted.

Bacterial strains and culture conditions

For cloning, *E. coli* DH5α and *E. coli* Top10 chemically competent maximum efficiency cells were used (Invitrogen). For heterologous expression, *E. coli* BL21(DE3) chemically competent cells (Agilent) were transformed with vectors containing *hsv* expression constructs (Table S4). The *hrpL* expression construct in pBAD vector was previously described (2). All overnight seed cultures were inoculated with a single colony and grown in 5 mL media in 14 mL Falcon culture tubes. Antibiotics were used in these concentrations, unless otherwise noted: 10 µg/mL tetracycline, 25 µg/mL chloramphenicol, 50 µg/mL kanamycin, 50 µg/mL spectinomycin, or 100 µg/mL ampicillin. All cultures for metabolomics were grown in 100 mL media with the appropriate antibiotic and 100 µL−2 mL of a saturated overnight culture. All *E. coli* cultures were grown in LB Media (Miller, granulated, Fisher) at 37 °C to an OD_{600} between 0.4 and 0.8. *E. coli* cultures were induced with 0.5 mM IPTG and then were incubated at 16 °C overnight, shaking at 225 rpm. *P. syringae* and *P. fluorescens* starter cultures were grown overnight in King's B Media (20 g/L Bacto Proteose Peptone #3, 1% glycerol by volume, 1.5 g/L K_2HPO_4, and 0.734 g/L $MgSO_4$, dissolved in water). *P.*

syringae cultures containing the pBAD plasmid were induced with 0.2% L-arabinose. All other *P. syringae* pv. *tomato* DC3000 and *P. fluorescens* cultures were not induced. Wildtype *P. fluorescens Pf*0-1 harboring the *hsv*-pBBR5 vector was grown in the presence of 50 µg/mL ampicillin and 50 µg/mL gentamycin. *P. fluorescens* harboring both *hsv*-pBBR5 and the T3SS (*Pf*0-1 +T3SS) was grown with 25 µg/mL tetracycline and 50 µg/mL gentamycin. After reaching an OD_{600} of >0.6 in King's B media, *P. fluorescens* and *P. syringae* cultures were washed with 100 mM $MgCl_2$ and resuspended in minimal media (12.8 g/L Na_2HPO_4 ● 7 H_2O, 3 g/L KH_2PO_4, 0.5 g/L NaCl, 1 g/L NH_4Cl, 1% glycerol by volume, 0.024 g/L $MgSO_4$, 0.0011 g/L $CaCl_2$, and 0.18 g/L mannitol, dissolved in water). Once resuspended in minimal media, these cultures were grown at 28 °C overnight and 16 °C for another 24 hours shaking at 225 rpm.

Protein expression and purification

Large-scale cultures for protein purification were grown in 1 L of media containing the appropriate antibiotic and 1−5 mL of overnight culture. At an OD600 of 0.5−0.8, a sample of 0.5 mM IPTG was added to induce protein expression. After 16 hours of protein expression, cultures were spun down and resuspended in HEPES lysis buffer (50 mM HEPES, 150 mM NaCl, 10% glycerol, pH 7.5). Cells were lysed by sonication at 30% amplitude for 3 minutes (0.5 seconds on and 1.5 seconds off). Cell debris was removed by centrifugation at 17,000 rpm for 40 minutes and the supernatant was filtered using a 0.45 µm filter (Corning). Each Hsv protein was purified using an AKTA FPLC using a 5 mL HiTrap nickel column (GE) at a flow rate of 3.0 mL/min. Wash buffer consisted of 50 mM HEPES, 150 mM NaCl, 25 mM imidazole, and 10% glycerol (pH 7.5). Elution buffer was the wash buffer with the addition of 250 mM imidazole. The wash step lasted for 5 column volumes (CVs). The proteins were eluted using a gradient of 0−100% of elution buffer over 10 CVs, and then held at 100% for 5 CVs. HsvB and HsvC were further purified using a HiLoad 16/600 Superdex 200 prep grade size exclusion column (GE) on the FPLC using the lysis buffer described above. The column was equilibrated with lysis buffer at a flow rate of 0.5 mL/min for 1.5 CVs, then

protein was loaded onto the column and eluted over 1.5 CVs using the same buffer and flow rate.

Amidinotransferase substrate assay conditions

To identify the preferred substrates of the amidinotransferase protein HsvA, L-arginine was incubated with potential substrates that accept the amidino group. Each reaction mixture contained two amino acids at 10 mM each (L-Arg and L-Lys, L-Arg and spermidine, or L-Arg and spermine). Each mixture also contained 100 mM HEPES (pH 7.5) and 20 µM purified HsvA to a final volume of 50 µL. Samples were incubated at 37 °C for 2 hours. Enzymes were omitted in negative controls. A sample of 10 µL was injected onto a Gemini C18 column (Phenomenex) on LC-MS and separated with a gradient of 2−73% acetonitrile (0.1% formic acid) over 25 minutes. This assay showed that HsvA catalyzes the transfer of the amidino group from L-Arg to spermidine, spermine, or L-lysine. Based on peak areas, the amidinospermidine product is present at the highest level, suggesting spermidine is the preferred substrate.

ATP-grasp substrate assay conditions

A malachite green dye assay (P_iColorLock, Innova Biosciences) was used to identify the preferred substrates of the ATP-grasp enzyme HsvB by quantifying free phosphate (P_i) release. Substrate assays were conducted in 100 µL scale in a microcentrifuge tube, and consisted of 2.0 mM amino acids, 10 µM of each enzyme, 10 mM $MgCl_2$, 5 mM ATP, and 50 mM HEPES (pH 7.5). After 30 minutes, reactions were diluted 1 in 10 with DI water into a 96-well plate to a final volume of 200 µL, then 50 µL Gold mix reagent and 20 µL stabilizer were added. After 30 minutes of incubation, UV-vis absorption of the products at 635 nm was measured on a Tecan infinite M1000 Pro plate reader. Assays containing L-Phe produced the most P_i, indicating that HsvB preferentially activates L-Phe.

Characterization of phevamine biosynthetic pathway

Sequential assays were conducted to elucidate the biosynthesis of phevamine A. Based on the structures of prephevamine, amidinotransfer by HsvA or condensation with L-Val

by HsvC may occur as the first step. This rationale led us to examine three potential biosynthetic pathways: HsvA → C → B, HsvC → A → B, and HsvC → B → A. An initial assay was conducted for either HsvA or HsvC. The HsvA assay consisted of 10 mM L-arginine, 10 mM spermidine, 100 mM HEPES (pH 7.5), 20 µM HsvA, and water in a 100 µL volume. Protein was removed after a 30 minute incubation at room temperature using a 3000 Da Amicon Ultra filter (Millipore) and the small molecule filtrate was collected. To this assay mixture, we added 2 mM $MgCl_2$, 1 mM ATP, 2 mM L-valine, and 10 µM HsvC. Protein was again removed after 30 minutes at room temperature with a 3000 Da filter and an aliquot was collected for LC-MS analysis. Finally, 2 mM L-phenylalanine and 10 µM HsvB were added, and the reaction was incubated at room temperature for 30 minutes before the reaction was quenched with acetonitrile at a ratio of 1:1 for 15 minutes, precipitated protein was removed by centrifugation, and the supernatant was analyzed by LC-MS. The initial HsvC assays consisted of 2 mM spermidine, 2 mM L-valine, 100 mM HEPES (pH 7.5), 2 mM $MgCl_2$, 1 mM ATP, 10 µM HsvC, and water in a 100 µL volume. After 30 minutes at room temperature, HsvC was removed with a 3000 Da filter. To one set of assays, 10 mM L-arginine and 20 µM HsvA were added. To the other set of assays, 2 mM L-phenylalanine and 10 µM HsvB were added. Both sets of reactions were incubated at room temperature for 30 minutes before removing protein with a 3000 Da filter. Aliquots were taken for LC-MS analysis. These reactions were then incubated with the remaining constituents that had not been added: 2 mM L-phenylalanine and 10 µM HsvB or 10 mM L-arginine and 20 µM HsvA. Reactions were incubated at room temperature for 30 minutes before they were quenched with acetonitrile at a ratio of 1:1 and the precipitated protein was removed by centrifugation. All aliquots were diluted 5 folds with water for LC-MS analysis. Phevamines were only produced when the reaction order was HsvA → HsvC → HsvB (Figure S10).

Purification of phevamine A

Assay supernatants were concentrated under reduced pressure and injected onto the prep HPLC at a flow rate of 15 mL/min with water and acetonitrile (both containing 0.1% trifluoroacetic acid) as mobile phases. The solvent gradient was held at 2% acetonitrile

for 10 minutes, then 5% acetonitrile for 5 minutes, and 10% acetonitrile for 15 minutes, before being ramped up to 95% over another 20 minutes. Fractions containing phevamine A (28–30 min retention time) were concentrated under reduced pressure and injected onto the analytical HPLC using the same mobile phases as those for the prep HPLC. The solvent gradient ramped from 2−30% acetonitrile over 35 minutes before ramping up to 95% for another 8 minutes (flow rate: 0.5 mL/min). Fractions containing phevamine A were collected at retention times of 20−25 minutes, and concentrated. To separate the two regio-isomers, a final round of purification was conducted on the analytical HPLC with an extended gradient at 10−20% acetonitrile for 25 min. Specifically, the solvent gradient started at 2−5% acetonitrile over 5 minutes, then 5−10% over another 5 minutes, and finished with 10−20% for another 25 minutes (flow rate: 0.5 mL/min). Fractions with retention times between 17.5–19.5 minutes were collected and concentrated. LC/MS analysis showed that the concentrated sample contained ~95% pure phevamine A (67% yield).

NMR spectroscopy for phevamine A and B

All spectra for *in vitro* purified phevamine A and B were obtained using a Bruker Avance^{III} HD (800 MHz ^{1}H reference frequency, 201 MHz for ^{13}C) equipped with a 5 mm CPTCL ^{1}H-^{13}C/^{15}N cryo probe. Non-gradient phase-cycled dqfCOSY spectra were acquired using the following parameters: 0.6 s acquisition time, 400−600 complex increments, 8, 16 or 32 scans per increment. Non-gradient HSQC and HMBC spectra were acquired with these parameters: 0.25 s acquisition time, 200−500 complex increments, 8−64 scans per increment. ^{1}H, ^{13}C-HMBC spectra were optimized for $J_{H,C}$ = 6 Hz. HSQC spectra were acquired without decoupling. NMR spectra were processed and baseline corrected using Mestrelabs MNOVA software packages. NMR assignments are shown in Tables S5 and S6.

Metabolite dependence on T3SS

The *hsv* operon was cloned into the pBBR5 plasmid containing a constitutive promoter and gentamycin resistance marker (3). *P. fluorescens Pf*0-1 and *Pf*0-1 + T3SS were both transformed with *hsv*-pBBR5 by electroporation using the method described by

Choi and Schweizer (4). Cultures (100 mL) were grown and extracted as described above to detect phevamine production and determine whether phevamine secretion is dependent on T3SS (Fig. S7).

Generation of Pseudomonas clean deletion mutants

Pseudomonas knockout clones were generated using MTN1907, a modified version of pLVC-D, which allows for *SacB* counter-selection (2, 5, 6). Overlapping primers MT1881, MT1880, MT1877, and MT1878 (Table S3) were used to generate a chimeric fragment composed of the ~200 bp sequence upstream of *hsvA* fused to the ~200bp region downstream of *hsvC*. The chimeric fragment was sub-cloned into MTN1907 and *Pseudomonas* was transformed with the plasmid to obtain a merodiploid after recombination. Two merodiploids, with a 3' end and a 5' end insertion, were selected to generate two independent *Pseudomonas* clones with clean *hsv* deletion for each parental strain (*Pto* DC3000, *Pto*-Cor $^{-}$, *Pto*Δ*hrcC*, *Pto*D28E) after growth on media containing 5% sucrose for the second recombination (see Fig. S29 and S30). For complementation, the *hsv* operon was sub-cloned into pBAV226 downstream of the *NptII* promoter (8) and transformed into *Pto*D28EΔ*hsv2* (see Fig. S30). The pBAV226 vector contains the sequence encoding the HA-tag downstream of the gateway cassette, but the HA tag was not included in the product of *hsvC* because the stop codon was retained.

Calcium burst measurement

Leaf disks of 3- to 4-week-old *A. thaliana* lines pMAQ2 expressing the apoaequorin gene under the control of the cauliflower mosaic virus 35S promoter (7) were collected in a 96-well plate and incubated overnight with 100 µM coelenterazine native (BYOSYNTH) (7). Luminescence was measured as in the ROS burst assay, with the exception that luminol and HRP were excluded from the reaction mix.

Synthesis of phevamine A

General information

Chemicals were purchased from commercial suppliers and used without further purification. Fmoc-derivatized amino acids were purchased from Alfa Aesar. N^1, N^4-bis-boc-spermidine was purchased from Chem-Impex International. Diethylamine and DIPEA were purchased from Sigma-Aldrich. *N,N′*-Di-Boc-1H-pyrazole-1-carboxamidine and trifluoroacetic acid were purchased from Acros Organics. HATU was purchased from Oakwood Products Inc. NMR solvents were purchased from Cambridge Isotope Laboratories. Normal-phase column chromatography was performed on silica gel (230−400 mesh). Reversed-phase chromatography was performed on C18-bonded silica, either on Phenomenex Kinetex C18 or Phenomenex Luna C18. High-resolution mass spectra (HRMS) were obtained using an Agilent 6520 Q-TOF LC/MS. Proton, carbon and fluorine magnetic resonance spectra (^{1}H NMR, ^{13}C NMR, and ^{19}F NMR) were recorded on a Bruker model DRX 400 or 600 (^{1}H NMR at 400 MHz or 600 MHz, ^{13}C NMR at 101 MHz or 151 MHz) or on a Bruker AVANCE III-OneBay500 (^{13}C NMR at 235 MHz) spectrometer. NMR experiments are reported in δ units, parts per million (ppm), and were referenced to $CDCl_3$ (δ 7.26 ppm for ^{1}H and 77.0 ppm for ^{13}C), DMSO (2.50 ppm), MeOD (3.31 ppm) or D_2O (4.79 ppm) as internal standards. ^{1}H NMR data are reported as follows: chemical shift, multiplicity (s = singlet, bs = broad singlet, d = doublet, dd = doublet of doublets, t = triplet, td = triplet of doublets, m = multiplet), coupling constants (Hz), and integration.

_N_-Boc-1,3-diaminopropane (1)

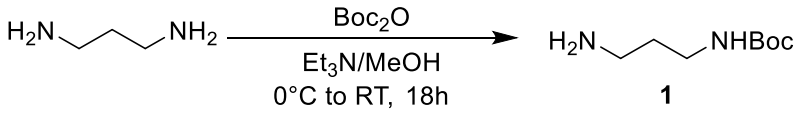

1

This synthesis followed a similar procedure as Kaur *et al.* (8). 1,3-Diaminopropane (3 g, 40.5 mmol, 1 eq.) was dissolved in a 10% solution of Et_3N in MeOH (30 mL); the mixture was cooled to 0 °C. In a flame dried flask, di-*tert*-butyl dicarbonate (4.4 g, 20 mmol, 0.5 eq.) was dissolved in MeOH and added to the cooled solution (via addition funnel). The reaction mixture, which did not appear homogeneous, was stirred overnight at room temperature (RT). The solvent was then removed under reduced pressure. The

crude mixture was treated with 10% Na_2CO_3 (10 mL, three times) and extracted with CH_2Cl_2. The combined organic phases were dried over anhydrous Na_2SO_4 and the solvent was removed under reduced pressure. The desired product (**1**) was obtained as a white solid (1.65 g, 23% yield) and used in the subsequent step without further purification.

^{1}H NMR (400 MHz, $CDCl_3$) δ 1.20 (bs, 1H), 1.44 (s, 9H), 1.64-1.57 (m, 2H), 2.76 (t, J = 6.6 Hz, 2H), 3.22-3.16 (m, 2H), 4.90 (bs, 1H).

N-(4-(3-Boc-1,3-diaminopropane)butyl)phthalimide (2)

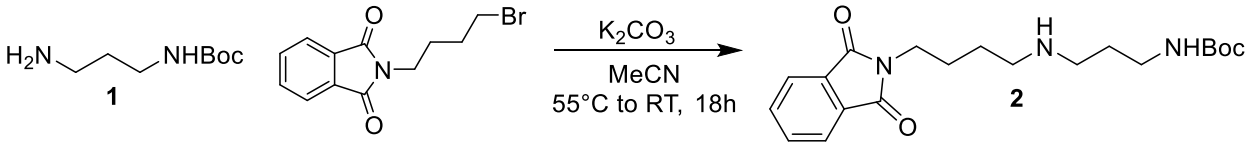

This reaction followed a procedure similar to that used by Wang *et al.* (2012) (9). *N*-Boc-1,3-diaminopropane (1.38 g, 7.9 mmol, 1.1 eq.) was dissolved in MeCN (15 mL) at RT and K_2CO_3 (3.43 g, 24.8 mmol, 5 eq.) was added. *N*-(4-Bromobutyl)phthalimide (2.2 g, 7.7 mmol, 1 eq.) was then added and the reaction mixture was heated to 50 °C and stirred at this temperature for 18 hours. Subsequently, the mixture was warmed up to RT and treated with H_2O. The mixture was extracted with EtOAc; the combined organic phases were dried over anhydrous Na_2SO_4 and the solvent was removed under reduced pressure. The desired product (**2**) was obtained (3 g, quantitative yield) and used in the subsequent step without further purification.

^{1}H NMR (400 MHz, $CDCl_3$) δ 1.90−1.82 (m, 2H), 1.40 (bs, 9H), 1.65-1.56 (m, 2H), 1.75−1.69 (m, 2H), 2.39−2.36 (m, 2H), 3.20-3.13 (m, 4H), 3.71−3.64 (m, 2H), 4.96 (bs, 1H), 7.75−7.72 (m, 2H), 7.82−7.79 (m, 2H),

N-(4-(*N*^{1},*N*^{3}-bis-Boc-1,3-diaminopropane)butyl)phthalimide (3)

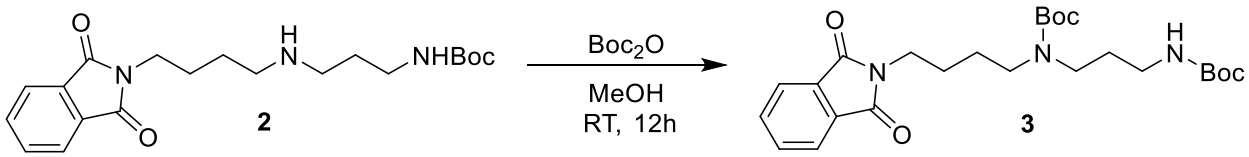

This reaction followed a similar procedure to that was used by Wang *et al.* (2014) (10). The substrate was dissolved in methanol (40 mL) and di-*tert*-butyl dicarbonate (1.7 g,

7.8 mmol, 1 eq.) was added. The reaction mixture was stirred at RT for 12 hours, then the solvent was removed under reduced pressure. The Boc-bisprotected product (**3**) was obtained as a pale, yellow oil (3.3 g, 87% yield) and used in the subsequent step without further purification.

^{1}H NMR (400 MHz, $CDCl_3$) δ 1.45−1.44 (m, 2H), 1.70−1.67 (m, 5H), 1.95−1.85 (m, 1H), 2.42 (bs, 2H), 3.27−3.10 (m, 4H), 3.76−3.70 (m, 2H), 7.75−7.72 (m, 2H), 7.88−7.84 (m, 2H).

***N*^{1}, *N*^{4}-bis-Boc-spermidine (4)**

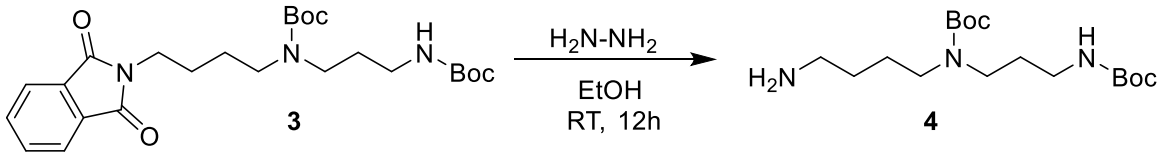

This reaction used a procedure similar to that was used by Wang *et al.* (2014) (10). To a solution of *tert*-butyl (3-((tert-butoxycarbonyl)amino)propyl)(4-(1,3-dioxoisoindolin-2-yl)butyl)carbamate (**3**) (780 mg, 1.64 mmol) in EtOH (30 mL), hydrazine hydrate (0.83 mL) was added and the reaction mixture was stirred for 12 hours at RT. The solvent was removed under reduced pressure and the residue was suspended in 10% ammonia and extracted with $CHCl_3$; the combined organic phases were dried on anhydrous Na_2SO_4 and the solvent was removed under reduced pressure. The desired product (**4**) was obtained as a pale, yellow oil (340 mg, 60% yield) and used in the subsequent step without further purification.

^{1}H NMR (400 MHz, $CDCl_3$) δ 1.48−1.46 (m. 18H), 1.66−1.57 (m, 7H), 2.43−2.40 (m, 1H), 2.49−2.46 (m, 1H), 2.74−2.71 (m, 1H), 3.26−3.12 (m, 4H), 3.69 (bs, 1H), 4.90 (bs, 1H), 5.78, 5.64 (bs 1H).

Fmoc-(*S*)-Val-bis-Boc-spermidine (5)

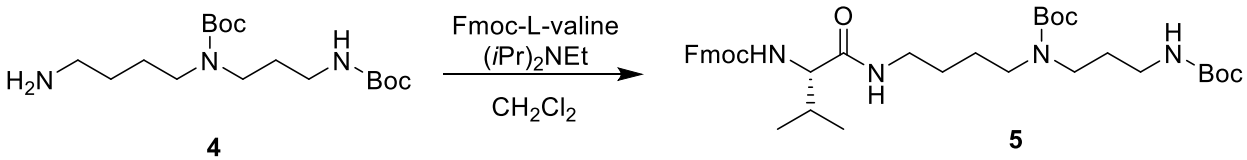

To a solution of N^1, N^4-bis-Boc-spermidine (**4**) (250 mg, 0.724 mmol, 1.0 eq.) in CH_2Cl_2 (20 mL) on ice, Fmoc-Val-OH (295 mg, 8.68 mmol, 1.2 eq.), and DIPEA (252.2 µL, 1.448 mmol, 2.0 eq.) were added. The reaction was stirred at room temperature for 16 hours. The crude reaction mixture was purified by flash chromatography (hexanes/ethyl acetate gradient) to afford pure product (**5**) (310 mg, 64% yield) as a white solid.

^{1}H NMR (400 MHz, $CDCl_3$) δ 0.97 (m, 6H), 1.46 (s, 9H), 1.47 (s, 9H), 1.52 (m, 2H), 1.66 (m, 2H), 2.15 (m, 2H), 3.07-3.35 (m, 9H), 4.23 (t, J = 7.0 Hz, 1H), 4.36 (m, 1H) 4.44 (m, 1H), 7.32 (t, J = 7.4 Hz, 2H), 7.42 (t, J = 7.6 Hz, 2H), 7.61 (d, J= 7.6 Hz, 2H), 7.78 (d, J = 7.2 Hz, 2H).

Fmoc-(*S*)-Phe-(*S*)-Val-bis-Boc-spermidine (6)

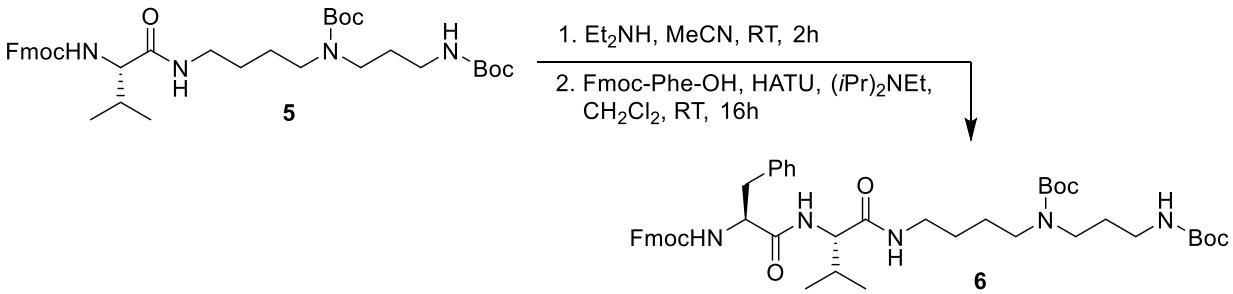

To a solution of Fmoc-(S)-Val-bis-Boc-spermidine (**5**) (310 mg, 0.465 mmol, 1.0 eq) in 20 mL MeCN, diethylamine (500 µL, 2.5% v/v) was added. The reaction was stirred at room temperature for 2 hours. The crude reaction mixture was concentrated under reduced pressure. Ethyl acetate (25 mL) was added, and the reaction mixture was concentrated again. The crude reaction mixture was dissolved in CH_2Cl_2 (20 mL) and added to a mixture of Fmoc-Phe-OH (216 mg, 0.558 mmol, 1.2 eq.), HATU (269 mg, 0.6975 mmol, 1.5 eq.), and DIPEA (162 µL, 0.742 mmol, 2.0 eq.) previously kept under stirring for 20 minutes on ice. The reaction was stirred at room temperature for 16 hours. The crude reaction mixture was purified by flash chromatography (hexanes/ethyl acetate gradient) to afford pure product (**6**) (190 mg, 50% yield) as a white solid.

^{1}H NMR (400 MHz, $CDCl_3$) δ 0.87 (d, J = 6.8 Hz, 3H), 0.92 (d, J = 6.8 Hz, 3H), 1.47 (s, 18H), 1.51 (m, 2H), 1.69 (m, 2H), 2.19 (m, 2H), 3.05−3.35 (m, 11H), 4.19 (t, 1H), 4.31 (m, 1H), 4.41 (m, 1H), 4.51 (m, 1H), 7.20 (m, 2H), 7.31 (m, 5H), 7.41 (t, J = 7.4 Hz, 2H), 7.54 (d, J = 7.6 Hz, 2H), 7.77 (d, J = 7.2 Hz, 2H).

Fmoc-(*S*)-Phe-(*S*)-Val-spermidine (7)

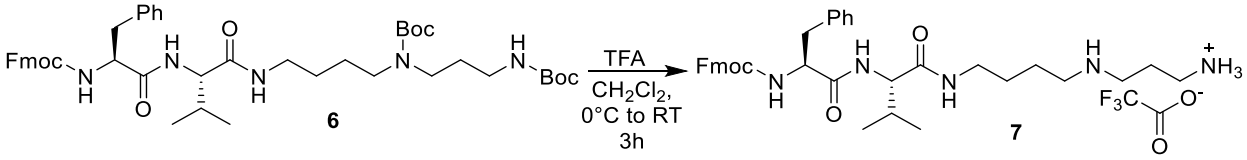

A solution of Fmoc-(*S*)-Phe-(*S*)-Val-bis-Boc-spermidine (**6**) (60 mg, 0.072 mmol) in CH_2Cl_2 (2 mL) was cooled to 0 °C and 800 µL of trifluoroacetic acid was added dropwise. The reaction was stirred at room temperature for 3 hours. The crude reaction mixture was concentrated under reduced pressure. Toluene was added, and the sample was concentrated under reduced pressure until dry. The pure product (**7**) (23 mg, 32% yield over two steps) was obtained as a white solid: ^{1}H NMR (400 MHz, MeOD) *δ* 0.96 (m, 6H), 1.59 (m, 2H), 1.70 (m, 2H), 2.07 (m, 3H), 3.00−3.27 (m, 10H), 4.08 (d, *J* = 7.2 Hz, 1H), 4.16 (t, *J* = 7.0 Hz, 1H), 4.26 (m, 1H), 4.34 (m, 1H), 4.42 (m, 1H), 7.16 (m, 1H), 7.21−7.32 (m, 5H), 7.40 (t, *J* = 7.6 Hz, 2H), 7.58 (d, *J* = 7.6 Hz, 2H), 7.81 (d, *J* = 7.6 Hz, 2H); HRMS (EI) *m/z* $[M + H]^+$ Calculated for $C_{36}H_{48}N_5O_4$ 614.370, observed 614.371.

Fmoc-(*S*)-Phe-(*S*)-Val-spermidine-*N,N'*-di-Boc-1*H*-guanidine (8)

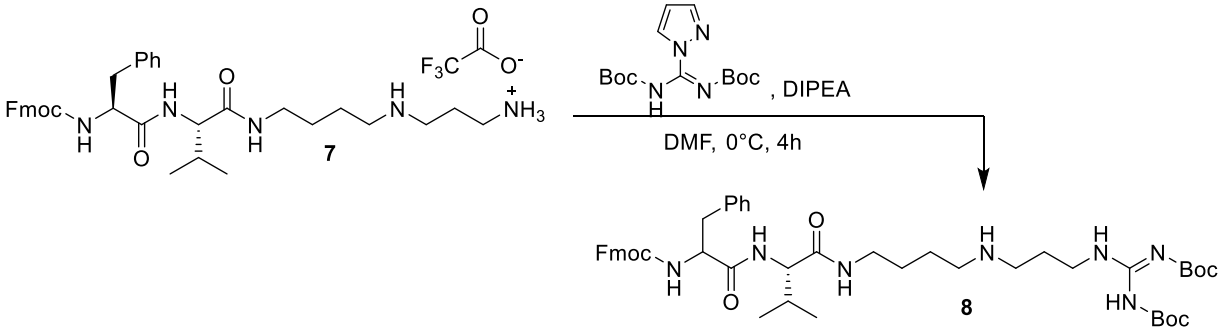

To a solution of Fmoc-(S)-Phe-(S)-Val-spermidine (**7**) in DMF (2 mL), which has been cooled to 0 °C, DIPEA (200 µL) and *N,N'*-Di-Boc-1H-pyrazole-1-carboxamidine (24 mg, 0.072 mmol, 1.0 eq.) were added. The reaction was stirred for 4 hours at room temperature. The crude reaction mixture was purified directly using reverse-phase prep HPLC (Phenomenex Luna C18, H_2O/MeCN gradient) and then purified using a second round of reverse-phase HPLC (Phenomenex Kinetex C18, H_2O/MeCN gradient). The product (**8**) was purified as a white solid (23 mg, 37% yield over 2 steps). ^{1}H NMR (600 MHz, MeOD) *δ* 0.96 (m, 6H), 1.49 (s, 9H), 1.55 (s, 9H), 1.60 (m, 2H), 1.72 (m, 2H), 1.95 (m, 2H), 2.07 (m, 1H), 3.02 (m, 4H), 3.14−3.23 (m, 2H), 3.24-3.35 (m, 2H) 3.47 (m, 2H),

4.08 (d, *J* = 7.2 Hz, 1H), 4.17 (t, *J* = 7.5 Hz, 1H), 4.26 (m, 1H), 4.35 (m, 1H), 4.42 (m, 2H), 7.23 (m, 2H), 7.30 (m, 5H), 7.40 (m, 2H), 7.58 (t, *J* = 6.9 Hz, 2H), 7.81 (d, *J* = 7.8 Hz, 2H); HRMS (EI) *m/z* $[M + H]^+$ Calculated for $C_{47}H_{66}N_7O_8$ 856.497, observed 856.499.

Phevamine A (9)

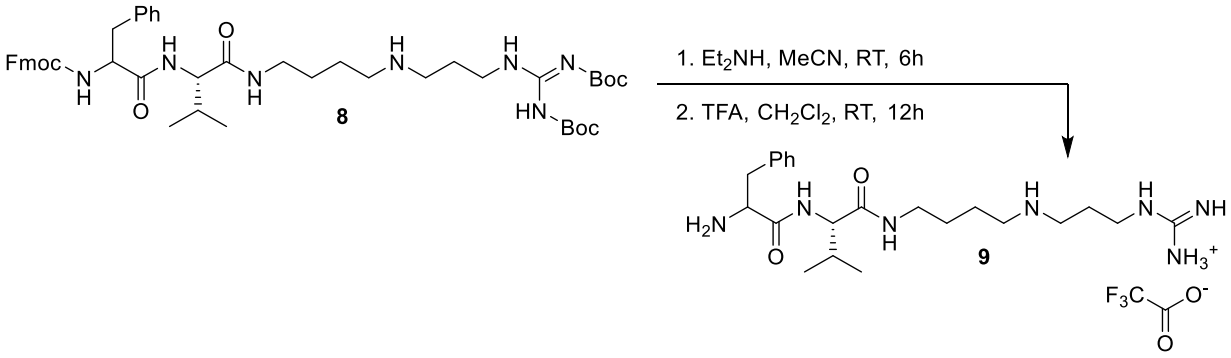

To a solution of Fmoc-(S)-Phe-(S)-Val-spermidine-*N,N'*-Di-Boc-1*H*-guanidine (**8**) (23 mg, 0.027 mmol) in 2.5 mL of MeCN, diethylamine (300µL) was added. The reaction was stirred for 6 hours at room temperature. The crude reaction mixture was concentrated under reduced pressure. Ethyl acetate was added, and the reaction mixture was concentrated again. The reaction mixture was dissolved in CH_2Cl_2 (3 mL) on ice and trifluoroacetic acid (350 µL) was added dropwise. The reaction was stirred at room temperature for 12 hours. The reaction mixture was concentrated under reduced pressure. Toluene was added and the reaction mixture was concentrated until dryness. The reaction mixture was purified by reverse-phase HPLC (Phenomenex Kinetex C18, H_2O/MeCN gradient). The final product phevamine A (**9**) was obtained as a white solid (9.8mg, 67% yield). ^{1}H NMR (400 MHz, D_2O) δ 0.79 (d, J = 6.8 Hz, 3H), 0.82 (d *J* = 6.8 Hz, 3H), 1.49 (m, 2H), 1.60 (m, 2H), 1.84 (m, 1H), 1.87 (m, 2H), 2.97−3.20 (m, 8H), 3.20 (t, *J* = 6.8 Hz, 2H), 3.87 (d, *J* = 8.4 Hz, 1H), 4.22 (t, *J* = 7.2 Hz, 1H), 7.15 (m, 2H), 7.29 (m, 3H); HRMS (EI) *m/z* $[M + H]^+$ Calculated for $C_{22}H_{40}N_7O_2$ 434.324, observed 434.323. ^{19}F NMR (400 MHz, D_2O) δ −75.67 (s).

Supplementary Tables

Name	Sequences (5' to 3')
hsv_pLIC-His_sense	**TACTTCCAATCCAATGCG**ATGTCATATCAAAAAGCAGAACCCGCTTAC
hsv_pLIC-His_anti	**TTATCCACTTCCAATGCGCTA**TCAACCACGCGCAGCTTCTGCATGC
hsv_pBBR5_sense	**GACAACAG<u>ACTAGT</u>**ATGTCATATCAAAAAGCAGAACCCG (SpeI site underlined)
hsv_pBBR5_anti	**GACAACAG<u>AAGCTT</u>** TCAACCACGCGCAGCTTC (HindIII site underlined)
hsvA_pRSF_BamHI_sense	**GACAACAG<u>GGATCC</u>**GATGTCATATCAAAAAGCAGAAC (BamHI site underlined)
hsvA_pRSF_HindIII_anti	**GACAACAG<u>AAGCTT</u>**TCAAATATAACGGTGCAGTCCT (HindIII site underlined)
hsvB_pACYC_SacI_sense	**GACAACAG<u>GAGCTC</u>**GATGCGCCCTACAAAAAAAATACTG (SacI site underlined)
hsvB_pACYC_HindIII_anti	**GACAACAG<u>AAGCTT</u>**TCACTCCTCAAACGGAGGG (HindIII site underlined)
hsvC_pCDF_BamHI_sense	**GACAACAG<u>GGATCC</u>**GATGGACAAAAATAAGCCAAACACTATTCTG A (BamHI site underlined)
hsvC_pCDF_HindIII_R	**GACAACAG<u>AAGCTT</u>**TCAACCACGCGCAGCTTCTG (HindIII site underlined)
MT1797	GTCCCGGATGAAGTAATCGGATCC
MT1881	GGGTACTGTCTAACGCCGCTATATTGACTGAAGGGGCG
MT1880	ATATAGCGGCGTTAGACAGTACCCGTCCGGGCATCCC
MT1877	**CACC**GTCTGAGGTTCTGATAGGACGGGG
MT1878	CTGCGCGACGAAATGCTCGCGGCGG
MT1967	GGGGTTCGTCCGGCCTTTCCGC
MT1968	GTGCTGATTGCGAGCACGGTCG
MT1969	GCTTCAGACCTTCCTCAAGGCG
MT1970	GTCTAATGGCTGACCGCCACTG
MT1971	AGAACCCACGTAGTGCCGGCTC
MT1972	ATGGACGCCATAGGGTGTGTAG

Table S3. Primers used for cloning of the *hsv* operon, cloning of individual *hsv* genes in *E. coli*, and generation of *hsv* knockouts. Nucleotides added for cloning are shown in bold. Restriction sites are underlined.

Insert	Plasmid	Host strain	Source
hsvA	pRSF-duet (Kan)	*E. coli* BL21	This study
hsvB	pACYC-duet (Cam)	*E. coli* BL21	This study
hsvC	pCDF-duet (Sm)	*E. coli* BL21	This study
hsvA-C	pLIC-His (Amp)	*E. coli* BL21	This study
		*P. fluorescens Pf*0-1	(11)
hrp/hrc		*EthAn Tn5 transposant of P. fluorescens Pf*0-1 (Tet)	(12)
hsvA-C	pBBR5 (Gent)	*P. fluorescens Pf*0-1	This study
		P. syringae pv. *tomato* DC3000	(2)
hrpL	pBAD (Tet)	*P. syringae* pv. *tomato* DC3000	(2)
*Tn*5::cfa6 (DC3118)		*P. syringae* pv. *tomato* DC3000	(13, 14)

Table S4. List of plasmids and strains used in this study.

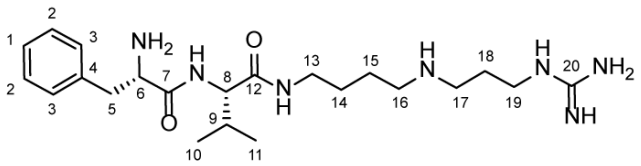

Position	δ_c	Proton	δH(J_{HH}[Hz])	HMBC
1	128.49	1-H	7.41($J_{1,2}$ = 6.9)	3
2	129.61	2-H	7.42($J_{2,1}$ = 6.9) ($J_{2,3}$ = 7.1)	2,4
3	129.86	3-H	7.26($J_{3,2}$ = 7.1)	1,3,5
4	134.07			
5	37.38	5-Ha	3.19($J_{5a,5b}$ = 14.4) ($J_{5a,6}$ = 7.5)	3,4,6,7
		5-Hb	3.23($J_{5b,5a}$ = 14.4) ($J_{5b,6}$ = 6.6)	3,4,6,7
6	54.65	6-H	4.33($J_{6,5a}$ = 7.5) ($J_{6,5b}$ = 6.6)	4,7
7	169.28			
8	60.45	8-H	3.98($J_{8,9}$ = 8.5)	7,9,10,11,12
9	30.71	9-H	1.95($J_{9,8}$ = 8.5) ($J_{9,10}$ = 6.8) ($J_{9,11}$ = 6.8)	8,10,11
10	18.49	10-3H	0.93($J_{10,9}$ = 6.8)	8,9,11
11	18.75	11-3H	0.90($J_{11,9}$ = 6.8)	8,9,10
12	172.58			
13	39.18	13-Ha	3.15($J_{13a,13b}$ = 13.3) ($J_{13a,14}$ = 7.0)	12,14,15
		13-Hb	3.29($J_{13b,13a}$ = 13.3) ($J_{13b,14}$ = 7.0)	12,14,15
14	26.02	14-2H	1.61($J_{14,13a}$ = 7.0) ($J_{14,13b}$ = 7.0) ($J_{14,15}$ = 7.6)	13,15,16
15	23.65	15-2H	1.73($J_{15,14}$ = 7.6) ($J_{15,16}$ = 7.6)	13,14,16
16	47.74	16-2H	3.10($J_{16,15}$ = 7.6)	14,15,17
17	45.29	17-2H	3.12($J_{17,18}$ = 8.0)	16,18,19
18	25.47	18-2H	2.00($J_{18,17}$ = 8.0) ($J_{18,19}$ = 6.7)	17,19
19	38.71	19-2H	3.31($J_{19,18}$ = 6.7)	17,18,20
20	157.38			

Table S5. ^{1}H (800 MHz) and ^{13}C (200 MHz) NMR spectroscopic data for phevamine A in D_2O. Chemical shifts were referenced to δ($C\underline{H}_3CO_2H$) = 2.08 ppm and δ($^{13}\underline{C}H_3CO_2H$) = 21.03. ^{13}C chemical shifts were determined via HMBC and HSQC experiments. ^{1}H, ^{1}H-*J*-coupling constants were determined from the acquired ^{1}H or dqfCOSY spectra. HMBC correlations are from the indicated proton(s) to the indicated ^{13}C atom.

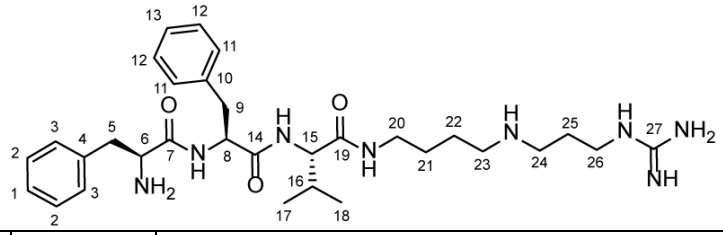

Position	δ_c	Proton	δH(J_{HH}[Hz])	HMBC
1	128.62	1-H	7.35($J_{1,2}$ = 7.0)	3
2	129.78	2-2H	7.38($J_{2,1}$ = 7.0) ($J_{2,3}$ = 7.1)	2,4
3	129.99	3-2H	7.23($J_{3,2}$ = 7.1)	1,3,5
4	134.05			
5	37.37	5-2H	3.18($J_{5,6}$ = 7.0)	3,6,7
6	54.66	6-H	4.25($J_{6,5}$ = 7.0)	4,7
7	169.12			
8	55.56	8-H	4.64($J_{8,9a}$ = 8.7) ($J_{8,9b}$ = 7.0)	7,9,13
9	37.93	9-Ha	2.99($J_{9a,9b}$ = 13.2) ($J_{9a,8}$ = 8.7)	10,11
		9-Hb	3.04($J_{9b,9a}$ = 13.2) ($J_{9b,8}$ = 7.0)	10,11
10	136.40			
11	129.78	11-2H	7.20($J_{11,12}$ = 7.5)	9,11,13
12	129.35	12-2H	7.34($J_{12,11}$ = 7.5) ($J_{12,13}$ = 7.0)	10,12
13	127.84	13-H	7.30($J_{13,12}$ = 7.0)	11
14	172.18			
15	60.39	15-H	3.85($J_{15,16}$ = 8.4)	14,16,18,19
16	30.81	16-H	1.91($J_{16,15}$ = 8.4) ($J_{16,17}$ = 6.8) ($J_{16,18}$ = 6.8)	18
17	18.87	17-3H	0.87($J_{17,16}$ = 6.8)	15,16,18
18	18.72	18-3H	0.91($J_{18,16}$ = 6.8)	15,16,17
19	172.85			
20	39.20	20-Ha	3.08($J_{20a,20b}$ = 13.5) ($J_{20a,21}$ = 7.0)	19,21,22
		20-Hb	3.18($J_{20b,20a}$ = 13.5) ($J_{20b,21}$ = 7.0)	19,21,22
21	26.07	21-2H	1.54($J_{21,20a}$ = 7.0) ($J_{21,20b}$ = 7.0) ($J_{21,22}$ = 7.0)	20,23
22	23.69	22-2H	1.67($J_{22,21}$ = 7.0) ($J_{22,23}$ = 7.8)	20,23
23	47.80	23-2H	3.05($J_{23,22}$ = 7.8)	21,22,24
24	45.35	24-2H	3.09($J_{24,25}$ = 7.8)	23,25,26
25	25.56	25-2H	1.98($J_{25,24}$ = 7.8) ($J_{25,26}$ = 7.0)	24,26
26	38.80	26-2H	3.28($J_{26,25}$ = 7.0)	24,25,27
27	157.47			

Table S6. ^{1}H (800 MHz) and ^{13}C (200 MHz) NMR spectroscopic data for phevamine B in D_2O. Chemical shifts were referenced to δ($C\underline{H}_3OH$) = 3.34 ppm and δ($^{13}\underline{C}H_3OH$) = 49.50. ^{13}C chemical shifts were determined via HMBC and HSQC experiments. ^{1}H, ^{1}H-*J*-coupling constants were determined from the acquired ^{1}H or dqfCOSY spectra. HMBC correlations are from the indicated proton(s) to the indicated ^{13}C atom.

Supplementary Figures

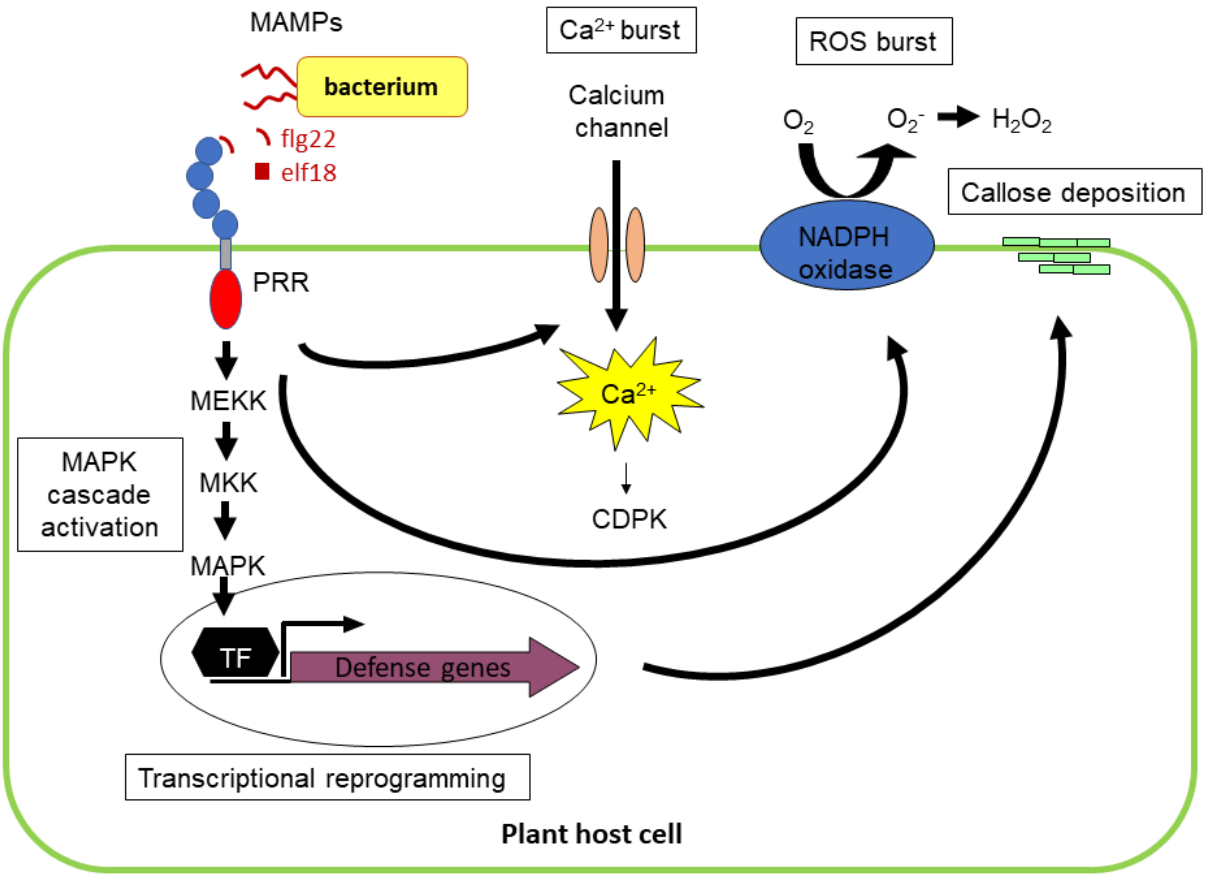

Figure S1. Plant immune response schematic. Diagram showing several MAMP-induced immune responses in a plant host cell. Upon elicitation by a MAMP, a plant cell may induce MAPK cascade activation, transcriptional reprogramming, calcium burst, ROS burst, synthesis of various secondary metabolites, and callose deposition. Collectively, these responses are sufficient to suppress pathogen proliferation. MAMP: microbe-associated molecular pattern, PRR: pathogen recognition receptor, TF: transcription factor, MEKK: mitogen-activated protein (MAP) kinase kinase kinase, MKK: MAP kinase kinase, MAPK: MAP kinase, CDPK: calcium-dependent protein kinase, ROS: reactive oxygen species.

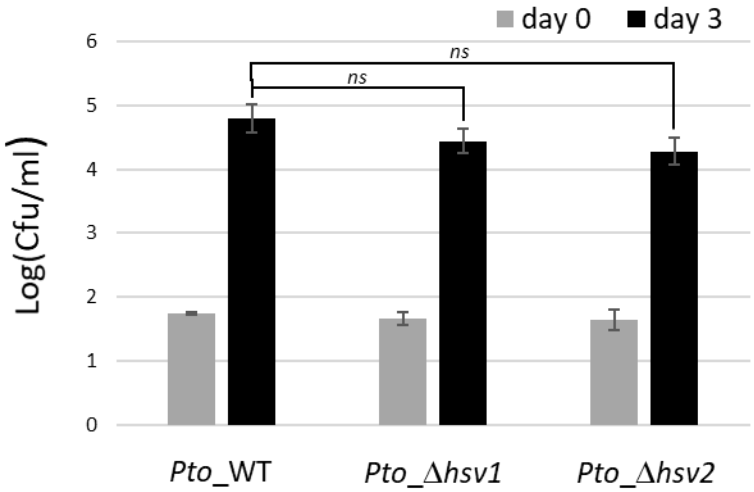

Figure S2. *Pto*_Δ*hsv* mutants do not display significantly reduced virulence on *A. thaliana*. Bacteria were counted after recovery from *Pto*-wildtype and *Pto*_Δ*hsv* mutants on *A. thaliana* seedlings. The experiment was repeated twice with similar results. The mutants in both experiments displayed slightly reduced growth but this was not statistically significant (Student's *t*-tests). ns: non significant. Error bars represent ± standard error.

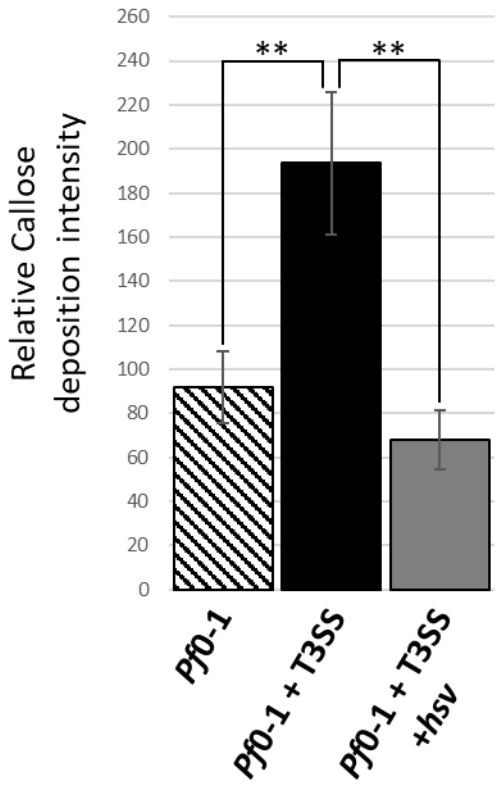

Figure S3. The *hsv* operon suppresses callose deposition in *A. thaliana* induced by components encoded by the T3SS locus. Leaves of 4-week-old *A. thaliana* were infiltrated with the *P. fluorescens* strains noted at bottom and stained with aniline blue, ~20 h post infiltration. **, *p*-value ≤ 0.01; *t*-test. Error bars represent standard errors. This experiment was repeated 3 times with similar results.

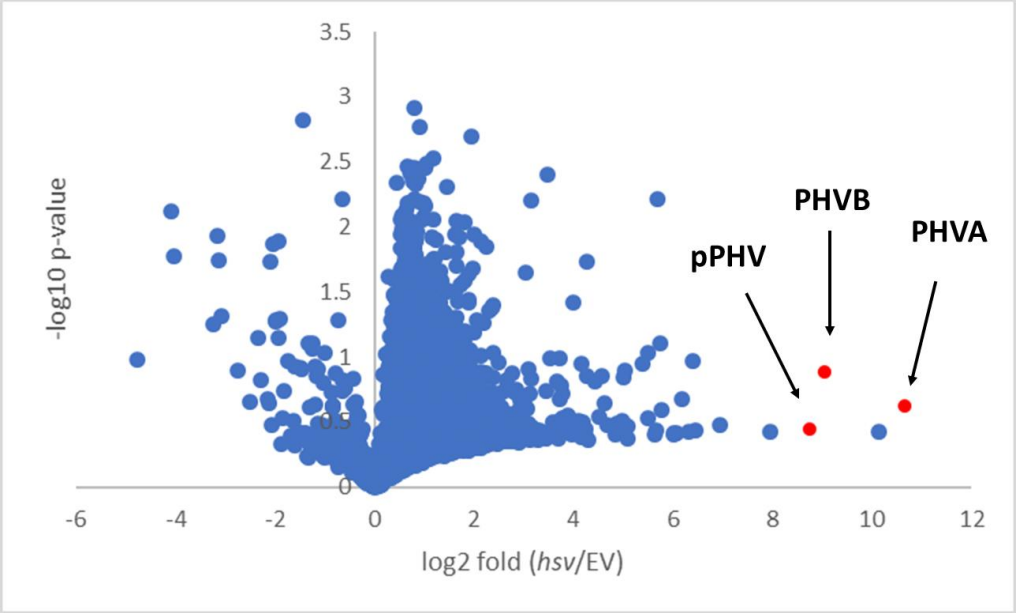

Figure S4. Identification of phevamines by comparative metabolomics. The LC-MS metabolic profiles are compared between the extract of *E. coli* overexpressing *hsv* and *E. coli* control containing the empty vector. The fold change ($\log_2$) for each metabolite is plotted against the *p*-value ($\log_{10}$) for that metabolite. Data points for prephevamine (pPHV), phevamine A (PHVA), and phevamine B (PHVB) are highlighted in red. The average fold change is very large for prephevamine (430 fold increase), phevamine A (1600 fold increase), and phevamine B (540 fold increase) comparing *hsv* overexpression and the empty vector control. When the fold change for a metabolite is large, the level in each sample tends to vary more. The relatively large *p*-values for these metabolites may be due to variable protein levels upon overexpression.

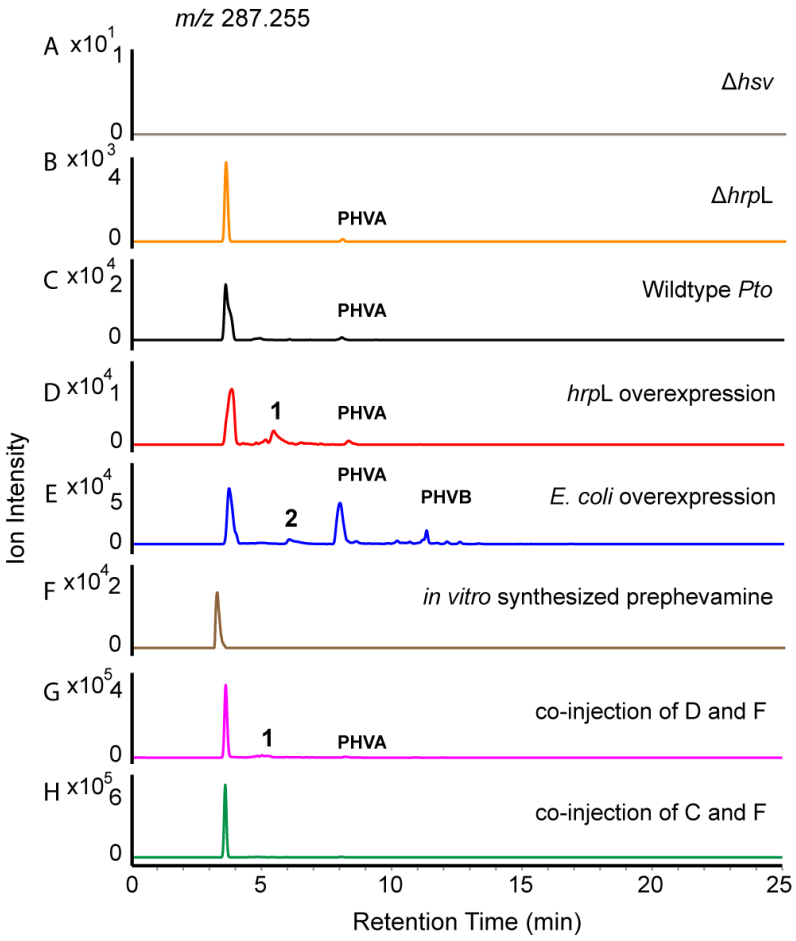

Figure S5. Production of prephevamine by different bacterial strains. Extracted ion chromatograms are shown for prephevamine (*m/z*, 287.255) detected in the extracts of each bacterial strain. The retention time of prephevamine is approximately 3.8 minutes. Prephevamine is not produced by *Pto*Δ*hsv* (*hsv* deletion mutant in *Pto*) (gray). Prephevamine is produced by *Pto*Δ*hrpL* (*hrpL* deletion mutant in *Pto*) (orange), wildtype *Pto* (black), *Pto* pBAD:*hrpL* overexpression (red), and *E. coli* overexpressing the *hsv* operon (blue). Prephevamine is also produced in the *in vitro* enzymatic reaction and was purified by HPLC (brown). The *in vitro* purified standard was co-injected with the *hrpL* overexpression extract (pink) and the wildtype *Pto* extract (green), both showing a single peak for prephevamine. In (*D*), (*E*), and (*G*), the additional prephevamine peaks result from in-source fragmentation of phevamine A or phevamine B as labeled. Lowering the fragmentor voltage reduced these in-source fragmentation peaks. Two metabolites from extractions, 1 and 2, are structurally unrelated to prephevamine based on LC/MS/MS analysis.

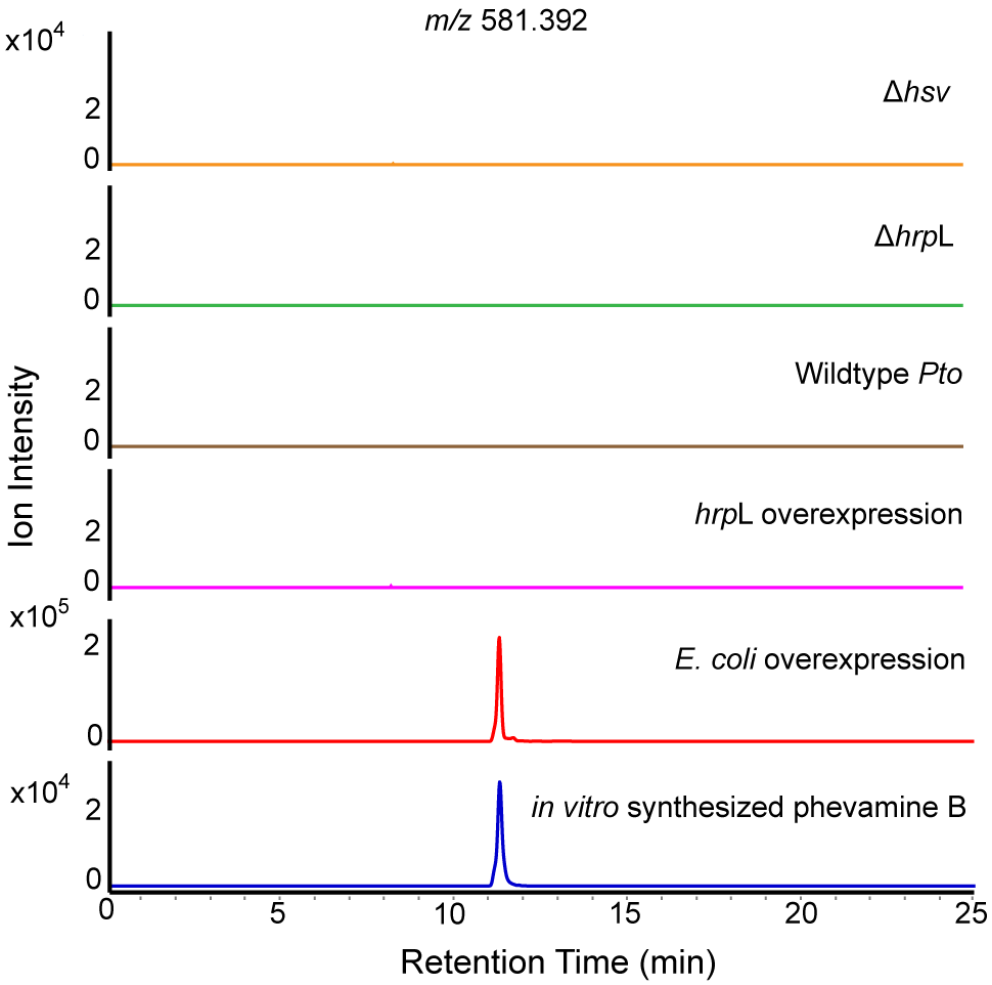

Figure S6. Production of phevamine B by different bacterial strains. Extracted ion chromatograms are shown for phevamine B (*m/z*, 581.392). Phevamine B is not produced by *Pto*Δ*hsv* (*hsv* deletion mutant in *Pto*) (orange), *Pto*Δ*hrpL* (*hrpL* deletion mutant in *Pto*) (green), wildtype *Pto* (brown), or *Pto* pBAD:*hrpL* overexpression (pink). Phevamine B is only detected in *E. coli* overexpressing *hsv* (red) and *in vitro* enzymatic reaction (blue).

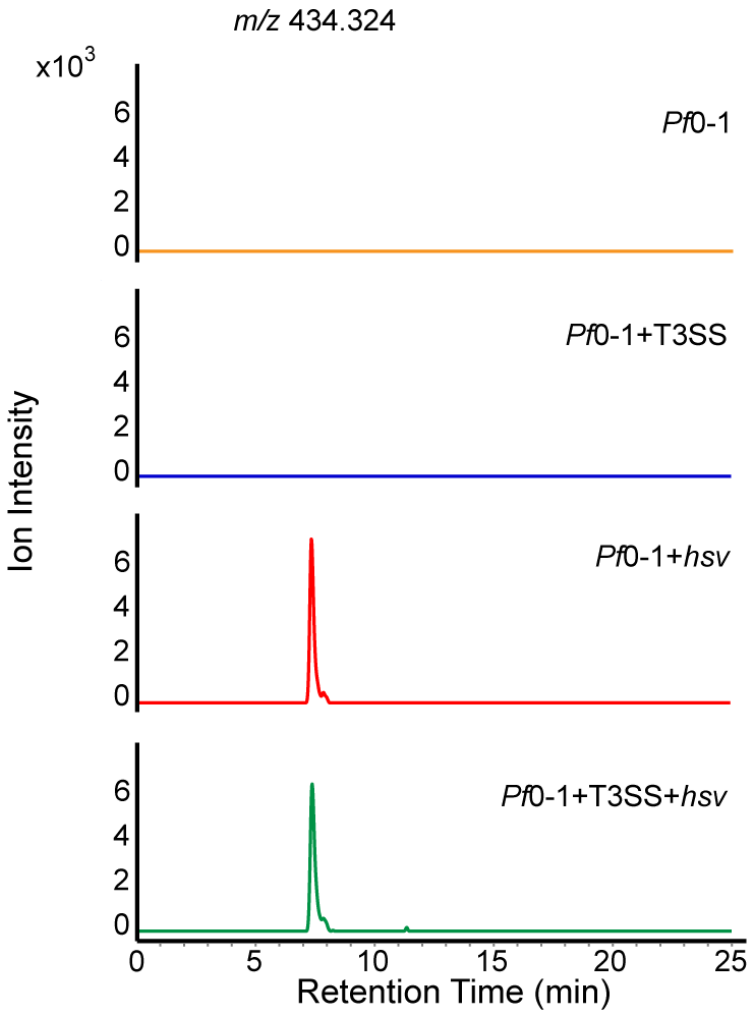

Figure S7. Phevamine A production in *P. fluorescens Pf*0-1 is independent of T3SS. Extracted ion chromatograms of phevamine A (*m/z* 434.324) are shown. Phevamine A is detected in both *Pf*0-1 strains expressing *hsv, Pf*0-1+T3SS+*hsv* (green) and *Pf*0-1+*hsv* (red), indicating that the T3SS is not required for the secretion of phevamine A. Phevamine A is not detected in the culture extracts of control strains without *hsv*, *Pf*0-1+T3SS (blue) or *Pf*0-1 (orange).

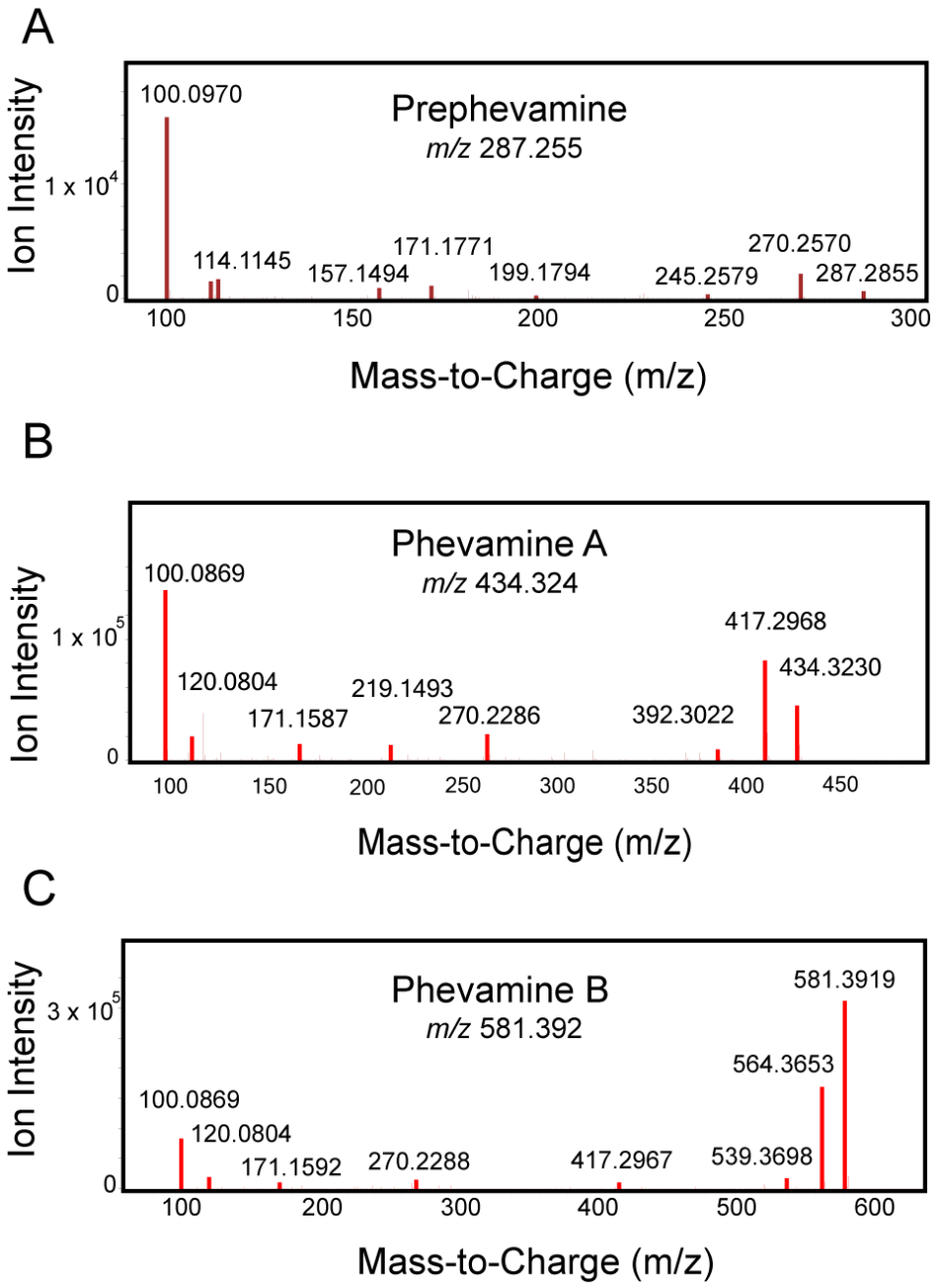

Figure S8. Structural analyses of prephevamine and phevamines by tandem mass spectrometry (LC-MS/MS). *(A)* MS/MS spectrum of prephevamine (*m/z* 287.255). *(B)* MS/MS spectrum of phevamine A (*m/z* 434.324). (*C)* MS/MS spectrum of phevamine B (*m/z* 581.392).

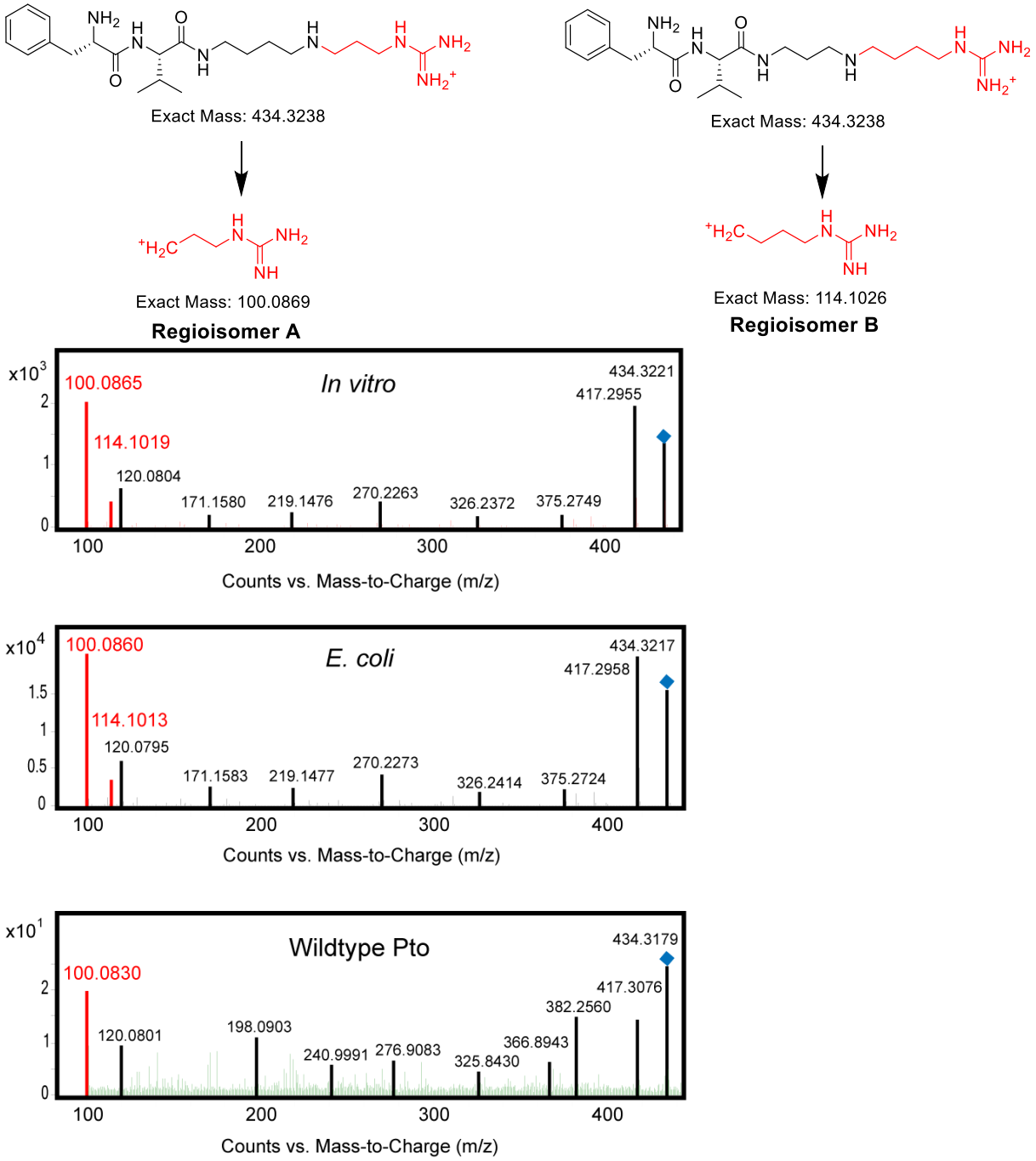

Figure S9. Identification of the regioisomers of phevamine A by LC-MS/MS. A 100 *m/z* fragment is unique to the amidinotransfer product on the propylamine end of spermidine (regioisomer A), and a 114 *m/z* fragment is unique to the amidinotransfer product on the butylamine end of spermidine (regioisomer B). Both isomers are detected from the *in vitro* reaction and *E. coli* overexpression. In culture extracts of wildtype *Pto*, only regioisomer A was detected.

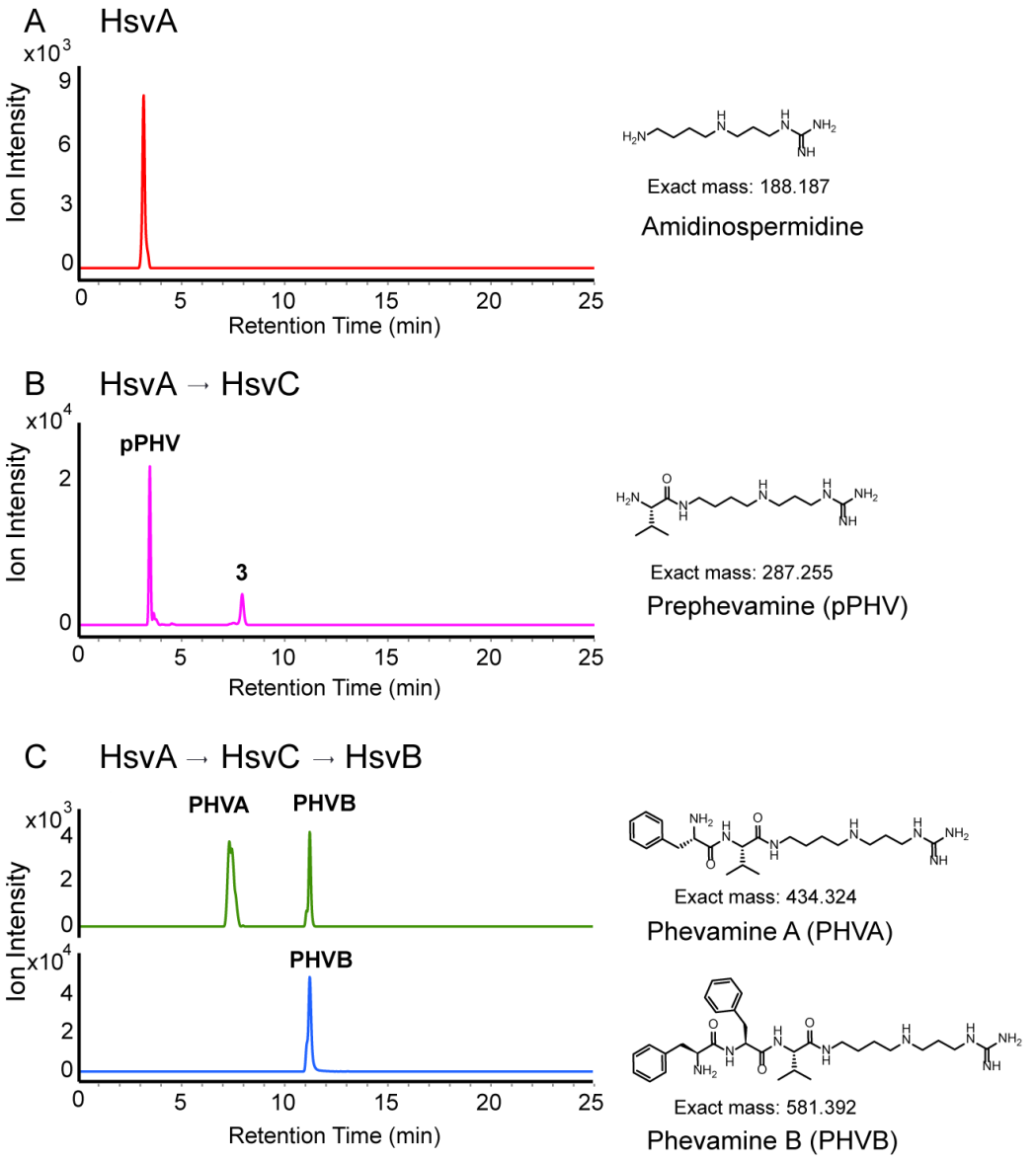

Figure S10. Production of phevamines and detection of pathway intermediates by sequential *in vitro* enzymatic assays. Extracted ion chromatograms are shown for *(A)* amidinospermidine (*m/z* 188.187) from HsvA reaction, *(B)* prephevamine (*m/z* 287.255) from HsvA reaction followed by HsvC reaction, and *(C)* phevamine A (*m/z* 434.324, green) and phevamine B (*m/z* 581.392, blue) from sequential reactions of HsvA, HsvC, and HsvB. In (*B*), the second small peak for prephevamine comes from in-source fragmentation of Compound 3, the mass of which corresponds to Val-Val-Val-amidinospermidine, an *in vitro* byproduct of the HsvC reaction. In (*C*), the second peak for phevamine A is the result of in-source fragmentation of phevamine B.

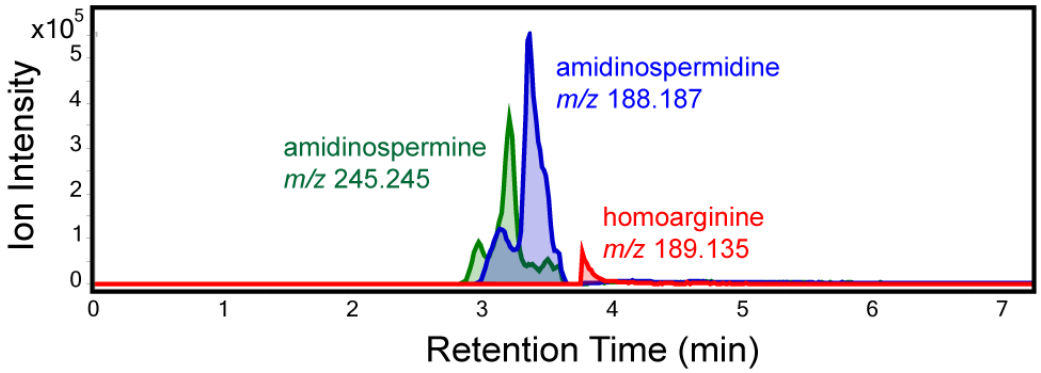

Figure S11. *In vitro* reconstitution of HsvA activity. HsvA was incubated with spermine, spermidine, and L-lysine as the acceptor of the amidino group and L-arginine as the donor of the amidino group. Extracted ion chromatograms are shown for amidinospermidine (*m/z* 188.187), amidinospermine (*m/z* 245.245), and homoarginine (*m/z* 189.135), which are the amidinotransfer products catalyzed by HsvA for spermidine, spermine, and arginine, respectively.

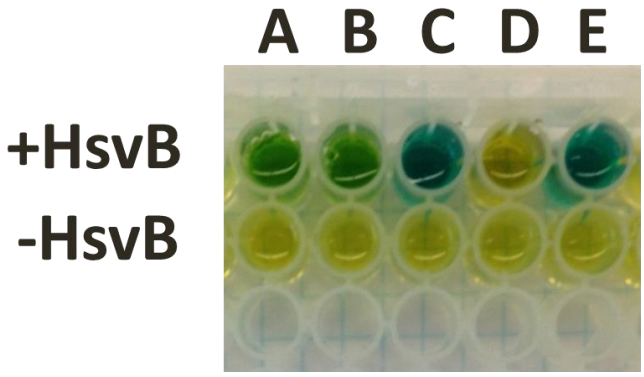

Figure S12. HsvB activates L-Phe as the preferred substrate. Several pairs of amino acids were incubated with HsvB and the released inorganic phosphate (P_i) was measured using the P_iColorLock assay described in the Methods. The amino acid pairs are (A) L-Ser and L-Orn, (B) L-Ala and L-Lys, (C) L-Ala and L-Phe, (D) L-Arg and L-Trp, and (E) 2x L-Phe. The assays containing L-Phe ((C) and (E)) produced the most P_i, indicating that L-Phe is the preferred substrate for HsvB.

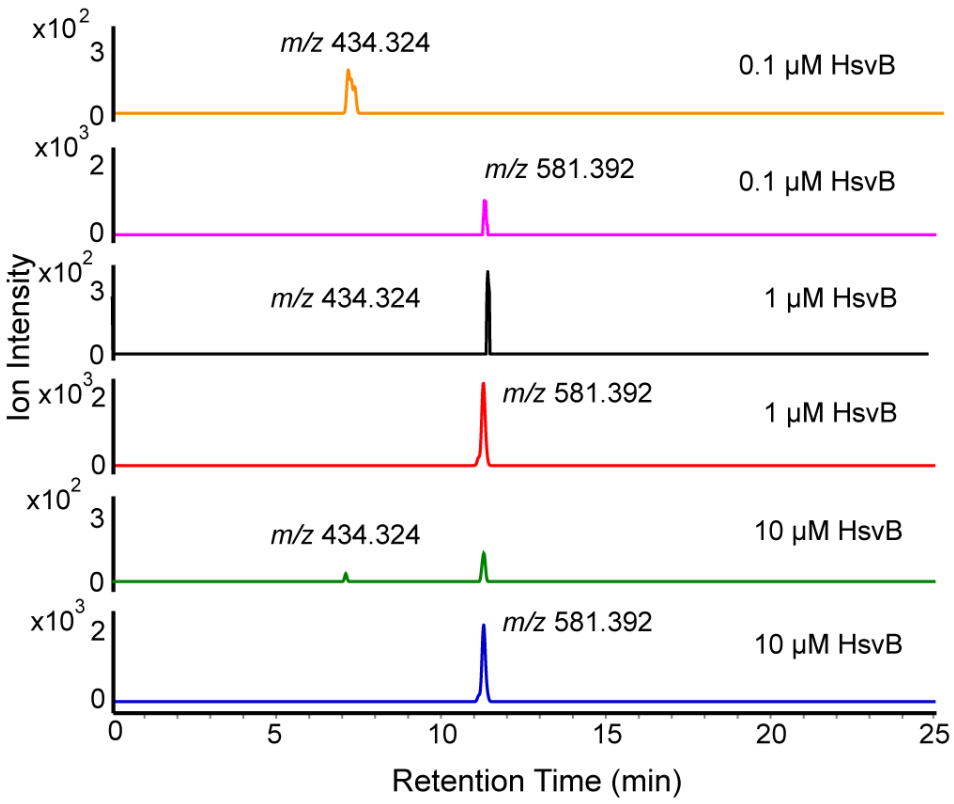

Figure S13. Production of phevamine A and B depends on HsvB concentration. Reaction mixtures containing 100 μM pPHV, 20 μM Phe, and varying amounts of HsvB were incubated at room temperature for 2 hours. As the concentration of HsvB increased, the amount of phevamine B (*m/z* 581.392) increased (pink, red, and blue). The ratio of phevamine A (*m/z* 434.324) (orange, black and green) to phevamine B is the highest at low concentration of HsvB. The peak around 11 minute retention time in phevamine A traces is a result of in-source fragmentation of phevamine B.

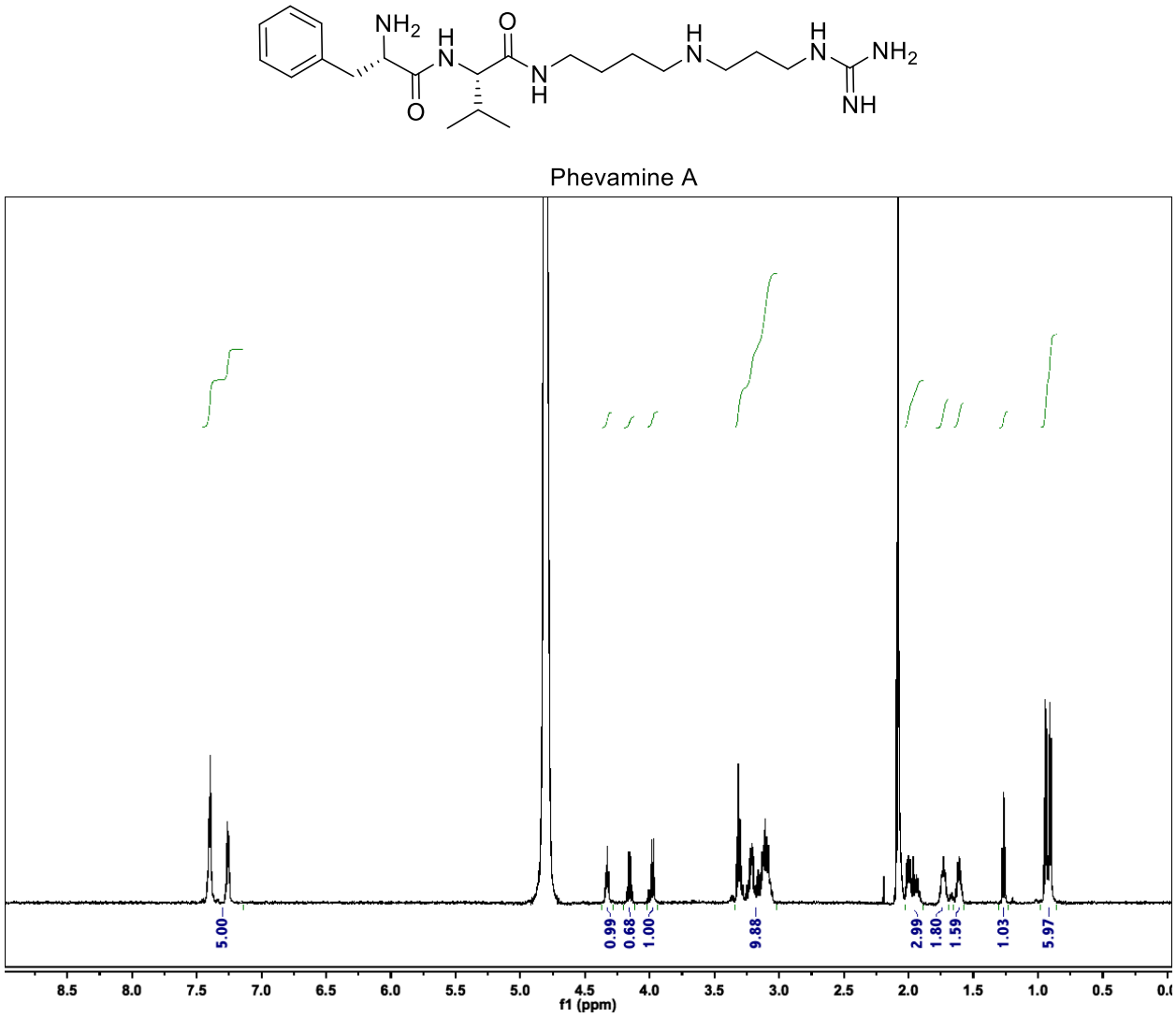

Figure S14. ^{1}H NMR (600 MHz) of *in vitro* synthesized and purified phevamine A. Spectrum acquired in D_2O.

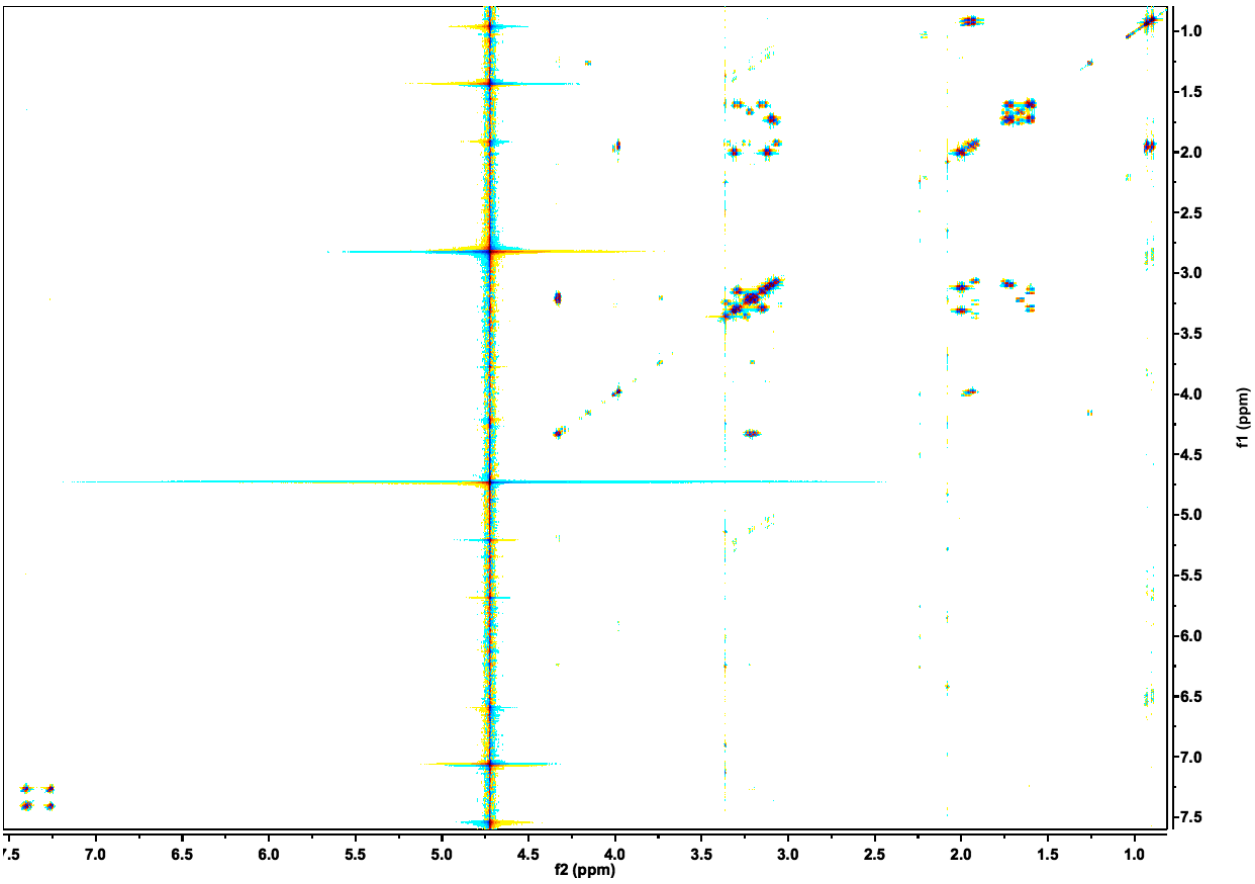

Figure S15. (^{1}H,^{1}H)-dqfCOSY spectrum (800 MHz) of *in vitro* synthesized and purified phevamine A. Spectrum acquired in CD_3OD.

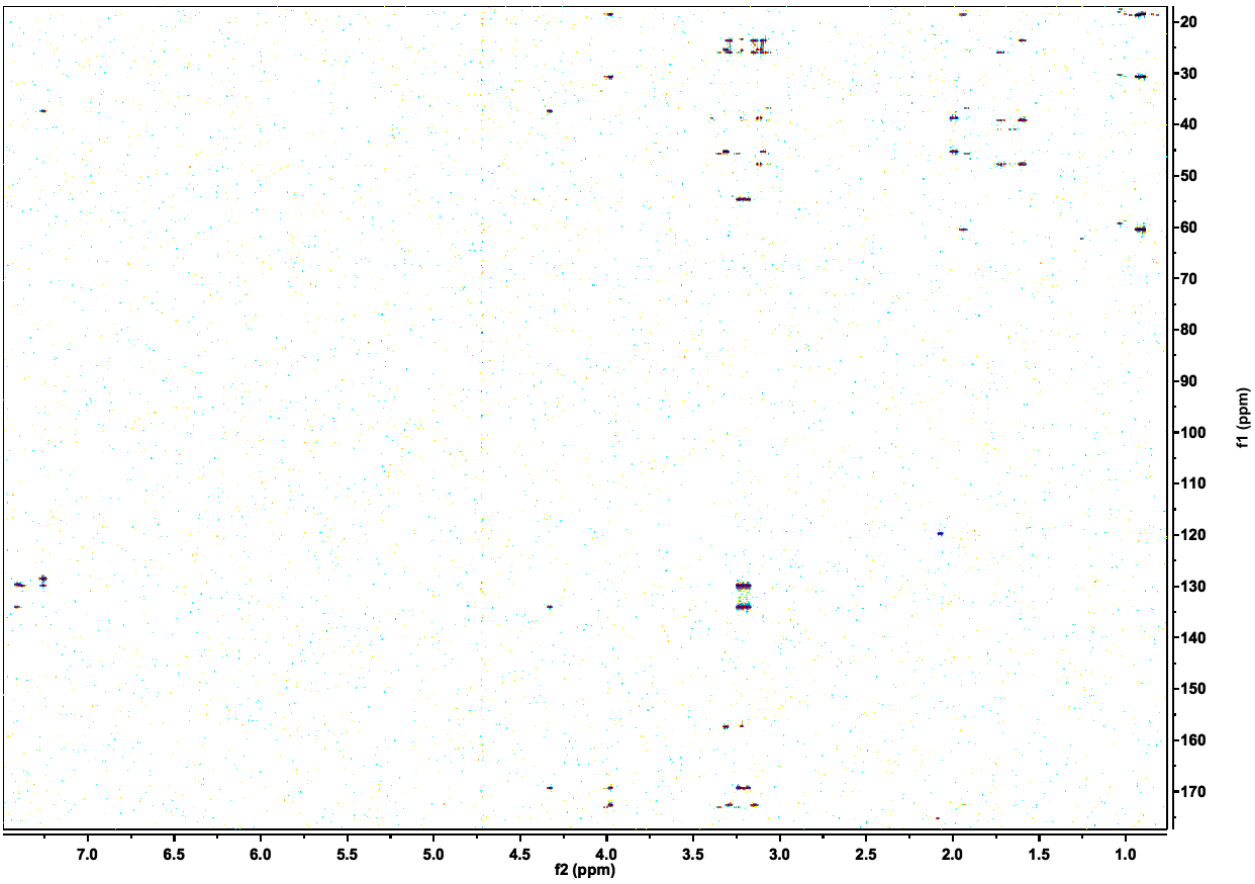

Figure S16. (^{1}H,^{13}C)-HMBC spectrum (800 MHz) of *in vitro* synthesized and purified phevamine A. Spectrum acquired in CD_3OD.

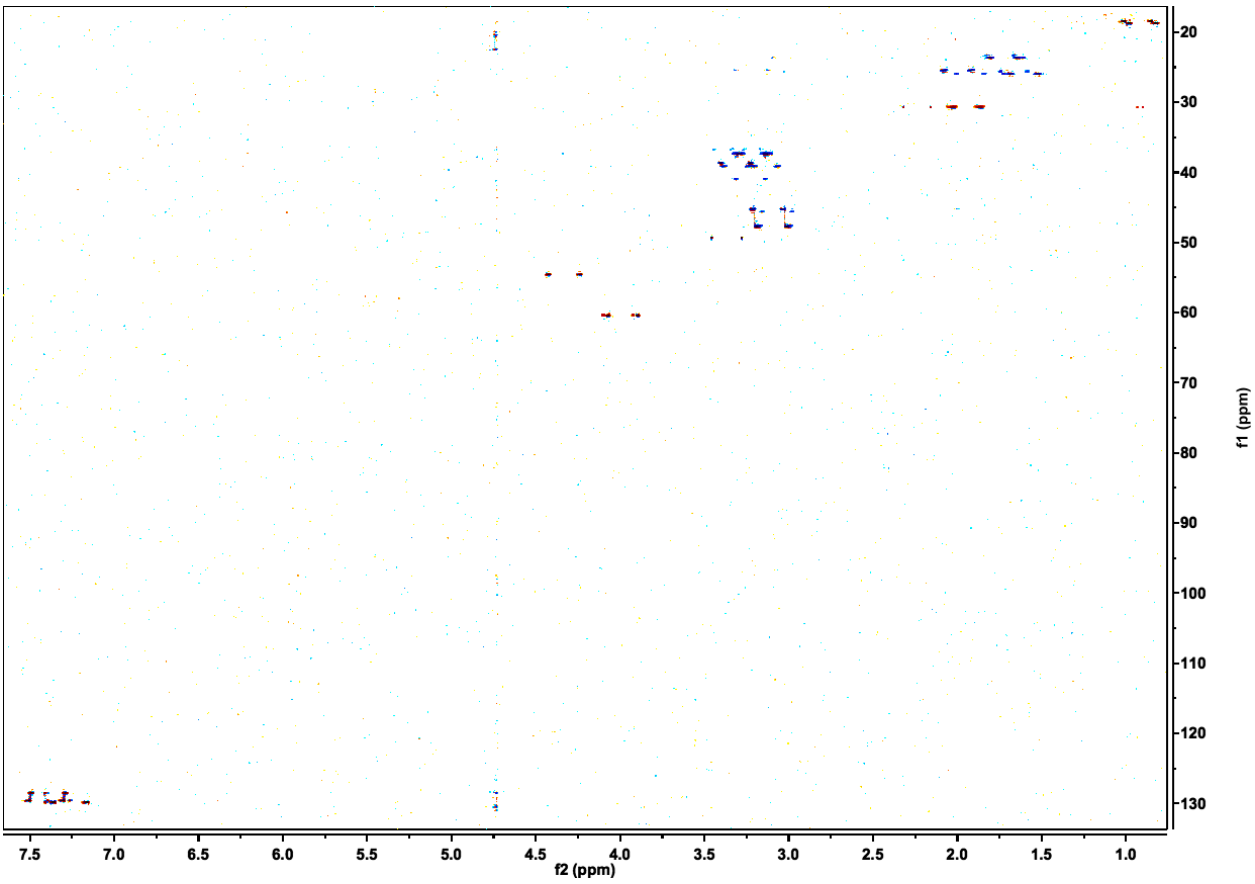

Figure S17. (^{1}H,^{13}C)-coupled-HSQC spectrum (800 MHz) of *in vitro* synthesized and purified phevamine A. Spectrum acquired in CD_3OD.

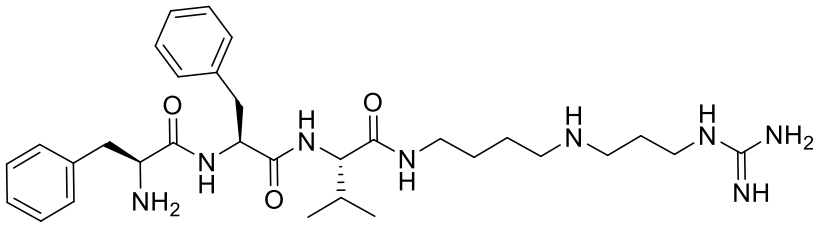

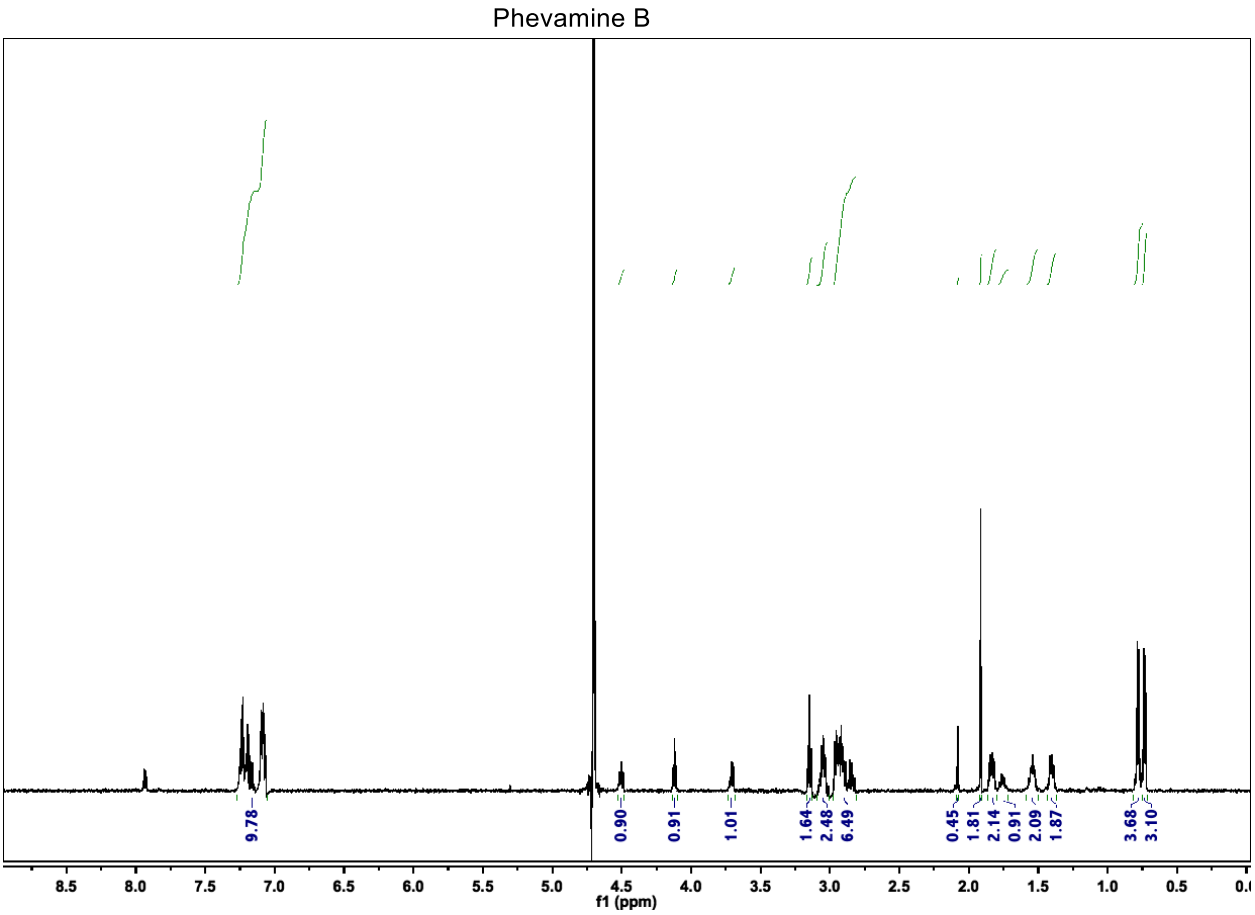

Figure S18. ^{1}H NMR (600 MHz) of *in vitro* synthesized and purified phevamine B. Spectrum acquired in CD_3OD.

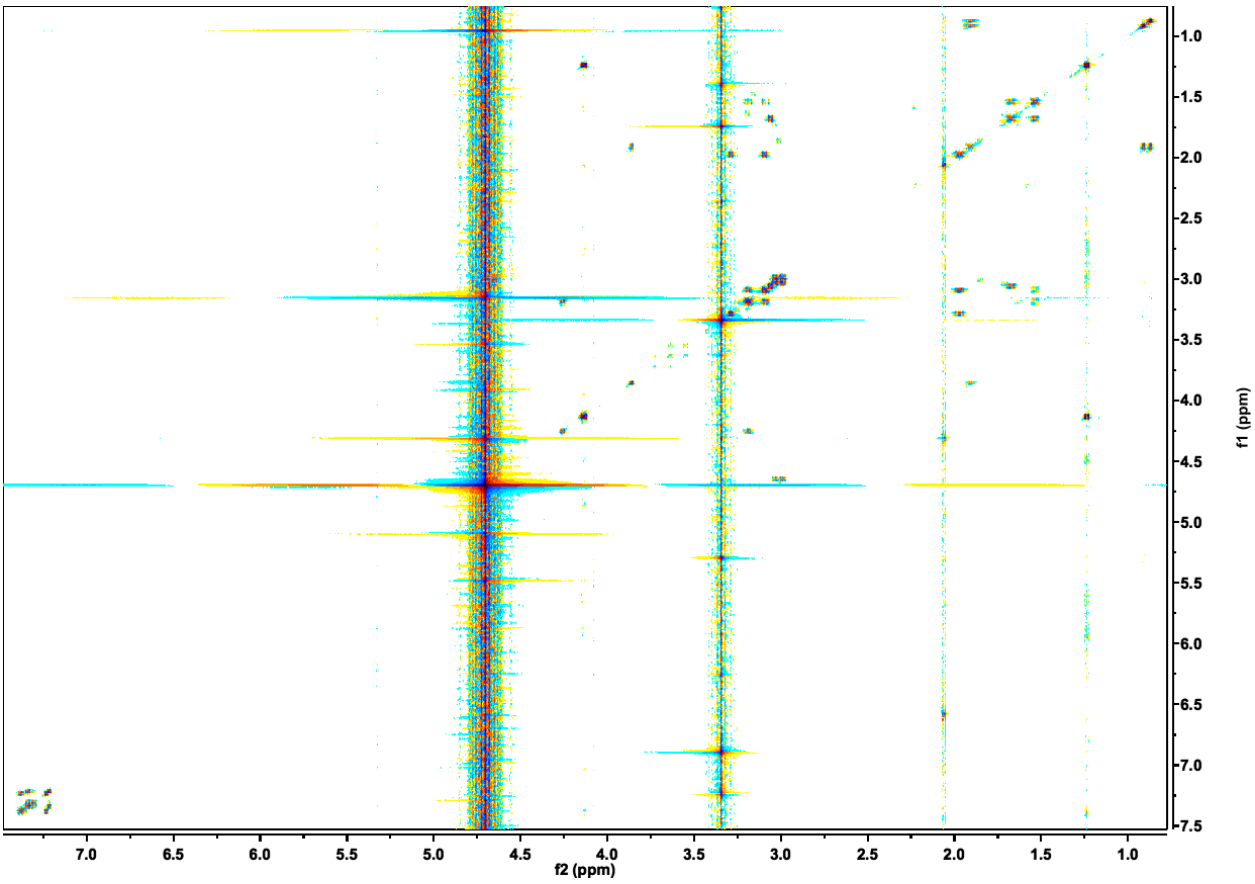

Figure S19. (^{1}H,^{1}H)-dqfCOSY spectrum (800 MHz) of *in vitro* synthesized and purified phevamine B. Spectrum acquired in CD_3OD.

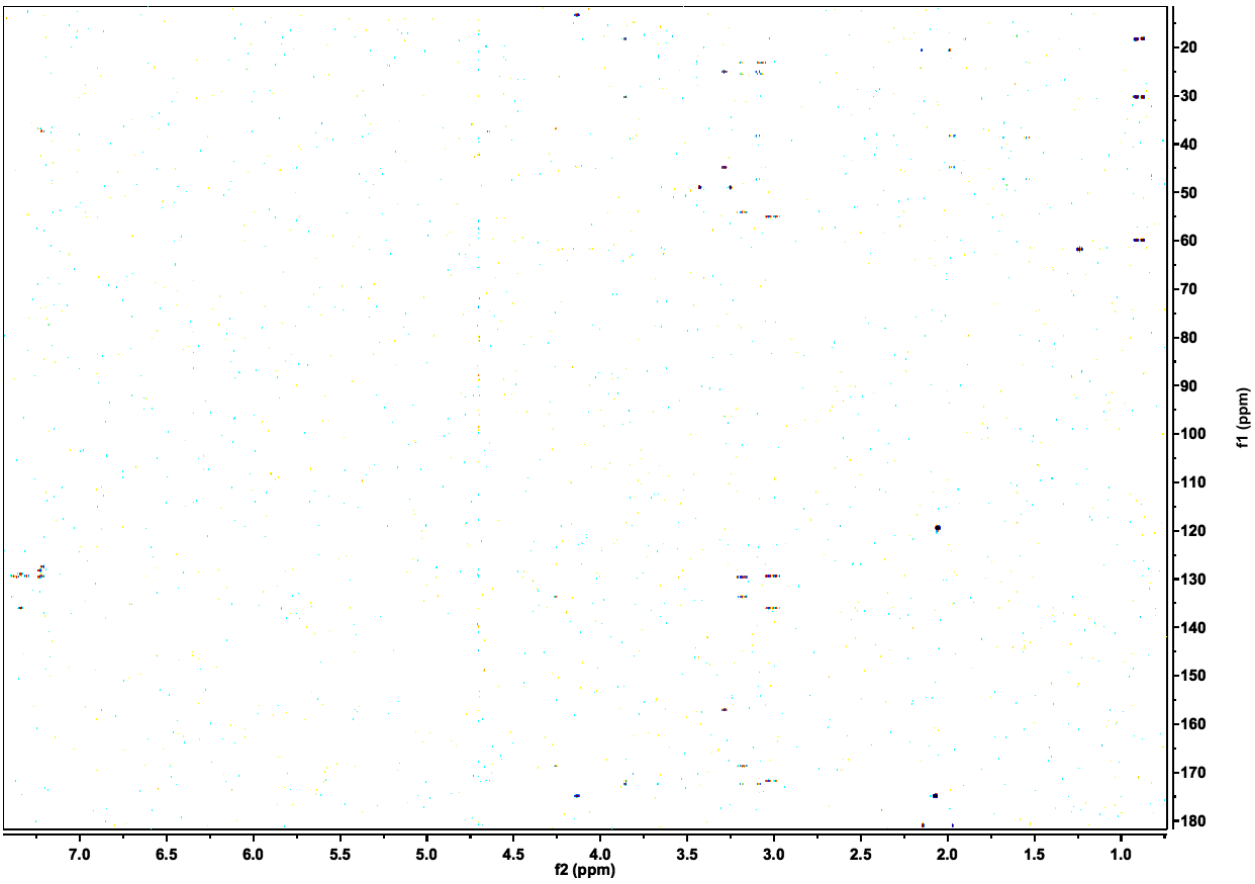

Figure S20. (^{1}H,^{13}C)-HMBC spectrum (800 MHz) of *in vitro* synthesized and purified phevamine B. Spectrum acquired in CD_3OD.

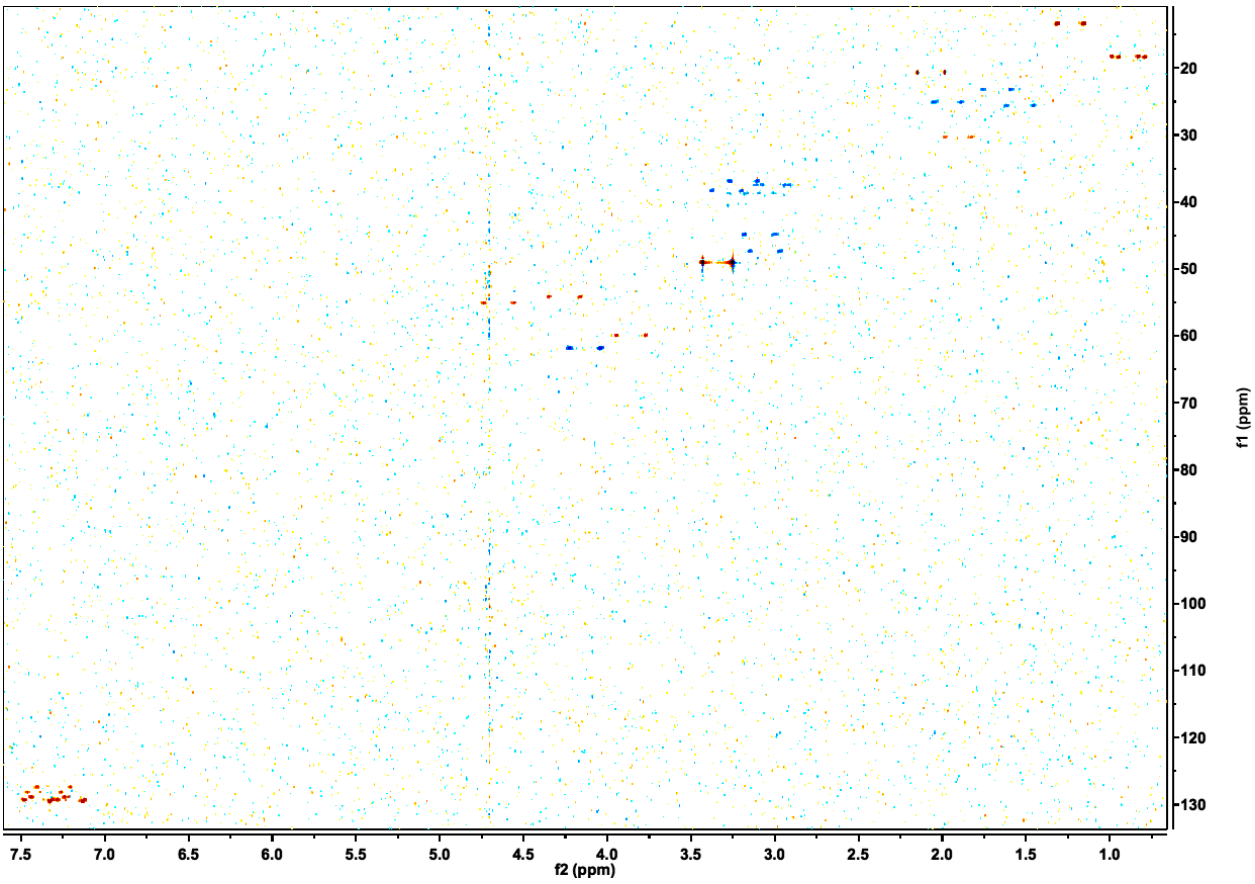

Figure S21. (^{1}H,^{13}C)-coupled-HSQC spectrum (800 MHz) of *in vitro* synthesized and purified phevamine B. Spectrum acquired in CD_3OD.

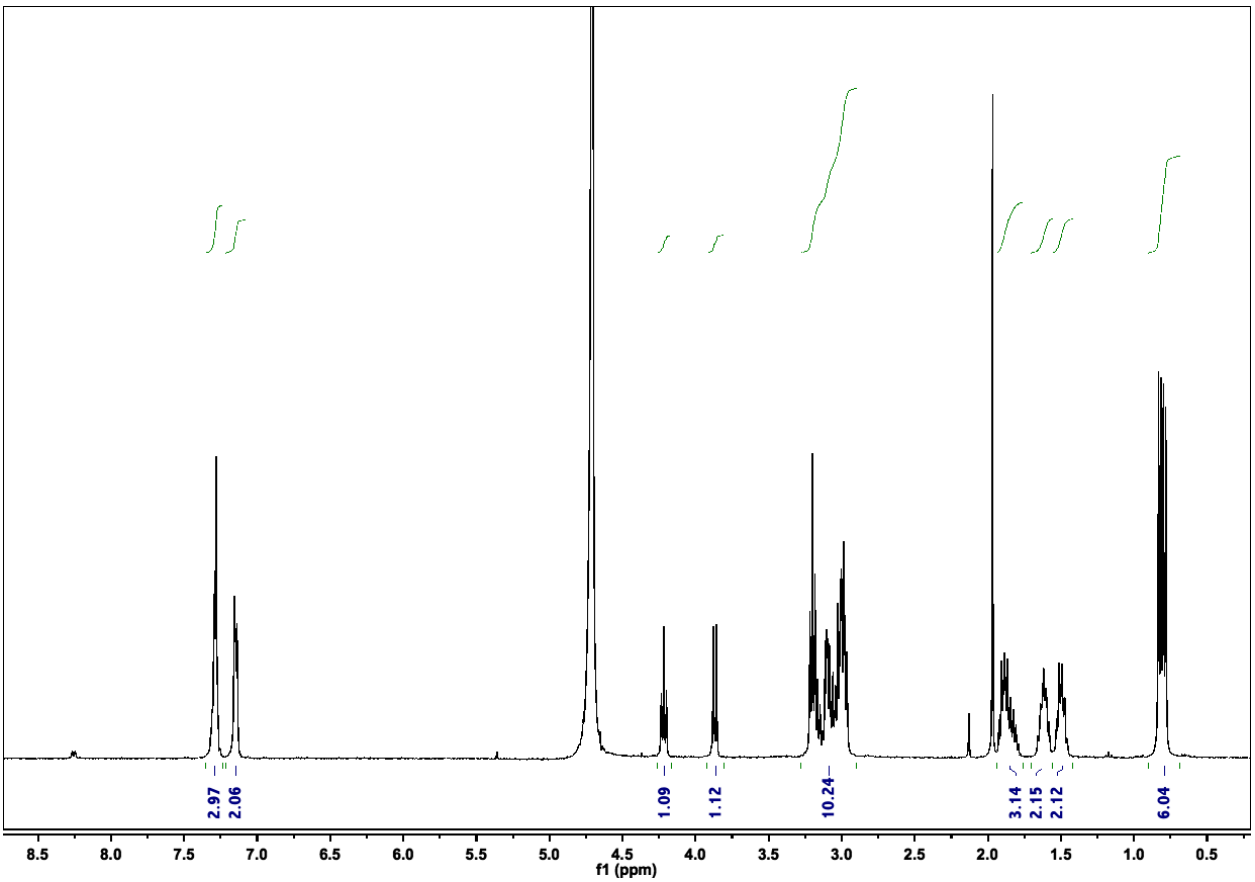

Figure S22. ^{1}H NMR (400 MHz) of the phevamine A synthetic standard (9). Spectrum acquired in D_2O.

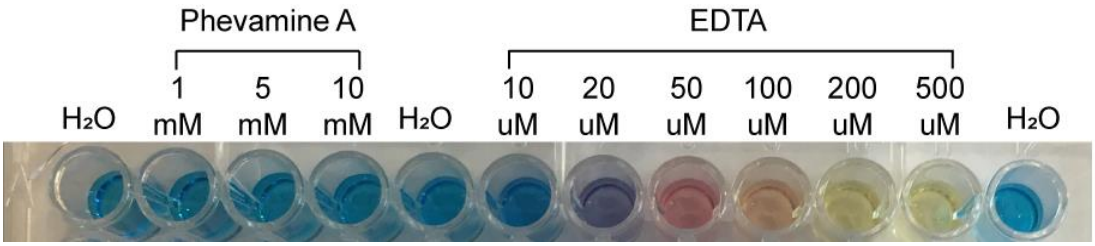

Figure S23. Iron binding activity of phevamine A. The ability of phevamine A to bind iron was tested and compared to EDTA standards using a chromeazurol S (CAS) assay. Upon binding of ferric iron, the chromeazurol S dye changes color from blue to yellow. No color change was observed for phevamine A at a concentration of up to 10 mM, thus it is unlikely that phevamine A acts as a siderophore to bind ferric iron.

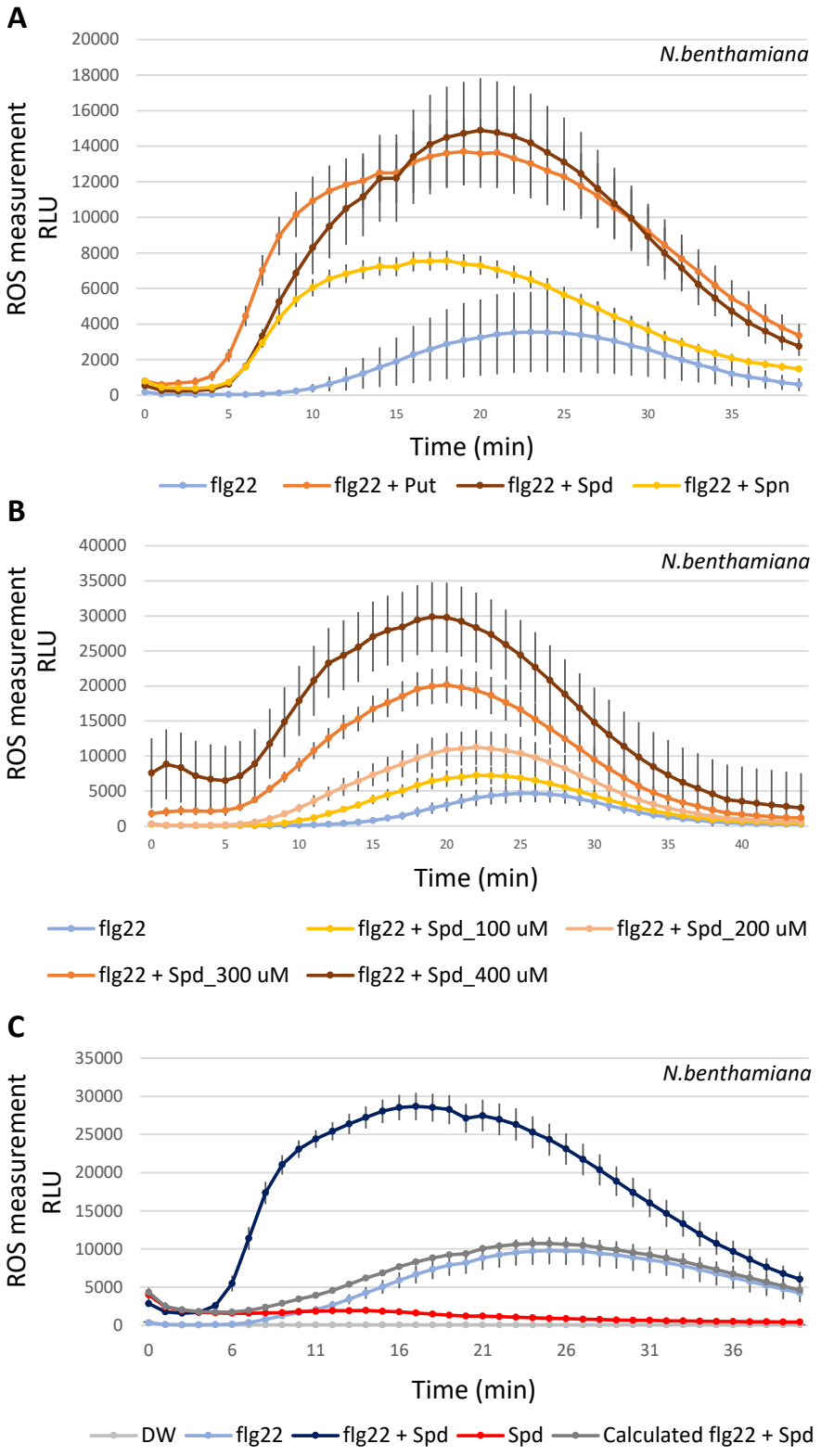

Figure S24. Polyamines enhance the flg22-induced ROS burst in *N. benthamiana*. *(A)* Various polyamines potentiate the flg22-induced ROS burst. Leaf disks were

challenged with 10 nM of flg22 with or without polyamines at 400 µM. Put: putrescine, Spd: spermidine, and Spn: spermine. *(B)* Dose-dependent effect of spermidine on the flg22-induced ROS burst. Leaf disks were challenged with 10 of nM flg22 and various concentrations of spermidine. *(C)* The increase of the flg22-induced ROS burst by spermidine is not due to an additive effect. Leaf disks were treated with distilled water (DW), 10 nM of flg22, 10 nM of flg22 with 400 µM of spermidine, or 400 µM of spermidine only. Experiments presented in panels (*A*) and (*C*) were performed more than 3 times with similar results. The experiment presented in panel (*B*) was done twice with similar results. Error bars represent standard errors.

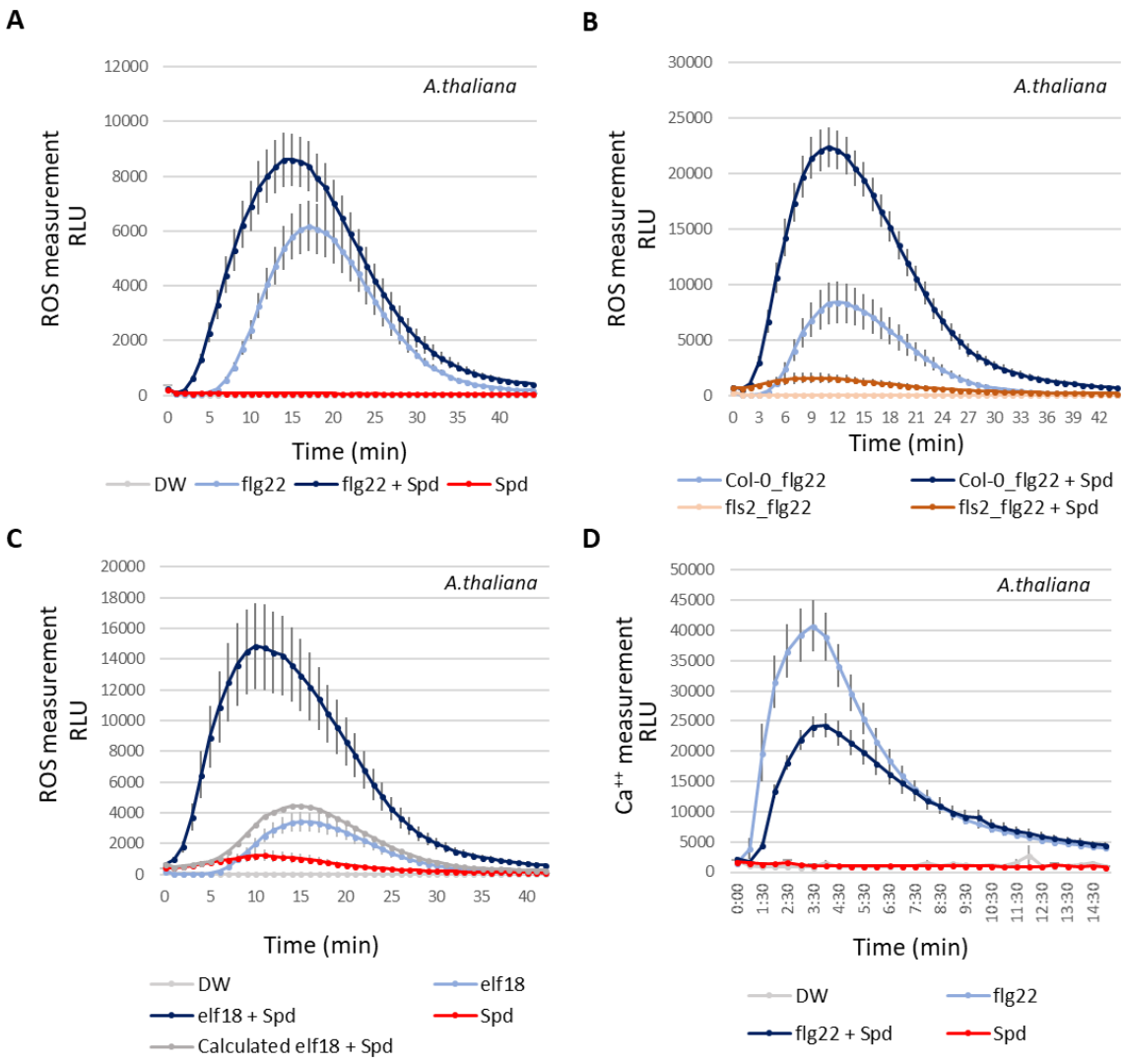

Figure S25. Effect of spermidine on early MTI responses in *A. thaliana*. (*A*) Spermidine potentiates the flg22-induced ROS burst. Leaf disks were treated with distilled water (DW), flg22 at 10 nM, flg22 with spermidine at 300 µM or spermidine only at 300 µM. ROS levels were measured. This assay was repeated more than 3 times with similar results. (*B*) Potentiation of the flg22 ROS burst by spermidine is dependent on FLS2. Leaf disks from Col-0 or the *fls2* mutant were challenged with flg22 only at 20 nM or with spermidine at 300 µM. This experiment was performed twice with similar results. (*C*) Spermidine potentiates the elf18-induced ROS burst. Leaf disks were challenged with DW, elf18 at 50 nM, elf18 supplemented with spermidine at 400 µM, or with spermidine only at 400 µM. This experiment was performed twice. (*D*) Spermidine suppresses the flg22-induced calcium burst. Col-0_pMAQ2 leaf disks were treated with DW, flg22 at 25 nM, flg22 at 25 nM with spermidine at 400 µM, or with spermidine only. This experiment was repeated more than 3 times. Error bars represent standard errors.

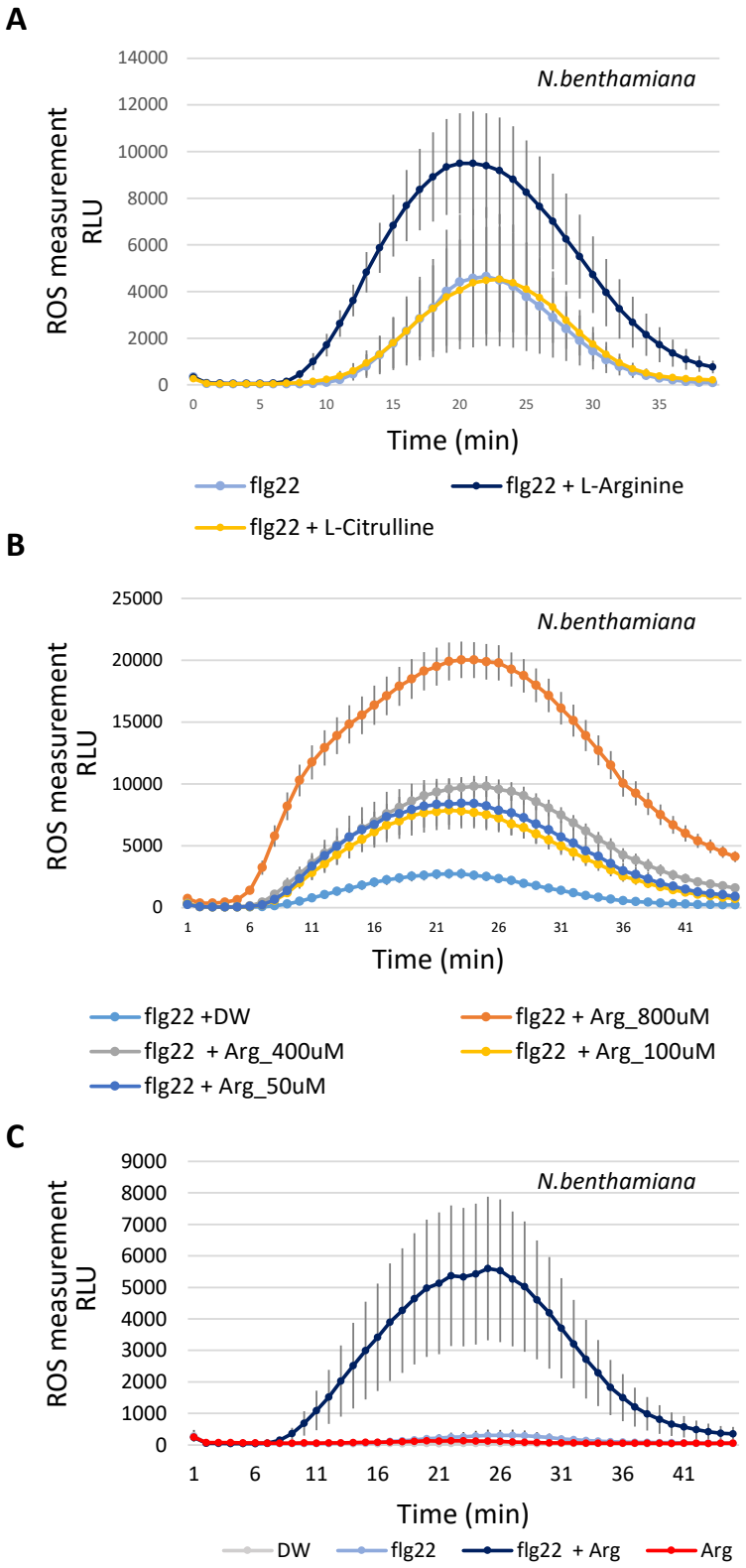

Figure S26. Arginine potentiates the flg22-induced ROS burst in *N. benthamiana*. *(A)* L-Arginine potentiates the flg22-induced ROS burst, but L-citrulline does not. flg22

was used at 10 nM, arginine and citrulline were used at 400 µM. This experiment was performed twice with similar results. *(B)* Dose-dependent effect of arginine on the flg22-induced ROS burst. flg22 was used at 100 nM and arginine at various concentrations. This experiment was performed twice with similar results. *(C)* The increase of the flg22-induced ROS burst by arginine is not due to an additive effect. flg22 was used at 10 nM and arginine at 400 µM. This experiment was repeated at least 3 times with similar results. Error bars represent standard errors.

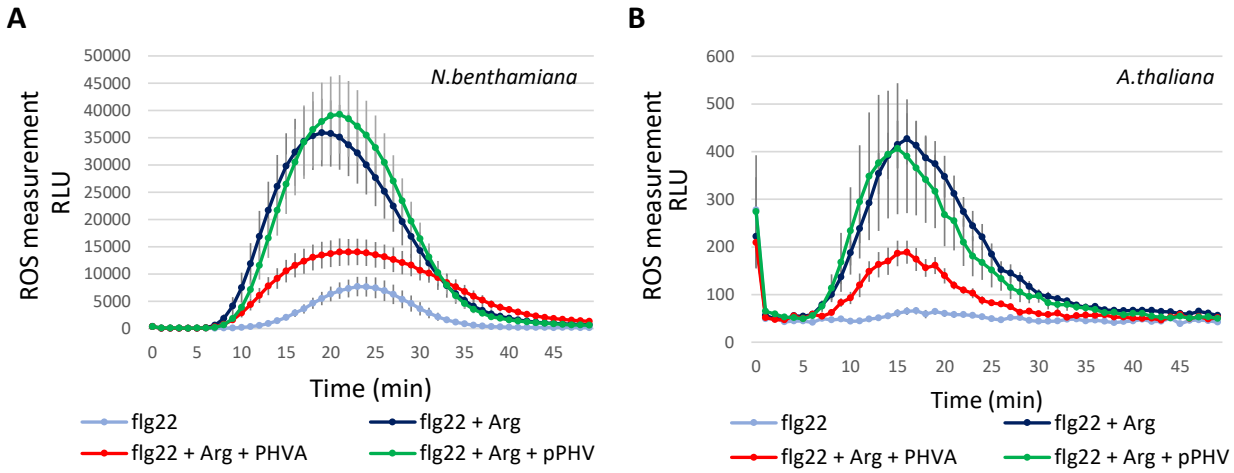

Figure S27. Phevamine A, but not prephevamine, suppresses the arginine potentiation of the flg22-induced ROS burst in both *N. benthamiana* and *A. thaliana*. *(A)* Phevamine A, but not prephevamine, suppresses the arginine ROS potentiation in *N. benthamiana.* flg22 was used at 5 nM; arginine, prephevamine and phevamine A at 300 µM. *(B)* Phevamine A, but not prephevamine, suppresses the arginine ROS potentiation in *A. thaliana.* flg22 was used at 5 nM; arginine, prephevamine, and phevamine A at 300 µM. PHVA: Phevamine A, pPHV: prephevamine. Experiments are representatives of 3 independent repeats with similar results.

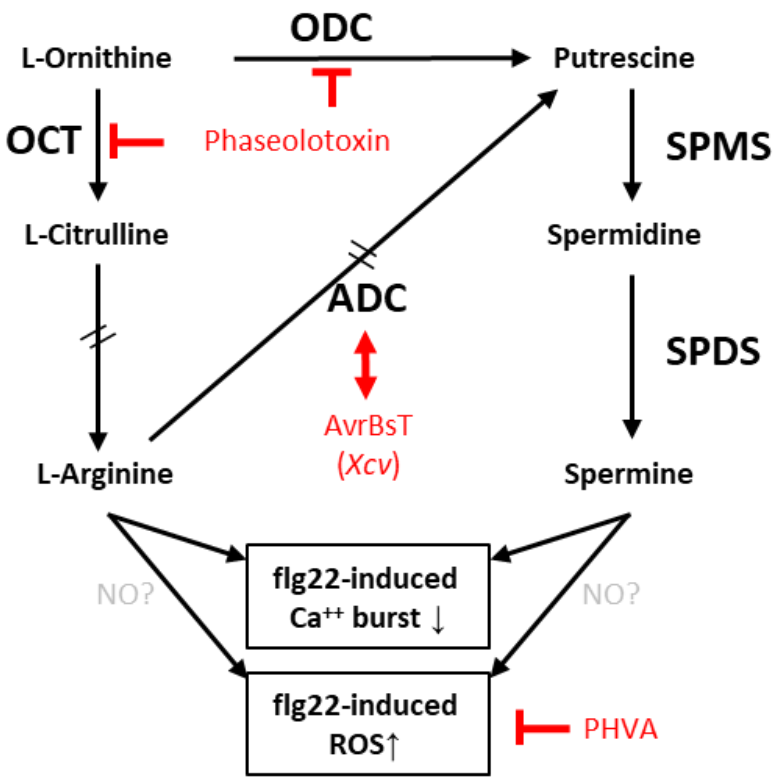

Figure S28. Arginine and polyamine biosynthetic pathways are targeted by pathogens via different mechanisms. Spermidine and L-arginine potentiate the flg22-induced ROS burst. The role of nitric oxide production in this potentiation remains uncertain (15). Phevamine A suppresses the spermidine/L-arginine potentiation of the flg22-induced ROS burst. Phaseolotoxin inhibits the synthesis of arginine and polyamines pathway by suppressing the activity of ODC and OCT, while phevamine A targets the potentiation mediated by spermidine and L-arginine. The effector AvrBsT from *Xanthomonas campestris* pv. *vesicatoria* (*Xcv*) interacts (red double arrow) with ADC1 in pepper (16). ODC: ornithine decarboxylase, OCT: ornithine carbamoyltransferase, ADC: arginine decarboxylase, SPDS: spermidine synthase, SPMS: spermine synthase, ROS: reactive oxygen species, NO: nitric oxide, PHVA: phevamine A. Double dashed arrows represent pathways with intermediates not shown. Reproduced from ref. (17) with permission from American Society for Microbiology.

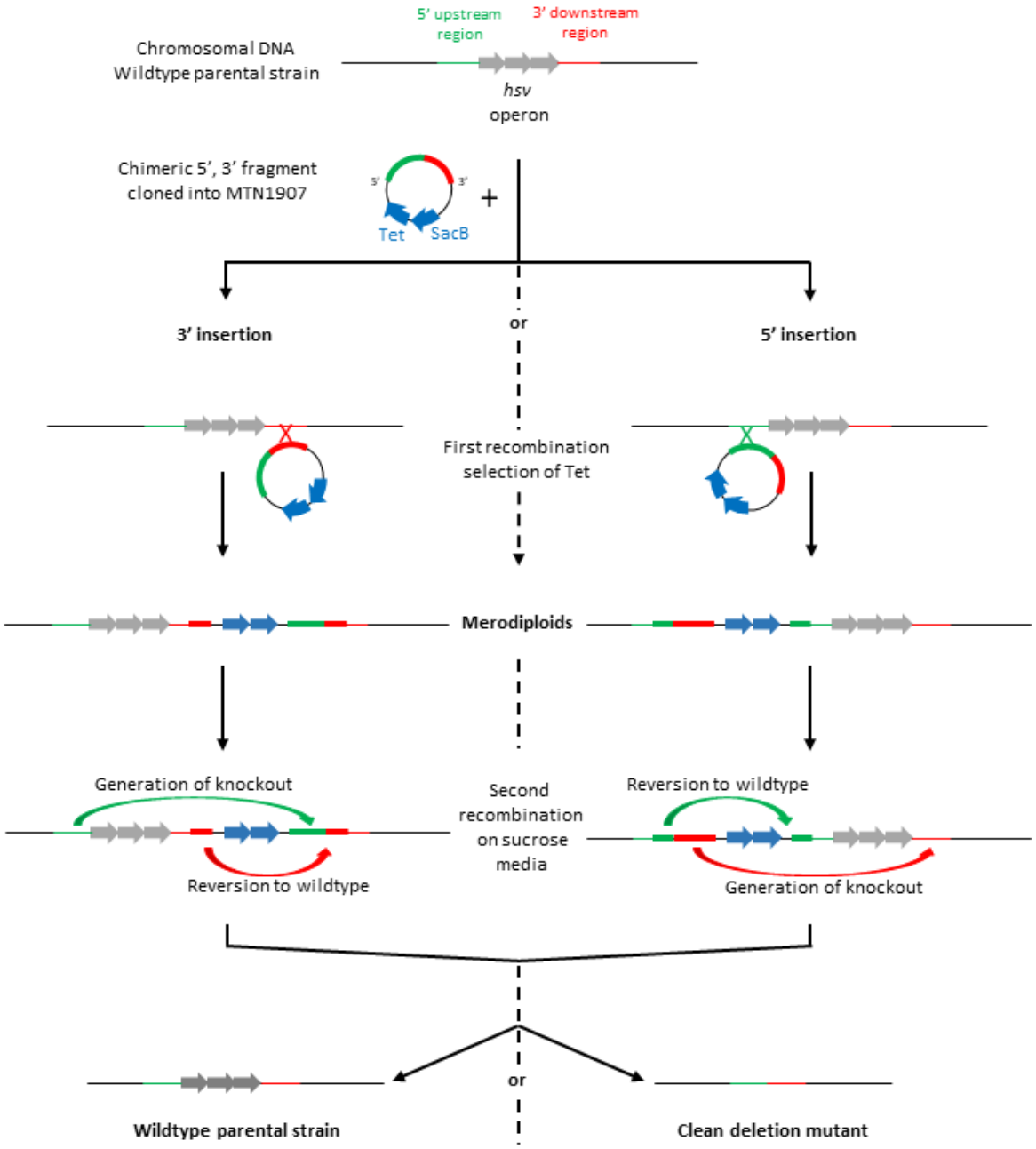

Figure S29. Strategy to generate *P. syringae* clean deletion mutants. A fusion of the 5' and 3' flanking region of the *hsv* operon was generated by chimeric PCR and cloned into MTN1907. After transformation of the parental strains (*Pto*, *Pto*-Cor $^{-}$, *Pto*D28E), the first recombination integrates the plasmid either at the 5 'or 3' end of the *hsv* operon. Merodiploids are selected on media containing tetracycline and genotyped by PCR. The second recombination event either leads to a reversion to the original locus or the generation of the clean mutant. Recombined strains were selected on plates containing sucrose (5%) and clean deletion mutants were identified by PCR (see Figure S30).

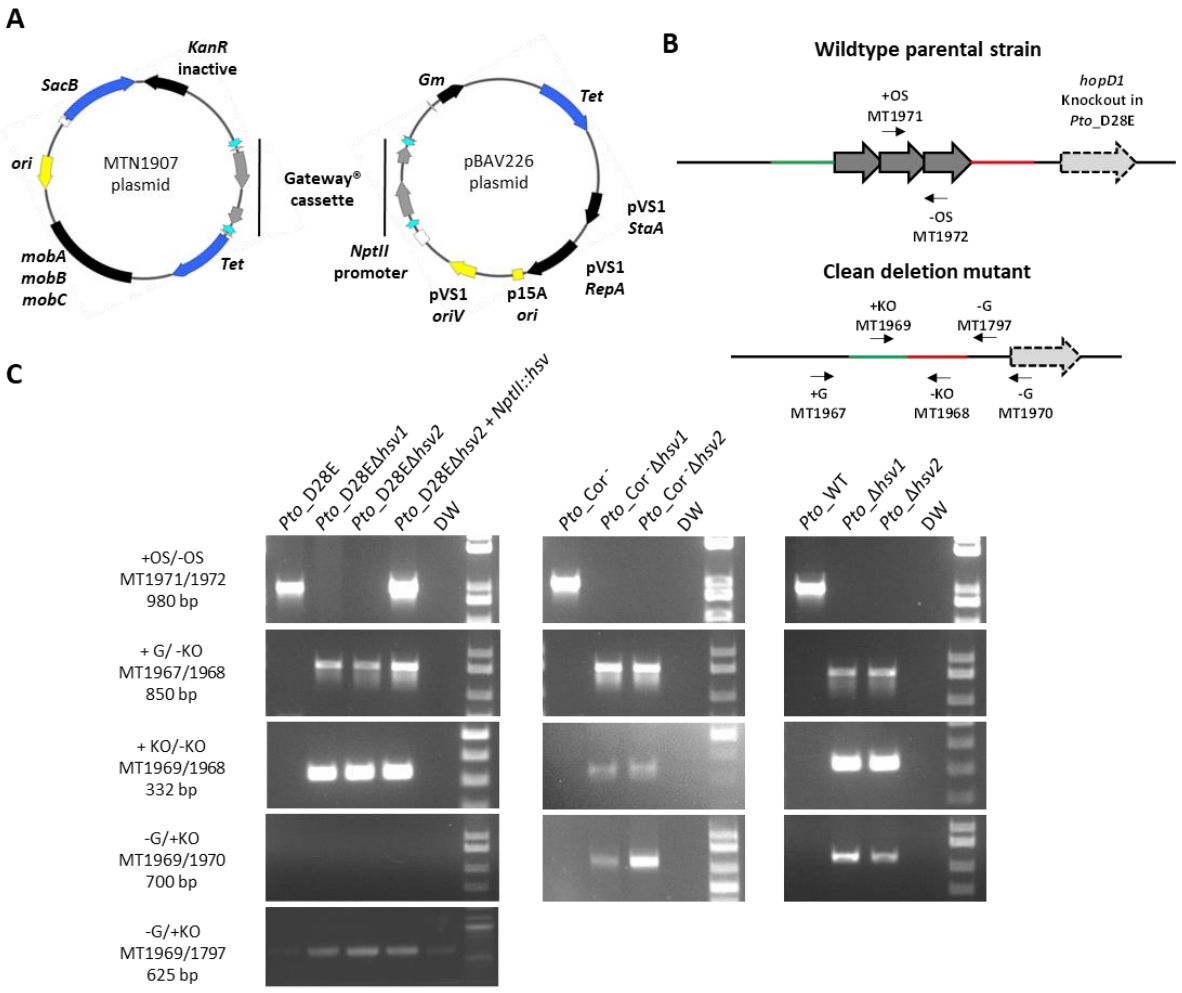

Figure S30. Genotyping of the clean deletion mutants and the complemented strain. *(A)* Graphical representation of the plasmids used for molecular manipulation of *P. syringae*. The left panel represents the MTN1907 plasmid used to engineer the mutants. The right panel represents the pBAV226 plasmid in which the *hsv* operon was cloned downstream of the *NptII* promoter for complementation of *Pto*D28E_Δ*hsv2*. Tet: confers resistance to tetracycline*; mobA, mobB, mobC*: RSF1010 mobilization genes; *ori*: high-copy-number origin of replication; *SacB*: a secreted levansucrase that renders bacteria sensitive to sucrose for counter-selection; *KanR*_inactive: aminoglycoside phosphotransferase gene inactive in *P. syringae*; pVS1 *StaA*: the stability protein from the *Pseudomonas* plasmid pVS1; pVS1 *RepA*: a replication protein; p15A *ori*: p15A origin of replication for propagation in *E. coli* cells; pVS1 *oriV*: origin of replication of the pVS1 plasmid; *Gm*: the gentamycin acetyltransferase. *(B)* Graphical representation of the *hsv* locus in the wildtype parental strains (*Pto*-WT, *Pto*-Cor ⁻, *Pto*D28E), and the clean deletion mutants. Arrows represent the primers used for the genotyping. OS: operon specific primer, G: genomic primer, KO: knockout primer, +: forward primer, -: reverse primer (see Supplementary Table S3 for primer sequences). (*C*) Analytical PCRs performed to confirm the genotype of the mutants generated in this study. PCR programs include a 1 min extension time, designed for amplification in mutant strains,

but too short for amplification in the wildtype parental strains with the exception of the PCRs using operon specific primers.

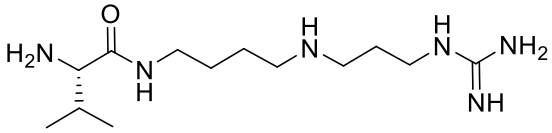

Prephevamine

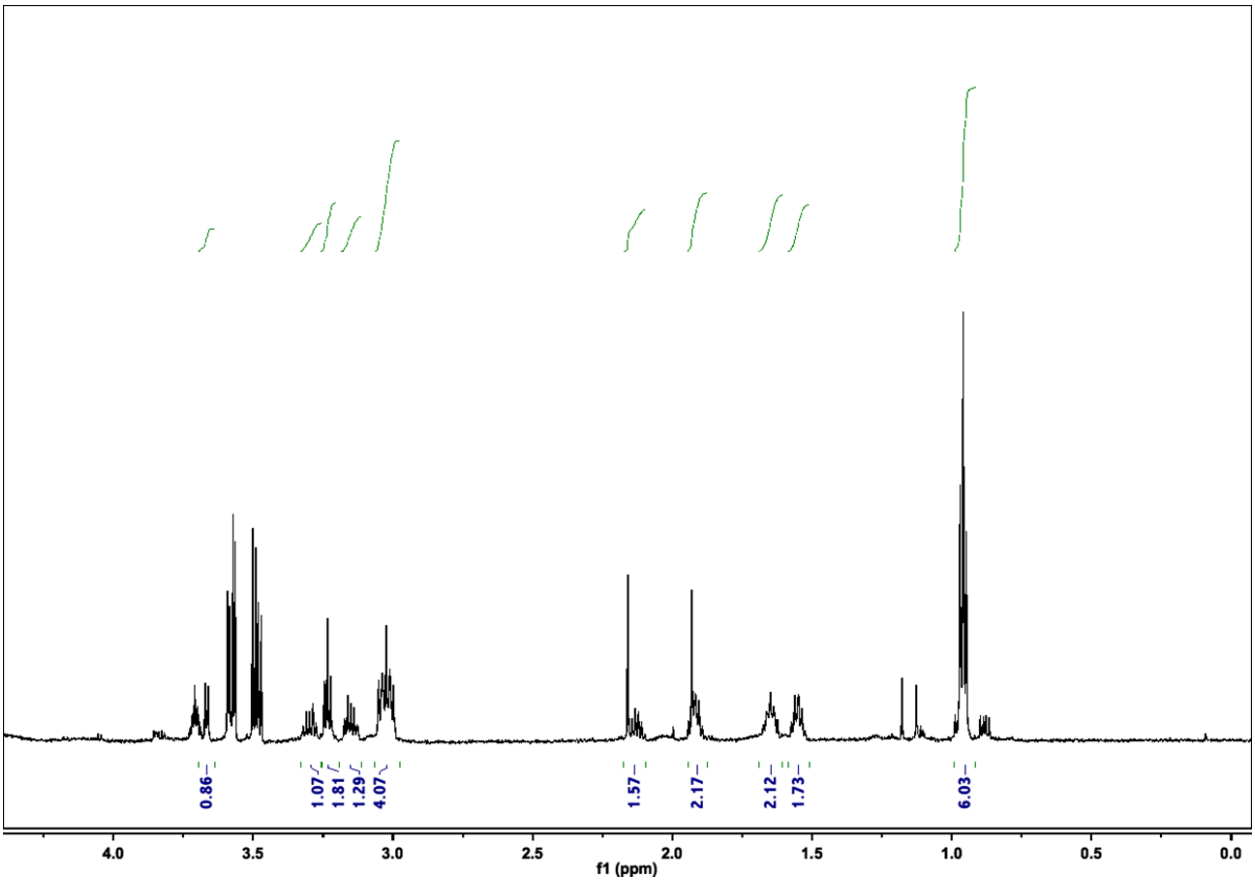

Figure S31. ^{1}H NMR (600 MHz) of *in vitro* purified prephevamine. Spectrum acquired in D_2O.

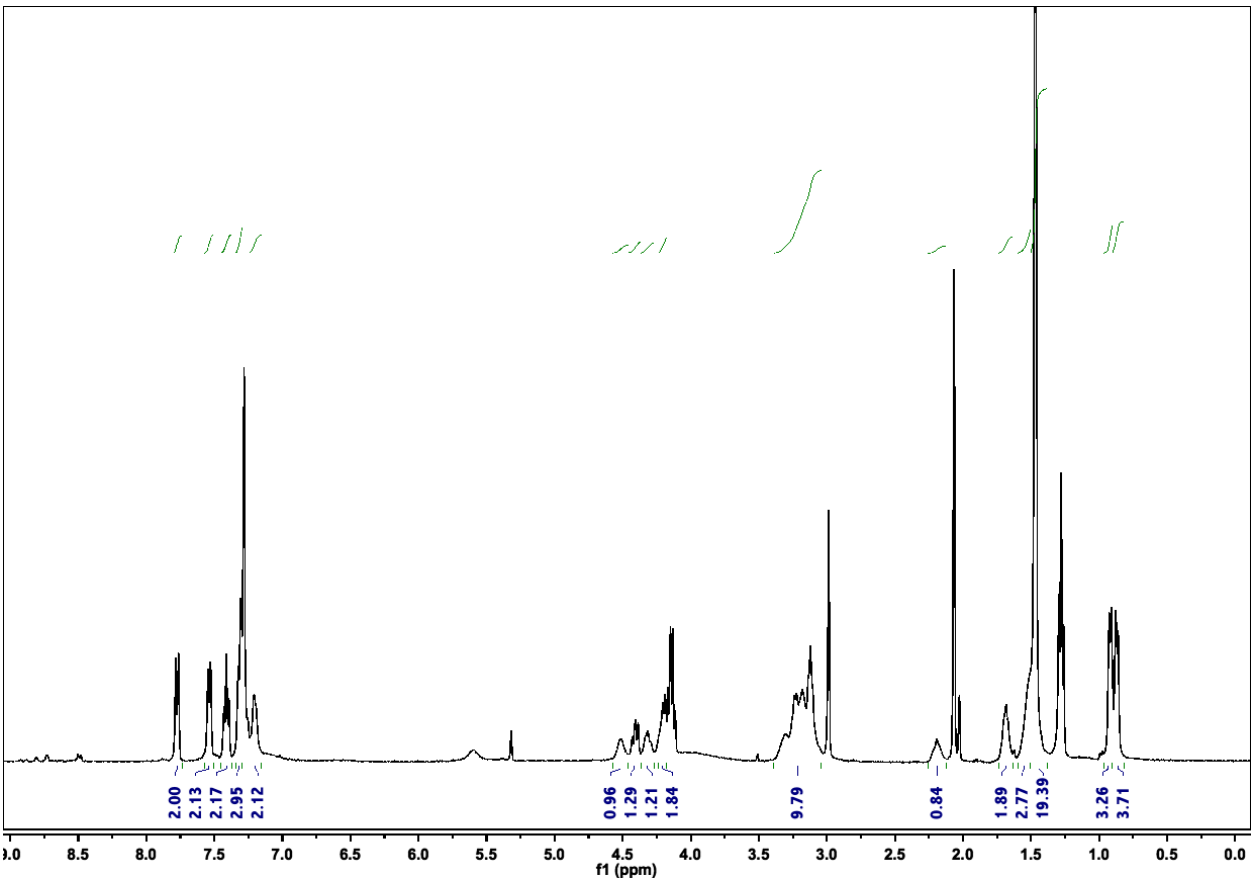

Figure S32. ^{1}H NMR (400 MHz) of Fmoc-(*S*)-Val-bis-Boc-spermidine (5). Spectrum acquired in $CDCl_3$.

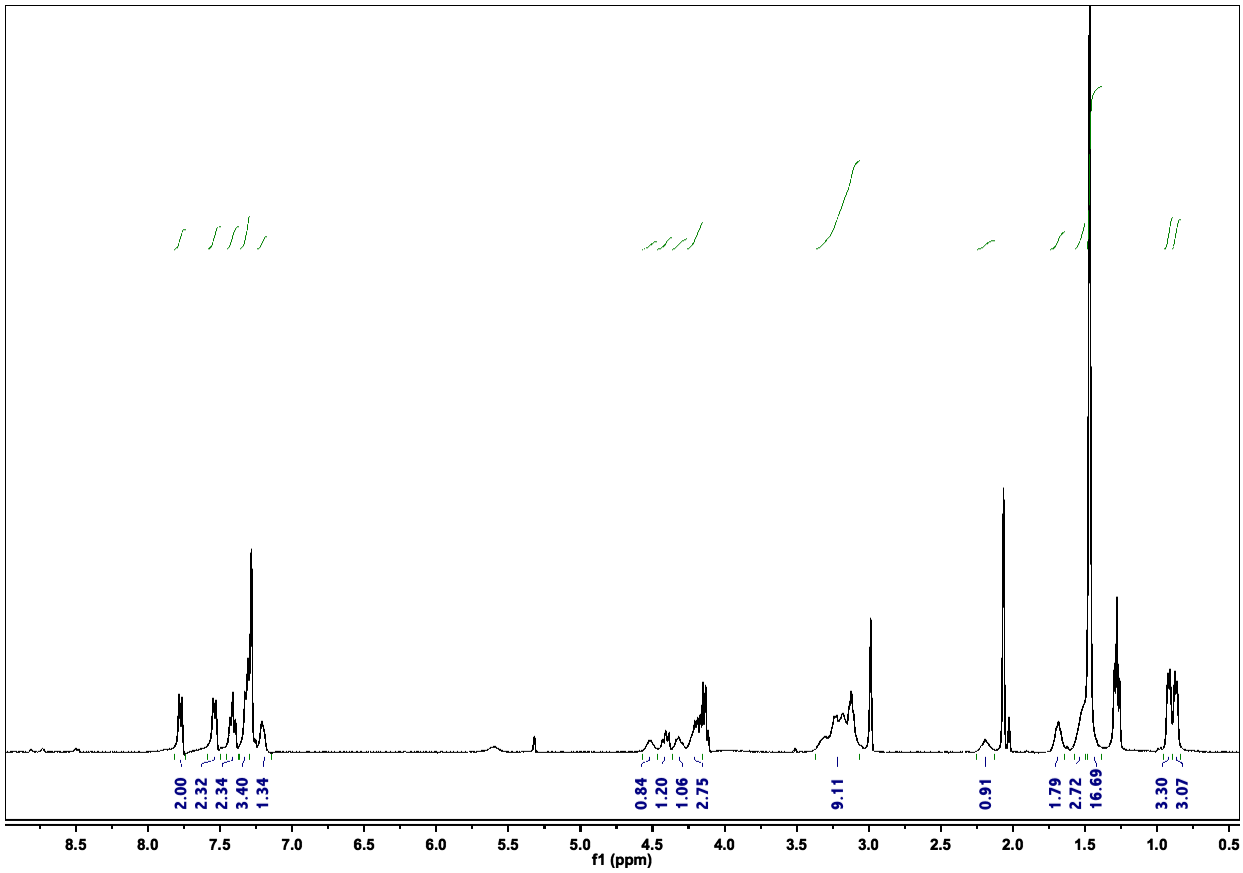

Figure S33. ^{1}H NMR (400 MHz) of Fmoc-(*S*)-Phe-(*S*)-Val-bis-Boc-spermidine (6). Spectrum acquired in $CDCl_3$.

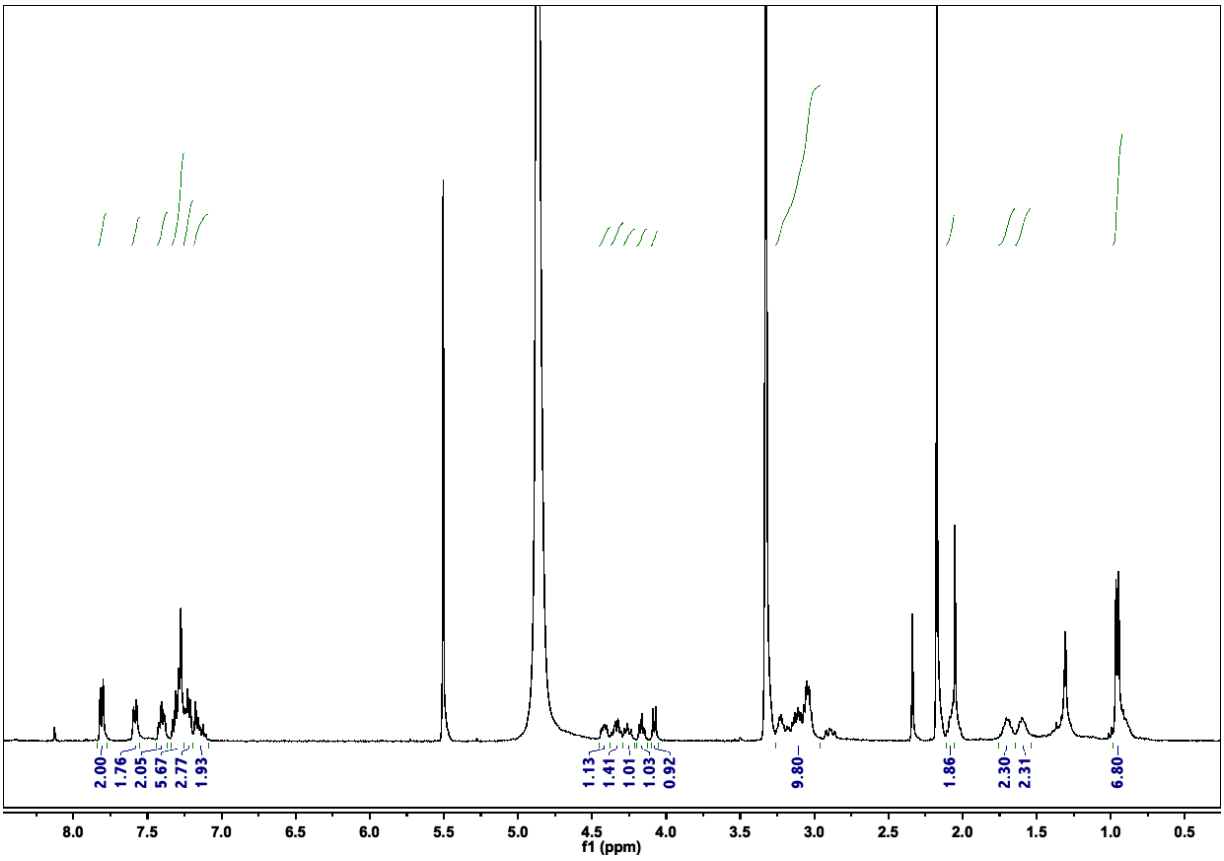

Figure S34. ^{1}H NMR (400 MHz) of Fmoc-(*S*)-Phe-(*S*)-Val-spermidine (7). Spectrum acquired in CD_3OD.

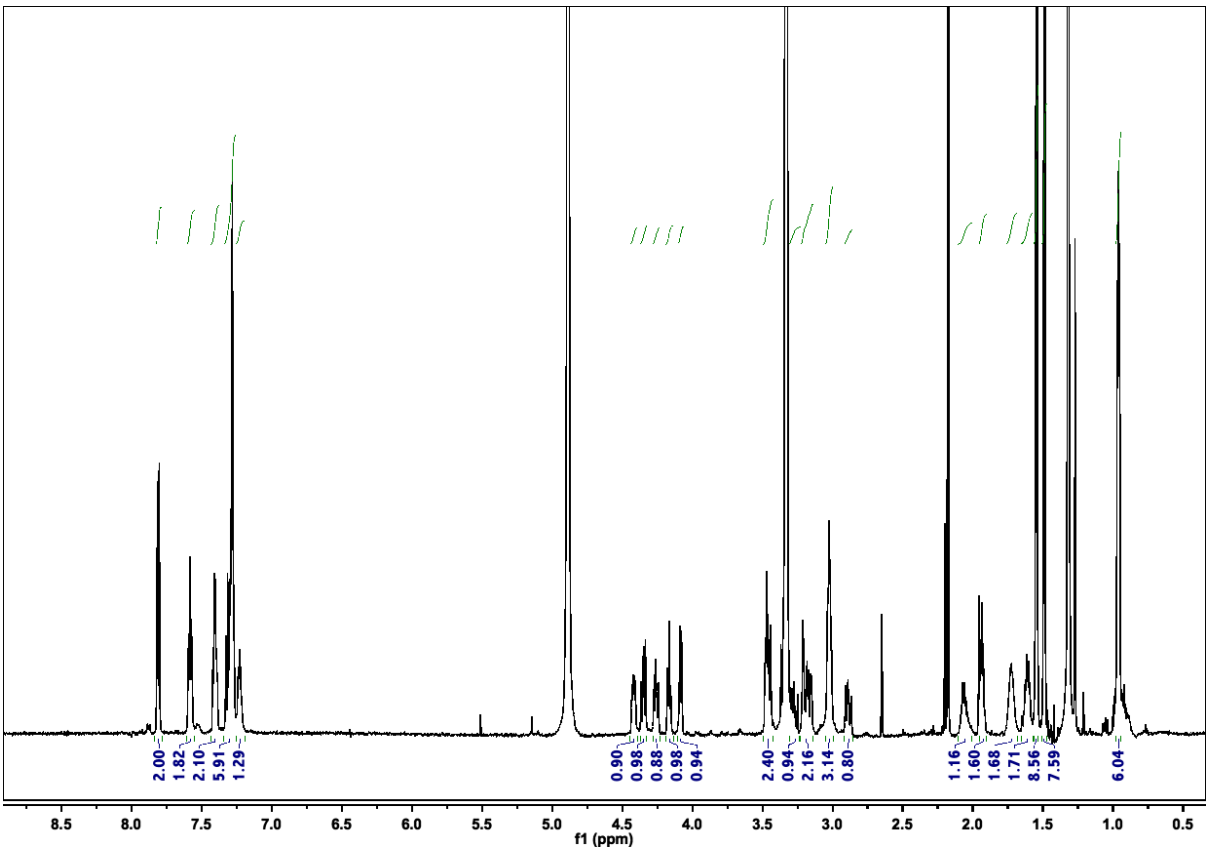

Figure S35. ^{1}H NMR (600 MHz) of Fmoc-(*S*)-Phe-(*S*)-Val-spermidine-*N,N*'-di-Boc-1*H*-guanidine (8). Spectrum acquired in CD_3OD.

References

1. Sambrook J & Russell D (2001) *Molecular Cloning: A Laboratory Manual* (Cold Spring Harbor, New York) 3rd Ed pp 6.4-6.12.
2. Mucyn TS*, et al.* (2014) Variable suites of non-effector genes are co-regulated in the type III secretion virulence regulon across the *Pseudomonas syringae* phylogeny. *PLoS Pathog* 10:e1003807.
3. Obranić S, Babić F, & Maravić-Vlahoviček G (2013) Improvement of pBBR1MCS plasmids, a very useful series of broad-host-range cloning vectors. *Plasmid* 70:263-267.
4. Choi K-H & Schweizer HP (2006) mini-Tn7 insertion in bacteria with single attTn7 sites: example *Pseudomonas aeruginosa*. *Nat Protoc* 1:153.
5. Marco ML, Legac J, & Lindow SE (2005) *Pseudomonas syringae* genes induced during colonization of leaf surfaces. *Environ Microbiol* 7:1379-1391.
6. Reyrat J-M, Pelicic V, Gicquel B, & Rappuoli R (1998) Counterselectable markers: untapped tools for bacterial genetics and pathogenesis. *Infect Immun* 66:4011-4017.
7. Knight H, Trewavas AJ, & Knight MR (1996) Cold calcium signaling in *Arabidopsis* involves two cellular pools and a change in calcium signature after acclimation. *Plant Cell* 8:489-503.
8. Kaur N*, et al.* (2008) Designing the polyamine pharmacophore: Influence of *N*-substituents on the transport behavior of polyamine conjugates. *J Med Chem* 51:2551-2560.
9. Wang J*, et al.* (2012) Synthesis, cytotoxicity, and cell death profile of polyaminoanthraquinones as antitumor agents. *Chem Biol Drug Des* 80:909-917.
10. Wang J*, et al.* (2014) Potent P-glycoprotein inhibition of emodin derivative: synthesis and biological evaluation. *Med Chem Res* 23:2106-2112.
11. Silby MW*, et al.* (2009) Genomic and genetic analyses of diversity and plant interactions of *Pseudomonas fluorescens*. *Genome Biol* 10:R51.
12. Thomas WJ, Thireault CA, Kimbrel JA, & Chang JH (2009) Recombineering and stable integration of the *Pseudomonas syringae* pv. *syringae* 61 hrp/hrc cluster into the genome of the soil bacterium *Pseudomonas fluorescens Pf*0-1. *Plant J* 60:919-928.
13. Ma S, Morris V, & Cuppels D (1991) Characterization of a DNA region required for production of the phytotoxin coronatine by *Pseudomonas syringae* pv. *tomato*. *Mol Plant Microbe Interact* 4:69-74.
14. Zeng W*, et al.* (2011) A genetic screen reveals *Arabidopsis* stomatal and/or apoplastic defenses against *Pseudomonas syringae* pv. *tomato* DC3000. *PLoS Pathog* 7:e1002291.
15. Yamasaki H & Cohen MF (2006) NO signal at the crossroads: polyamine-induced nitric oxide synthesis in plants? *Trends Plant Sci* 11:522-524.
16. Kim NH, Kim BS, & Hwang BK (2013) Pepper arginine decarboxylase is required for polyamine and γ-aminobutyric acid signaling in cell death and defense response. *Plant Physiol* 162:2067-2083.
17. Carrión VJ*, et al.* (2013) The *mangotoxin biosynthetic operon* (*mbo*) is specifically distributed within *Pseudomonas syringae* genomospecies 1 and was acquired only once during evolution. *Appl Environ Microb* 79:756-767.